Doctoral Thesis

Structural basis for the Gip1-mediated sequestration of heterotrimeric G proteins in the cytosol for wide-range chemotaxis

Takero Miyagawa

Graduate School of Frontier Biosciences
Osaka University

March 2019

General Summary

Cells can sense and respond to the environmental change. G protein-coupled receptor (GPCR) and heterotrimeric G proteins play pivotal role in sensing extracellular signals in eukaryotic cells. GPCR is activated by extracellular signals, and the activated GPCR stimulates heterotrimeric G proteins on the surface of plasma membrane by exchanging guanine nucleotide bound to G proteins, consequently resulting in the appropriate responses. One important biological phenomenon relating to GPCR signaling is chemotaxis. Chemotaxis is a behavior with which cells sense extracellular chemicals and move along the chemical gradient. This phenomenon is observed in a wide variety of life events, for example, neurogenesis, embryogenesis, wound healing, and immune response. Chemotactic cells show sensing ability against chemoattractant over broad range. Indeed, a social amoeba *Dictyostelium discoideum* can chemotax at the concentration of chemoattractant over 10^5 – 10^6-fold range. Recent studies revealed that *Dictyostelium* extends its chemotactic dynamic range by regulating the subcellular localization of G proteins from the cytosol to the plasma membrane dependent on the chemoattractant stimulation, called “G protein shuttling”. Although this kind of spatial regulation mechanism of G proteins is physiologically important for the effective signal transduction, it remains elusive how heterotrimeric G proteins regulate their subcellular localization.

This doctoral thesis reveals the structural basis of G protein sequestration in the cytosolic pool in *Dictyostelium*. G proteins utilized their prenyl-modification on Gγ subunit for binding with a cytosolic protein named G protein interacting protein 1, Gip1. Gip1 had a hydrophobic cavity, which was required for binding with G proteins and chemotactic behavior. Since mammalian cells encode TNFAIP8 family proteins that are structurally similar to Gip1, TNFAIP8 family proteins could serve as regulators of G protein shuttling in mammalian cells. It is remarkably important to regulate the activity of heterotrimeric G proteins because GPCR signaling relates to several biological phenomena in eukaryote, including human

diseases. This doctoral thesis provide the possibility that G protein shuttling is observed even in mammalian cells as a regulation mechanism of heterotrimeric G proteins in the different way from guanine nucleotide exchange.

Abstract

A social amoeba *Dictyostelium discoideum* moves toward the source of chemoattractant along the wide-range chemical gradient using G protein-coupled receptors. In a cell, heterotrimeric G proteins are sequestered in the cytosol and translocated from the cytosol to the plasma membrane in a chemoattractant-dependent manner, resulting in the wide-range chemotaxis. This G protein shuttling is mediated by G protein interacting protein 1 (Gip1). However, it remains elusive how G proteins are sequestered in the cytosol at the resting state. Here, I unveil the structural basis of the Gip1-mediated sequestration of heterotrimeric G proteins in the cytosol. A structure of G protein binding region of Gip1 showed a central hydrophobic cavity accommodating a phospholipid. Another form of Gip1 structure obtained in this study showed that rotational movements around α1- and α6-helices changed the cavity shape. The overall structure of G protein binding region of Gip1 was distinct from solubilization factors but similar to tumor necrosis factor-α-induced protein 8 (TNFAIP8) family proteins. Biochemical experiments indicated that the geranylgeranyl moiety on Gγ subunit of heterotrimeric G proteins was essential for complex formation with Gip1 in the cytosol, although Gip1 did not bind to other prenyl-modified proteins. Further studies of tryptophan and alanine mutagenesis revealed that the hydrophobic cavity and a C-terminal tail region were required for the complex formation. Finally, mutations in both the cavity and the C-terminal tail impaired the chemotactic ability at the higher concentration. These researches elucidate the significance of the hydrophobic cavity of Gip1 for the G protein sequestration in the cytosol. There are some proteins solubilizing and trafficking small G proteins inside a cell, but it is the first report revealing the structural mechanism of solubilizing heterotrimeric G proteins. Since mammalian cells encode TNFAIP8 family proteins, whose molecular mechanism has not been well studied, the G protein shuttling could be a widely conserved mechanism regulating the activity of heterotrimeric G proteins.

Abbreviation

cAMP	cyclic adenosine 3',5'-monophosphate
cAR	cAMP receptor
DTT	dithiothreitol
GAP	GTPase activating protein
GDI	guanine nucleotide dissociation inhibitor
GDP	guanosine 5'-diphosphate
GEF	guanine nucleotide exchange factor
Gip1	G protein interacting protein 1
GPCR	G protein-coupled receptor
GRK	G protein-coupled receptor kinase
GTP	guanosine triphosphate
IPTG	isopropyl β-D-1-thiogalactopyranoside
LatA	latrunculin A
LEGI	local excitation and global inhibition
PDEδ	δ subunit of phosphodiesterase 6
PE	phosphatidylethanolamine
PG	phosphatidylglycerol
PH domain	Pleckstrin homology domain
PIP2	phophatidylinositol (4,5)-bisphosphate
PIP3	phophatidylinositol (3,4,5)-trisphosphate
REP	Rab escort protein
RGS	regulatory of G protein signaling
TIPE	TNFAIP8-like
TMR	tetramethyl rhodamine
TNFAIP8	tumor necrosis factor-α-induced protein 8

I. Introduction

I-1 Sensing mechanism in eukaryotic chemotaxis

Living organisms sense and respond to the environmental change. These phenomena are observed not only in a multicellular organism but also in an individual single cell. Cells can response to many extracellular signals, for example, light, heat, electricity, gravity, chemicals, etc. The motilities in response to the outer stimulation are called taxes. Specifically, the taxis toward chemicals is named as chemotaxis. Chemotaxis is widely observed phenomenon over prokaryotic cells to eukaryotic cells. Both cells can sense the chemical concentration and migrate toward chemoattractant or away from chemorepellent. Bacterial cells randomly swim and temporally sense the concentration of chemicals. By temporally sensing and comparing the chemical concentration, cells change the frequency of straight swimming and turn to change move direction by regulating the rotational direction of flagella [Macnab & Koshland, 1972; Tsang *et al.*, 1973]. For this chemotactic feature called "biased-random walk", bacterial cells utilize temporal sensing mechanism.

Eukaryotic chemotaxis is observed in many motility cells, for example neutrophil and *Dictyostelium discoideum* [Konijn *et al.*, 1969a; Konijn *et al.*, 1969b; Zigmond, 1974; Devreotes & Zigmond, 1988]. Neutrophils show chemotactic ability against formylmethionyl peptides (e.g. *N*-folmyl-methionyl-leucyl-phenylalanine (fMLP) peptide) [Schiffmann *et al.,* 1975]. Since formylmethionyl peptides are secreted from bacteria, the chemotactic ability enables neutrophils to chase and phagocyte infected bacteria for an immune response. *Dictyostelium* is a social amoeba with chemotactic ability toward cyclic adenosine 3',5'-monophosphate (cAMP) [Konijn *et al.*, 1969a; Bonner *et al.*, 1969; Konijn *et al.*, 1969b]. The amoebae usually behave as single cells. Once cells are in starvation, they secrete cAMP and aggregate each other (known as "cAMP relay"). In this developmental stage, aggregating cells periodically produce cAMP generated by adenylyl cyclase and degraded by phosphodiesterase, resulting in cAMP oscillation [Tomchik & Devreotes, 1981]. Aggregated

cells transform to a multicellular slug, and finally to the fruiting body to tolerate in the harsh environment. Through the chemotaxis, cells show chemotactic ability over broad-range chemoattractant concentration. In case of *Dictyostelium* cells, cells can chemotax at the concentration over 10^5- to 10^6-fold range [Fisher *et al.,* 1989]. Eukaryotic chemoatxis comprises the three processes: directional sensing, polarity, and cell motility (Fig. 1) [Swaney *et al.,* 2010]. In contrast to bacterial cells, eukaryotic cells are larger in the size and slower in the speed. In these aspects, eukaryotic cells use spatial sensing mechanism rather than temporal sensing mechanism with which cells do not need to move to sense the chemical gradient. Both neutrophil and *Dictyostelium* are model organisms for studying eukaryotic chemotaxis, and utilize G protein-coupled receptors (GPCRs) for receiving chemoattractants [Murphy *et al.*, 1992; Klein *et al.,* 1988]. Although the signaling network is shared to some extent between neutrophil and *Dictyostelium*, signaling pathways have been well studied especially in *Dictyostelium* [Swaney *et al.,* 2010; Devreotes *et al.,* 2017]. *Dictyostelium* has GPCRs for cAMP, named cAMP receptors (cARs). There are four types of cARs, cAR1 to cAR4, whose expressions are regulated dependent on the developmental stage [Klein *et al.*, 1988; Saxe *et al.*, 1991; Saxe *et al.*, 1993; Johnson *et al.*, 1993]. During the aggregation stage, the amoebae express cAR1 that is uniformly distributed on the plasma membrane [Jin *et al.,* 2000]. While, downstream heterotrimeric G proteins distribute along shallow gradient [Jin *et al.,* 2000], and other chemotactic factors (e.g. Ras, phosphatidylinositol (3,4,5)-trisphosphate (PIP3), PTEN, F-actin, myosin II) polarize at the front or back side of a cell along the gradient of cAMP on the plasma membrane [Yumura *et al.,* 1984; Parent *et al.,* 1998; Iijima & Devreotes, 2002; Sasaki *et al.,* 2004]. Some factors are able to polarize even in the absence of F-actin cytoskeleton [Parent *et al.,* 1998]. In addition to the regulation mechanism at the GPCR level (described in the section I-2), transient recruitment of chemotactic factors to the plasma membrane regulates the signal transduction. For example, NfaA accelerates Ras dissociation from the plasma membrane and terminates Ras activation [Zhang *et al.,* 2008]. In another

case, C2GAP1 inhibits the sustainable Ras localization on the plasma membrane and extends the chemotactic dynamic range [Xu *et al.,* 2017]. For the explanation of the gradient sensing, cells use local excitation and global inhibition (LEGI) model [Levchenko & Iglesias, 2002; Tang *et al*., 2014]. In this model, an input signal (*S*) stimulates both a local excitor (*E*) and a global inhibitor (*I*). *E* rapidly activates downstream response regulator (*RR*), while *I* slowly inhibits *RR*. Since *RR* is only activated in the vicinity of *E*, signal transduction occurs only near the stimulated *E*. Applying the model to the signaling network in *Dictyostelium*, *S* is cAMP, *E* is heterotrimeric G proteins. In the chemotactic signaling pathways, very few factors have been identified as binding partners of heterotrimeric G proteins (ElmoE for Gβ and Ric8 for Gα2) [Yan *et al.,* 2012; Kataria *et al.,* 2013], and the connection between G proteins and downstream effectors (e.g. RasG, RasC, sGC) remained enigmatic [Devreotes *et al.,* 2017]. So far, no candidates have been identified as *I*.

I-2 Regulation mechanisms of GPCR signal transduction

GPCRs are membrane proteins embedded in the cell membrane with seven-transmembrane α-helices. They are classified into six groups according to the sequence homology: rhodopsin-like for class A, secretin receptor family for class B, for metabotropic glutamate for class C, fungal mating pheromone receptors for class D, cyclic AMP receptors for class E, and Frizzled/smoothened for class F [Alexander *et al.,* 2017], although classes D and E are not found in vertebrates. GPCRs mainly function as sensors for external stimuli including odorants, tastes, hormones, neurotransmitters, chemoattractants, and even photons of light. Many GPCRs are remained as orphan GPCRs whose ligands are unknown. Approximately 800 GPCRs are encoded in the human genome, and many of them are drug targets. Nowadays, many GPCR structures have been solved. Especially, recent technological advances have made it possible to determine the complex structures of GPCR with heterotrimeric G proteins or arrestin [Rassmussen *et al.*, 2011; Kang *et al.*, 2015]. Ligand-bound GPCRs change their

structure and function as guanine nucleotide exchange factors (GEFs) of downstream heterotrimeric G proteins. Activated GPCRs also interact with G protein-coupled receptor kinases (GRKs). GRKs phosphorylate the C-terminal region of GPCRs, leading to the recruitment of β-arrestin. Arrestin-bound GPCRs are internalized into the cell and removed from the cell surface, resulting in desensitization [Ferguson *et al.*, 1996]. In *Dictyostelium*, cAMP stimulation induces cAR1 phosphorylation at its C-terminal tail region, although it is not important for chemotaxis [Hereld *et al.,* 1994; Caterina *et al.,* 1995; Kim *et al.,* 1997]. It remains elusive what GRKs phosphorylates cAR1. Phosphorylated cAR1 interacts with arrestin and internalized, resulting in the modulation of the frequency of cAMP oscillation [Cao *et al.,* 2014].

Heterotrimeric G proteins are downstream target of ligand-bound GPCRs, composed of Gα subunit and tightly bound Gβγ subunit. As an inactive state, Gα contains guanosine 5'-diphosphate (GDP) and complexes with Gβγ. Once interacted with ligand-bound GPCRs, Gα exchanges GDP to guanosine triphosphate (GTP), and dissociates from Gβγ. Dissociated Gα and Gβγ are activated and individually interact with downstream target proteins, leading to stimulating several signal transduction pathways. Gα has an intrinsic GTPase activity, however it is too weak to hydrolysis GTP to GDP. GTPase activating protein (GAP), which is called in another name as regulatory of G protein signaling (RGS), interacts with Gα-GTP and catalyzes GTP hydrolysis. Gα-GDP associates with Gβγ and returns to inactivated ternary Gαβγ complex. In conclusion, heterotrimeric G proteins modulate their activity dependent on the bound guanine nucleotide, and are regarded as a molecular switch catalyzed by two enzymes GEF and GAP (Fig. 2). This switch mechanism is conserved in other small G proteins including Ras superfamily. Recent studies revealed that there are cytosolic non-receptor GEF enzymes (e.g. Ric8 and GIV/Girdin) [Tall *et al.*, 2003; Garcia-Marcos et al., 2009; Oner *et al.*, 2013]. Furthermore, non-canonical G protein signal transduction mechanism has been found [Zha *et al.*, 2015]. In *Dictyostelium*, cAMP stimula-

tion induces the Gα2Gβγ complex dissociation inside a cell with *K*d value of 1-10 nM [Janetopoulos *et al.,* 2001; Miyanaga *et al.*, 2018].

Gα comprises of a GTPase domain, which is structurally similar to small G proteins, and a helical domain connected by linker regions [Noel *et al.*, 1993; Lambright *et al*., 1994; Lambright *et al*., 1996]. Among the Gα structure, there are three flexible loops named switch I, II and III regions. These regions locate near the bound γ-phosphate of GTP and dramatically change their configuration between GDP- and GTP-bound forms [Noel *et al.*, 1993; Lambright *et al*., 1994]. Gβ is a β-propeller family protein containing seven β-sheets, each containing four antiparallel β-strands like a blade of a propeller. There are the characteristic WD repeats (Trp-Asp bipeptide) in the blade-like regions [Sondek *et al.*, 1996; Lambright *et al*., 1996]. Gγ tightly encircles the β-propeller fold of Gβ. Many effector proteins of Gβγ share almost the same binding interface with Gα [Lambright *et al*., 1996; Gaudet *et al.*, 1996; Ford *et al.*, 1998; Leow *et al.*, 1998; Tesmer *et al*., 2005; Davis *et al.*, 2005]. This is why Gβγ can switch its signal transduction activity by association or dissociation with Gα.

Both Gα and Gγ are subjected to acylation and prenylation at their N and C terminus, respectively. At the N terminus of Gα, there are glycine at position 2 (Gly2) or Cys. These Gly and Cys are possible to be subjected to myristoylation (saturated 14-carbon fatty acyl chain; (C14:0)) and palmitoylation (C16:0), respectively [Resh, 2006]. Myristoylation and palmitoylation are catalyzed by N-myristoyl transferase (NMT) and palmitoyl acyl transferase (PAT), respectively. On the other hand, Gγ has a CAAX motif (C for Cys; A for aliphatic amino acid; X for any amino acid) at its C terminus. Final X determines the type of prenylation of Cys in CAAX motif: Leu for geranylgeranylation (C20), and the other for farnesylation (C15) [Jiang *et al.*, 2018]. Prenylation is catalyzed by geranylgeranyltransferase I (GGTaseI) for geranylgeranylation, and farnesyltransferase (FTase) for farnesylation, respectively [Resh, 2006]. C-terminal AAX motif is removed after prenyl-modification, and the remained prenylated cysteine is methylated. Among these lipid-modifications, palmitoylation

is reversibly removed but the other lipid-modifications are not. The reversible palmitoylation regulates the trafficking and localization to the membrane [Rocks *et al.*, 2005; Rocks *et al.*, 2010].

I-3 Translocation of G proteins

Heterotrimeric G proteins function on the plasma membrane by anchoring via lipid-modifications at N terminus of Gα and C terminus of Gγ. However, some reports say that G proteins dynamically change their positions inside a cell.

One of the most famous examples is the translocation of transducin (GαtGβγ) in a vertebrate rod photoreceptor cell in a retina. A rod has compartments called the outer segment, which is a specialized ciliary organelle, and the inner segment. Proteins are synthesized in the inner segment and trafficked to the outer segment. There are many phototransduction proteins, including rhodopsin and transducin, in the outer segment. Once the rod is illuminated with bright light, transducin moves out from the outer segment to the inner segment [Philp *et al.*, 1987; Brann & Cohen, 1987]. Photon-stimulated rhodopsin activates transducin and leads to the dissociation of transducin into Gαt and Gβγ. Gβγ interacts with phosducin and is translocated to the inner segment at the different rate to that of Gαt [Lee *et al.*, 1987; Sokolov *et al.*, 2002; Sokolov *et al.*, 2004]. During the dark adaptation, Gαt in the inner segment binds to UNC119 regardless of guanine nucleotide form and moves back to the outer segment [Zhang *et al.*, 2011; Sinha *et al.*, 2013]. Through the translocation of transducin, lipid-modifications of both Gαt and Gβγ are important [Zhang *et al.*, 2011; Brooks *et al.*, 2018].

In another case, Gβγ translocate from the plasma membrane to the endomembrane like Golgi [Akgoz *et al.*, 2004]. This translocation is induced by ligand-stimulated GPCR and activation of Gα [Azpiazu *et al.*, 2006; Chisari *et al.*, 2007]. The direction of Gβγ translocation is from the plasma membrane to the endomembrane by agonist stimulation, and from the

endomembrane to the plasma membrane by antagonist stimulation [O'Neill *et al.*, 2012]. Furthermore, the rate of translocation depends on the Gγ C-terminal region including prenyl-modification regardless of the move direction [Akgoz *et al*., 2006; Saini *et al*., 2007; Karunarathne *et al.*, 2012; O'Neill *et al.*, 2012]. These Gγ dependent subcellular translocations modulate some physiological events: the fragmentation of Golgi, the pulse oscillation of calcium ions, and cell migration [Sanini *et al*., 2010; Giri *et al.*, 2014; Senarath *et al*., 2018]. However, it has not been elusive what factors relate to the Gβγ translocation.

As is the case with heterotrimeric G proteins, small G proteins also translocate inside a cell. One of the most studied phenomena is the translocation of KRas4B by δ subunit of phophodiesterase 6 (PDEδ). There are three isoforms of Ras proteins: H-, N-, and KRas. KRas4B is a splice variant of KRas (KRas4A and KRas4B). KRas4B has the C-terminal hypervariable region (HVR) including positively charged poly-lysine and the farnesyl-modification, although other Ras isomers have no polybasic regions and are subjected to some palmitoylations on their HVR [Nancy *et al*., 2002; Chandra *et al.*, 2012]. PDEδ was originally discovered as a subunit that solubilizes membrane-bound cGMP phosphodiesterase in rod [Florio *et al.*, 1996]. PDEδ interacts with KRas4B via the farnesyl-modification and facilitates free diffusion through a cell in complex with KRas4B [Chandra *et al.*, 2012]. PDEδ releases KRas4B on the target membrane by interacting with activated Arl2/3 (Arl2/3-GTP), resulting in the accumulation of KRas4B on the plasma membrane (Fig. 3) [Chandra *et al.*, 2012; Schmick *et al.*, 2014]. PDEδ can also interact with other Ras subfamily proteins (e.g. HRas, NRas, RheB, INPP5E) in prenyl-modification-dependent manners after depalmitoylation [Nancy *et al*., 2002; Hanzal-Bayer *et al*., 2002; Chandra *et al.*, 2012; Fansa *et al.*, 2016]. Because of this feature, PDEδ is called in another name as prenyl binding protein (PrBP). Since Arl3-GTP binds to PDEδ more specific than Arl2-GTP, PDEδ dissociates from the prenyl-modified proteins that show higher affinity to PDEδ by interaction with Arl3-GTP but not with Arl2-GTP [Fansa *et al.*, 2016]. In addition to PDEδ, there is a report

showing that KRas4B is translocated from the plasma membrane to Golgi and early endosome by calmodulin [Fivaz & Meyer, 2005; Sperlich *et al.*, 2016].

I-4 Solubilization factors

Solubilization factors enable membrane-bound proteins to dissociate from the membrane and freely diffuse in the soluble cytoplasmic environment in a cell. Solubilization factors facilitate the subcellular trafficking of lipid-modified proteins, called cargos, between intracellular membrane compartments. PDEδ is a solubilization factor for KRas4B and other Ras subfamily proteins. The structures of PDEδ have already determined in complex with some prenyl-modified proteins [Ismail *et al.*, 2011; Dharmaiah *et al.*, 2016; Fansa *et al.*, 2016]. The structure of PDEδ is an immunoglobulin-like β-sandwich fold and shows a hydrophobic cavity. Co-crystallizaed prenyl-modified proteins bind to PDEδ with their prenyl-moieties through the cavity. The cavity size does not significantly change whether PDEδ interacts with cargo proteins or not [Qureshi *et al*., 2018], however largely decreases when PDEδ binds to Arl2-GTP [Hanzal-Bayer *et al.*, 2002; Ismail *et al.*, 2011]. These structural studies support a model that PDEδ rapidly catches a cytosolic cargo protein, which dissociates from the plasma membrane, through the constantly open cavity. PDEδ freely diffuses inside a cell in complex with a cargo and releases the cargo at the proper location where activated Arl2/3 resides (Fig. 3). Regarding on the binding specificity, C-terminal amino acids at the position of -1 and -3 from the prenylated cysteine and carboxymethylation are important [Dharmaiah *et al.*, 2016; Fansa *et al.*, 2016].

PDEδ shows structural homology with UNC119 and guanine nucleotide dissociation inhibitor (GDI) of Rho (RhoGDI) (Fig. 4) [Keep *et al.*, 1997; Hoffmann *et al*., 2000; Scheffzek *et al.*, 2000; Grizot *et al*., 2001; Tnimov *et al.*, 2012; Zhang *et al.*, 2011; Ismail *et al.*, 2012; Jaiswal *et al.*, 2016]. Compared to PDEδ, RhoGDI has an extended N-terminal helix-loop-helix arm. This arm interacts with the switch region of cargos, resulting in the re-

striction of the complex form with inactivated GDP-formed cargo proteins [Hoffmann *et al*., 2000; Scheffzek *et al.*, 2000; Grizot *et al*., 2001; Tnimov *et al.*, 2012]. Furthermore, this N-terminal arm is required for inhibiting the GTPase activities of cargos [Gosser *et al.*, 1997]. According to these functional features, the N-terminal arm is called as a "regulatory arm". In contrast to PDEδ, the cavity size of RhoGDI is small in absence of cargos, but enlarges when RhoGDI binds to a cargo. Because of this feature, RhoGDI first binds to membrane-bound cargos through the regulatory arm, orients to the proper direction, and then captures the prenyl-moiety that transiently dissociates from the membrane (Fig. 3) [Nomanbhoy *et al.*, 1996].

In addition to RhoGDI, there is another GDI group for Rab as RabGDI. The structure of RabGDI is totally different form those of RhoGDI, PDEδ, and UNC119. The overall structure is rather similar to that of Rab escort protein (REP), which facilitates geranylgeranylation of Rab in cooperation with GGTaseII [Schalk *et al.*, 1996; An *et al.*, 2003; Rak *et al*., 2003; Pylypenko *et al.*, 2006].

I-5 TNFAIP8 family proteins

Some proteins transfer not only lipid-modified proteins but also lipid compounds. Recently identified examples are tumor necrosis factor-α-induced protein 8 (TNFAIP8) family proteins. TNFAIP8 family is composed of TNFAIP8, TNFAIP8-like 1 (TIPE1), TIPE2, and TIPE3. TNFAIP8 was originally discovered as a protein up-regulated by tumor necrosis factor-α (TNF-α) induction [Kumar *et al.*, 2000]. TNFAIP8 localizes in the cytosol and suppresses apoptosis by inhibiting the activity of caspase-8 [You *et al.*, 2001; Kumar *et al.*, 2004]. Past reports show that TNFAIP8 interacts with Gαi3-GTP and Rac1-GTP [Laliberté *et al.,* 2010; Porturas *et al*., 2015].

Among the TNFAIP8 family proteins, TIPE2 is the most well studied one. TIPE2 suppresses the immune responses against signals from toll-like receptors (e.g. lipopolysac-

charide, double-stranded RNA, CpG oligodeoxynleotide, peptidoglycan) [Sun *et al.*, 2008; Wang *et al.*, 2012; Sun *et al*., 2012]. In contrast to TNFAIP8, TIPE2 enhances apoptosis induced by Fas [Sun *et al.*, 2008]. TNFAIP8 interacts with caspase-8 and modulates its activity [Sun *et al.*, 2008]. TIPE2 also interacts with RalGEF and consequently inhibits inflammation and cancer metastasis [Gus-Brautbar *et al.,* 2012]. Other studies suggest that TIPE2 binds to Rac-GTP, resulting in the inhibition of phagocytosis and oxidative burst in neutrophils, and cell growth and metastasis in hepatocellular carcinoma [Wang *et al.*, 2012; Cao *et al.*, 2013]. Furthermore, TIPE2 involves in the neutrophil chemotaxis, especially in directionality and mobility [Fayngerts *et al.*, 2017]. Through the chemotactic processes, TIPE2 facilitates the appropriate localization of F-actin, Rac, and AKT, besides TIPE2 itself weakly localizes in front of a cell. TIPE2 also serves as a phophatidylinositol (4,5)-bisphosphate (PIP2) transfer protein [Fayngerts *et al.*, 2017].

Few reports have been published so far about TIPE1 and TIPE3. TIPE1 is down-regulated as progress of hepatocellular carcinoma, and inhibits apoptosis by directly inhibiting Rac1 activation [Zhang *et al.*, 2015]. On the other hand, TIPE3 is overexpressed in many tumor cells and increases cell number, volume, size and colonies by activating phosphoinositide 3-kinase. In contrast to other TNFAIP8 family proteins, TIPE3 does not interact with Rac. Instead, TIPE3 binds to phosphatidylinositols and serves to transfer PIP2 to the plasma membrane [Fayngerts *et al.*, 2014]. To sum up, TNFAIP8 family proteins involve in immunity, inflammation, apoptosis, and cancer, although detailed mechanism remains enigmatic.

Nowadays, crystal structures of TNFAIP8, TIPE2 and TIPE3 are determined [Zhang *et al.,* 2009; Fayngerts *et al.,* 2014; Kim *et al.,* 2017]. All of them share the similar structural features, a hydrophobic cavity at their center (Fig. 5). The cavity is thought to be important for transferring phospholipids [Fayngerts *et al.,* 2014; Kim *et al.,* 2017]. There are some residues around the cavity entrance significant for physiological functions [Fayngerts *et*

al., 2014; Antony *et al*., 2016; Kim *et al*., 2017].

I-6 G protein interacting protein 1

G protein interacting protein 1 (Gip1) was first discovered in *Dictyostelium* cells as a binding partner of Gβγ subunit [Kamimura *et al.,* 2016]. As a phenotypic study, *gip1* gene disruption induces the severe defect in chemotactic ability specifically at the high cAMP stimulation over 1 μM. In other word, Gip1 is required for extension of chemotactic dynamic range to the higher chemoattractant concentration (Fig. 6). During the chemotactic processes, polarity and motility are not significantly affected. So, Gip1 involves in the chemotactic process of directional sensing. In *Dictyostelium* cells, it was reported that the G proteins are recruited to the plasma membrane dependent on the cAMP stimulation [Elzie *et al.,* 2009]. Further studies revealed that Gip1 is a regulator of the subcellular localization of heterotrimeric G proteins in the cAMP-dependent manner [Kamimura *et al.,* 2016]. Since Gip1 sequesters G proteins in the cytosol at the resting state, Gip1 can be said as a solubilization factor.

Gip1 is composed of N-terminal Pleckstrin homology (PH) domain and C-terminal DUF758 domain, whose function is unknown, annotated with Pfam server (http://pfam.xfam.org/) [El-Gebali *et al.*, 2019]. PH domain is required for regulation of cAMP-dependent G protein translocation. On the other hand, C terminal region is essential for both the binding ability with G proteins and cytosolic sequestration. At the resting state, G proteins exists in the cytosolic pool in *Dictyostelium* cells. Once cells receive cAMP stimulation, G proteins translocate from the cytosol to the plasma membrane in a Gip1-dependent manner (Fig. 7). In addition, more G proteins are translocated to the membrane exposed with higher cAMP rather than with lower cAMP. In summary, molecular functions of Gip1 are (1) sequestration of heterotrimeric G proteins in the cytosolic pool, (2) regulation of subcellular G protein translocation dependent on cAMP stimulation, and (3) biased redistribution of G proteins (Fig. 7).

Now, there are mainly three remaining questions on the Gip1 functions. First, how does Gip1 sequester heterotrimeric G proteins in the cytosol at the resting state? Second, what factors regulates the translocation of heterotrimeric G proteins between the cytosol and the plasma membrane? Third, how does heterotrimeric G proteins ununiformly translocate to the plasma membrane on the cAMP rich side? Among these three questions, here I aim to unveil how Gip1 stably sequesters heterotrimeric G proteins in the cytosolic pool.

I-7 Aim of this doctoral thesis

This doctoral thesis aims to reveal the molecular mechanism underlying the sequestration of heterotrimeric G proteins in the cytosol via Gip1. First, I determined and analyzed the crystal structures of G protein binding region of Gip1. Next, I investigated the significance of prenyl-modification of G proteins and the hydrophobic cavity of Gip1. Finally, I validated the structural-function relationship of Gip1.

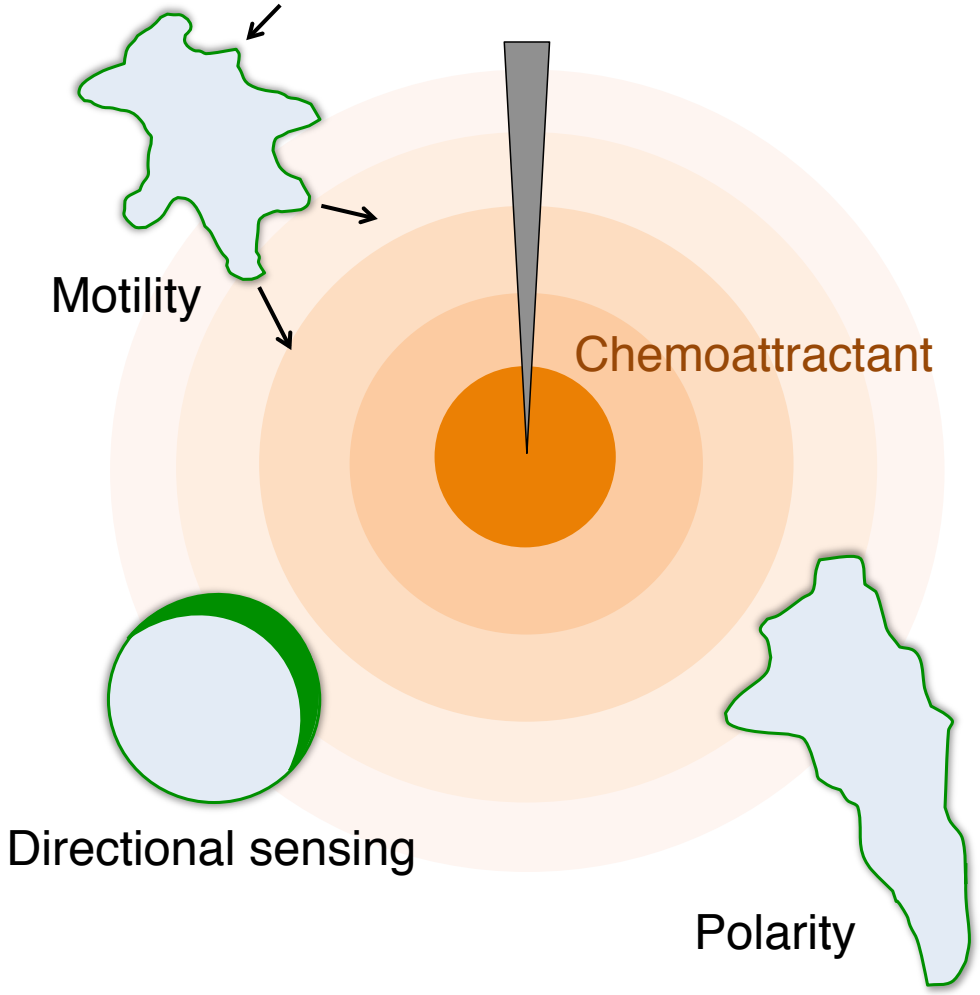

Fig. 1 Three features for chemotactic cells.

Cells are elongated and show the front and the back (Polarity). Cells move by extending or retracting psudophodia (Motility). Cells sense the direction of the source of chemoattractant resulting in the local accumulation of chemotactic factors (e.g. PIP3 colored in green) on the plasma membrane even if the cells do not move (Directional sensing). In this figure, chemo-attractant is secreted from a tip of a centrally located needle. Chemoattractant is colored in orange.

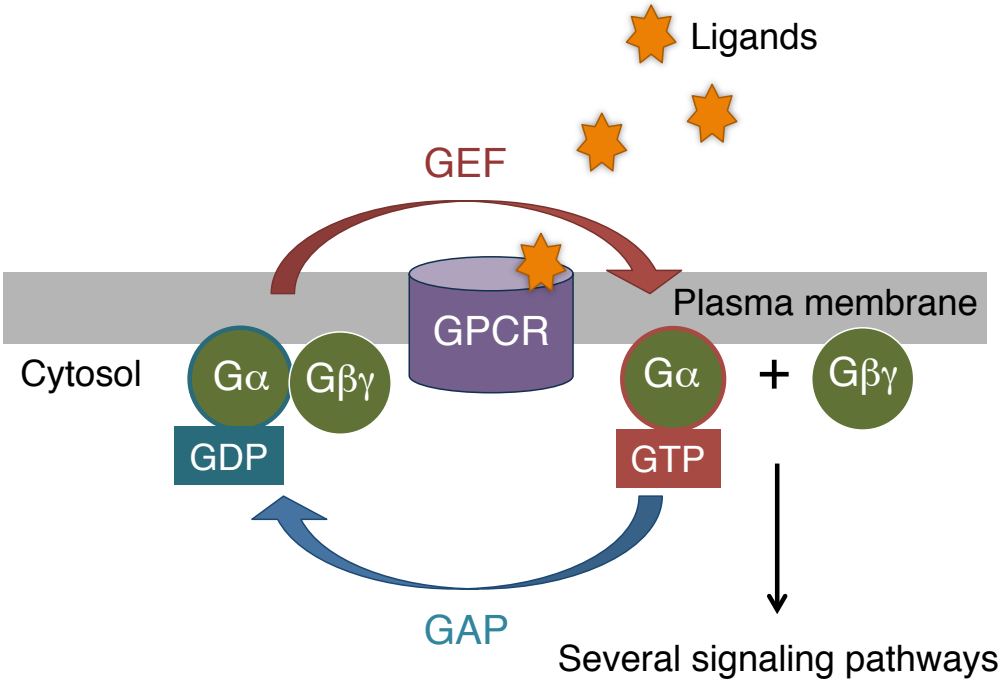

Fig. 2 Traditional regulation mechanism of heterotrimeric G proteins.

Gα and Gβγ subunits locate on the plasma membrane. Gα subunit containing GDP is complexed with Gβγ and in inactive state. Ligand-bound GPCR shows GEF activity and exchange GDP to GTP, leading to the dissociation of Gα and Gβγ. Both G protein subunits transduce signals until Gα hydrolyses bound-GTP to GDP and re-associates to Gβγ with the help of GAP.

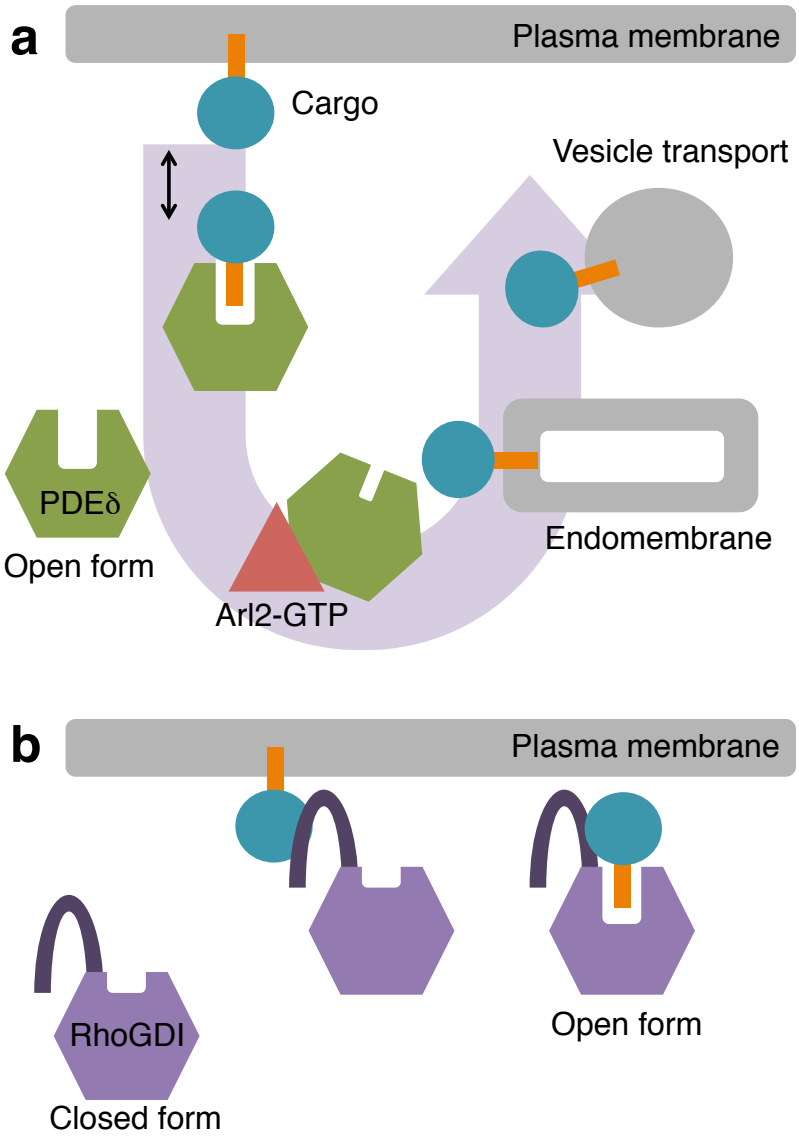

Fig. 3 Molecular functions of PDEδ and RhoGDI.

(a) PDEδ has a hydrophobic cavity. PDEδ captures a prenylated cargo protein spontaneously dissociated from the cell membrane via the open cavity. Freely diffusing PDEδ releases the cargo to the target membrane by reducing the cavity size resulted from the interaction with Arl2-GTP. Cargos are transferred to the plasma membrane with the help of vesicular transport system. **(b)** RhoGDI has a hydrophobic cavity. In contrast to PDEδ, the cavity is closed in absence of cargos. RhoGDI interacts with membrane-bound cargos through N-terminal regulatory arm, and then captures the prenyl-moiety of the cargo transiently dissociated from the plasma membrane.

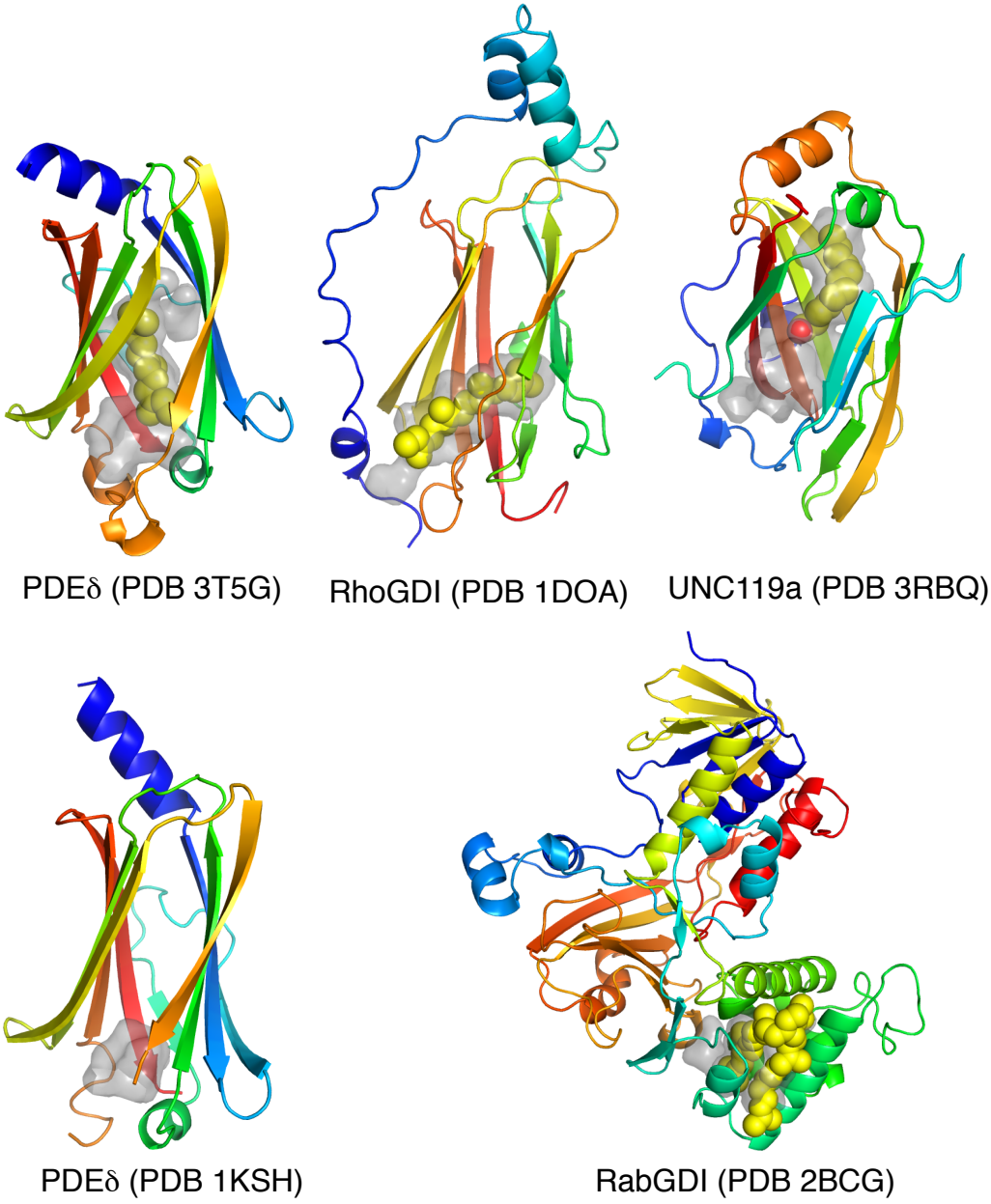

Fig. 4 Overall structures of solubilization factors.

Known solubilization factors are shown as cartoon models. Each structure is colored in rainbow from blue (N terminus) to red (C terminus). Lipid compounds are shown as ball models colored in yellow. Cargo proteins are not shown (Rheb for 3T5G; Cdc42 for 1DOA; peptide of Gαt for 3RBQ; Arl2-GTP for 1KSH; Ypt1 for 2BCG). The surface of a cavity is depicted in gray.

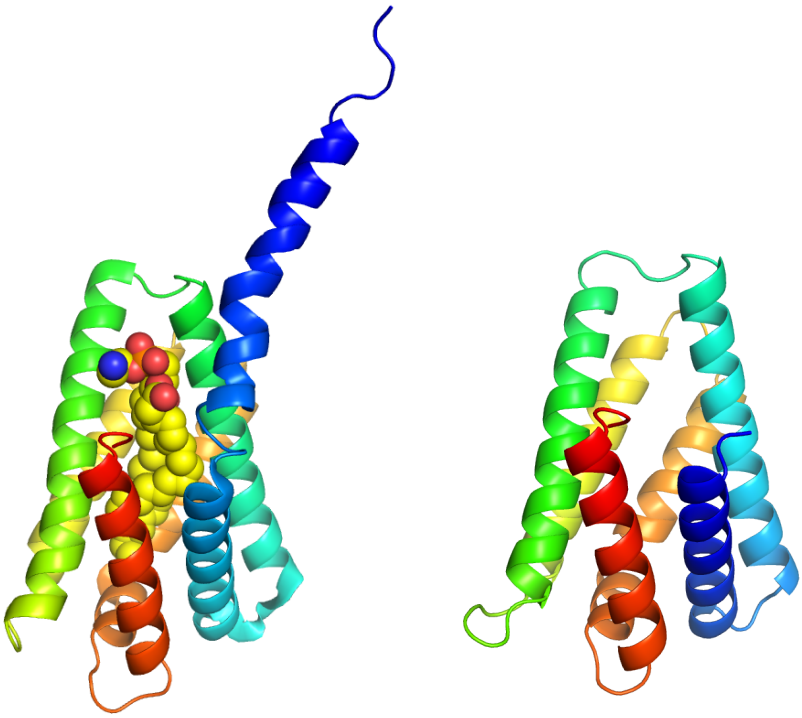

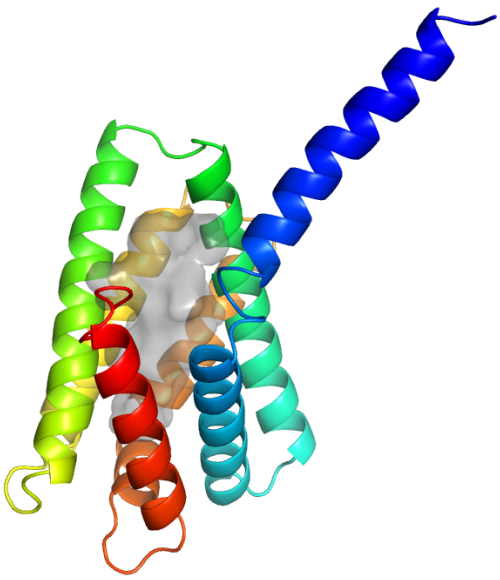

Fig. 5 Overall structures of TNFAIP8 family proteins.

Structures are depicted as cartoon models colored in rainbow from N terminus (blue) to C terminus (red). Lipid compound is shown as a ball model. Only TIPE3 shows the cavity surface colored in gray.

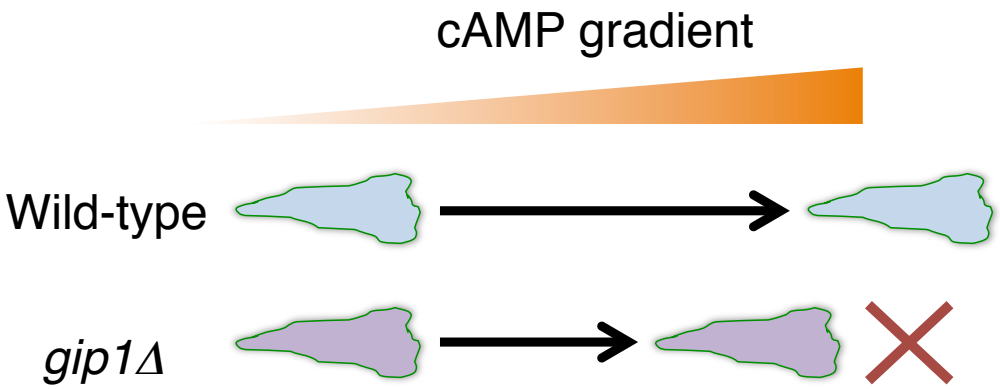

Fig. 6 Phenotypic behavior of *gip1Δ* cells on eukarotic chemotaxis.

Knockout of *gip1* gene impairs the chemotactic ability at the higher cAMP concentration. In other word, Gip1 is required for the extension of chemotactic dynamic range in *Dictyostelium* cells.

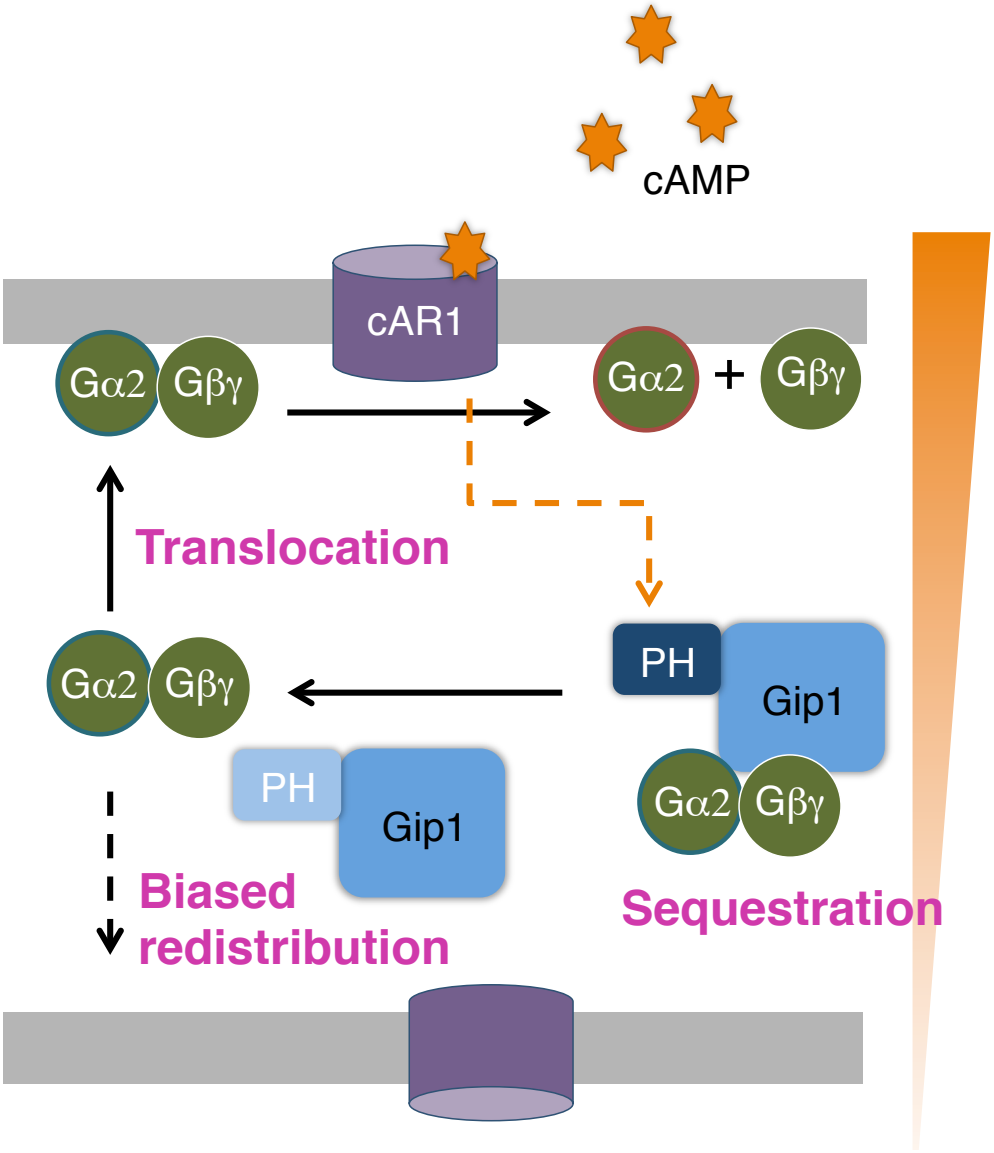

Fig. 7 Schematic model of molecular functions of Gip1 in a *Dictyostelium* cell.

Heterotrimeric G proteins (Gα2Gβγ) bind to Gip1 through Gβγ and stay in the cytosol in the resting state (Sequestration). Ligand-bound cAR1 transduces a signal to Gip1 via its PH domain, resulting in the dissociation of Gα2Gβγ from Gip1. Gα2Gβγ are translocated to the plasma membrane exposed by more cAMP (Translocation, Biased redistribution), and then stimulated by ligand-bound cAR1.

II. Materials and methods

Plasmid construction

For the crystallization, I constructed a plasmid vector pE-8HisSUMO-3C by modifying pE-SUMOstar (LifeSensors) with elongating the number of N-terminal poly-histidine from 6 to 8 and inserting a PreScission cleavable site immediately after the SUMO sequence. The DNA fragment encoding Gip1(146-310) was amplified by PCR and cloned into pE-8HisSUMO-3C vector by the In-Fusion technique (Clontech Laboratories).

For the biochemical and imaging experiments, I constructed plasmids by the In-Fusion technique (Clontech Laboratories). pTX-Flag-Flag-GFP (pTX-F_2G), pTX-F_2G-Gγ, pJK1-Gip1-GFP-Flag (pJK1-Gip1-GFPF), pJK1-Gα2-GFPF, pHK12-Gα2-Halo, and pHK12-Halo-Gγ were used in lab stocks. pTX-F_2G-Gγ(ΔCAAX) was created by cloning the DNA fragment encoding Gγ that lacked the last four amino acids (CSVL) and inserting into pTX-F_2G vector. pTX-F_2G-RasG(178-189) was created by cloning the DNA fragment encoding the last 12 amino acids of RasG (a.a. 178-189) including CTLL (CAAX box), and inserting into pTX-F_2G vector. pTX-F_2G-RasG, -Rac1A, and -Rap1 were also created as the same processes by amplifying DNA fragments encoding intact genes by PCR. pJK1-Gip1(ΔC-tail)-GFPF was created by cloning the DNA fragment encoding Gip1(a.a. 1-303) and inserting into pJK1-GFPF vector. pJK1-Gα2(G2A,C4G)-GFPF was created by using 5'-end forward primer including mutated codons to replace Gly2 to Ala and Cys4 to Gly. pJK1-Gip1(4A)-GFPF was created by replacing Lys181, Lys185, Lys189 and Arg260 to Ala. All used plasmids and primers are summarized in Table 1 and 2.

Overproduction and purification of Gip1(146-310)

Gip1(146-310) was overproduced in Rosetta (DE3) competent *Escherichia coli* cells (New England Biolabs Japan). The cells were transformed with pE-8HisSUMO-3C-Gip1(146-310) plasmid, cultivated at 37 °C until OD_{600} of 0.8-1.0, and harvested one day after induction of

0.1 mM isopropyl β-D-1-thiogalactopyranoside (IPTG) at 18 °C. Collected cells were rinsed with saline solution consisting of 0.9% NaCl and stored at -80 °C. Used cell strains are listed in Table 3.

The collected cells were resuspended with lysis buffer (20 mM HEPES-NaOH (pH 7.0) and 350 mM NaCl) containing 30 mM imidazole, 5 mM $MgCl_2$, and 10 μg/ml DNaseI and disrupted with a UD-201 ultrasonic disruptor (TOMY Seiko). Insoluble debris were removed from the supernatant containing Gip1(146-310) by centrifugation at 72,000 × *g* with a himac CP80WX centrifuge (HITACHI). Recombinant Gip1(146-310) was first purified by binding to nickel-chelating resin (Ni-NTA, Qiagen), washed with 60 times as much as the lysis buffer containing 40 mM imidazole, and eluted with the same amount of the lysis buffer containing 350 mM imidazole divided into 5 fractions. To cleave the N-terminal 8His-SUMO tag, the collected elution fractions were mixed with dithiothreitol (DTT) at a final concentration of 1 mM and Turbo3C protease (Novagen), and dialysed in the lysis buffer containing 0.5 mM DTT overnight at 4 °C. The protease reaction mixture was applied at least 10 times to the nickel-chelating resin substituted by the lysis buffer containing 1 mM DTT and 5 mM imidazole. The flow-through containing tag-free Gip1(146-310) was collected. Finally, Gip1(146-310) was subjected to size-exclusion chromatography with Superdex 75 10/300 GL (GE Healthcare) in 20 mM HEPES-NaOH (pH 7.5) and 150 mM NaCl. Purified Gip1(146-310) was concentrated to 6.1 mg/ml by ultrafiltration using Amicon Ultra with 3-kDa MWKO (Merck Millipore). Purified Gip1(146-310) was finally measured in the concentration by using a spectrophotometer NanoDrop 2000 (Thermo Fisher Scientific) before frozen with liquid nitrogen and stored at -80 °C.

Crystallization and X-ray diffraction data collection

Before every crystallization experiments, protein samples were subjected to centrifugation at 20,400 × *g* for at least 15 min at 4 °C to remove insoluble debris. I first checked the mono-

dispersity of purified Gip1(146-310) samples by dynamic light scattering using Zetasizer Nano (Malvern Panalytical). For the first crystallization screen step, I mixed the same volume of protein solution (Gip1(146-310) (6.1 mg/ml)) and reservoir solution by using a robot for crystallization, mosquito Crystal (TTP LabTech). Used screening kits were Index, SaltRx1, SaltRx2, PEGRx1, and PEGRx2 (Hampton Research). Crystals were grown by the sitting-drop vapor-diffusion method for few days at 4 or 20 °C. Conditions for crystallizing Gip1(146-310) at the first screening are listed in Table 4. Through the optimized crystallization screen, I obtained crystals by the hanging-drop vapor-diffusion method. The crystallization reagent was composed of 14-20% (v/v) PEG 20,000 and 100 mM Bicine (pH 8.0-9.0). Equal volumes of protein solution and reservoir solution were mixed and incubated at 20 °C. The obtained crystals were also soaked into the reagent containing 3 mM *N*-acetyl-*S*-geranylgeranyl-L-cysteine (Santa Cruz Biotechnology) and 0.025% DMSO. The aim of the soaking experiment was to obtain the crystals comprised of Gip1(146-310) whose ligand were exchanged to the geranylgeranyl-derivative, but the resulting structure was to found not to exchange the original ligand (Form II). The crystals were transferred into reservoir solution containing 30% PEG 400 as a cryoprotectant and flash-cooled with liquid nitrogen.

Diffraction data sets were collected at BL26B1 and B2 at SPring-8 (Harima, Japan) with a charge-coupled device detector MX225-HE (Raynonix). All X-ray experiments were conducted under a cryostream at 100 K. The diffraction data of native crystals were collected with X-ray wavelength of 1.0000 Å and 1.7000 Å for Form I and Form II, respectively. Diffraction data were processed and scaled with HKL2000 [Otwinowski & Minor, 1997] (HKL Research) for Form I and XDS [Kabsch, 2010] for Form II.

Structural determination and refinement

The initial structure for the refinement of Gip1(146-310) was determined by molecular re-

placement using a polyalanine model of a.a. 51-150 of TIPE2 (PDB 3F4M), which included four of the six α-helices, as a search model. Molecular replacement was conducted with Phaser [McCoy *et al.*, 2007]. The side chains were modelled by using Autobuild [Terwilliger *et al.*, 2008] implemented in Phenix [Adams *et al*., 2010]. The obtained model structure was modified manually with Coot [Emsley *et al.*, 2010] and refined with Refmac5 [Vagin *et al*., 2004] implemented in the CCP4 program suite [Winn *et al.*, 2011] and phenix.refine [Afonine *et al*. 2012] implemented in Phenix. The exogenous two ligands, phosphatidylethanolamine (PE) and phosphatidylglycerol (PG), were modelled by using restraint files of di-palmitoyl-3-sn-phosphatidylethanolamine (PEF) and 1,2-dipalmitoyl-phosphatidyl-glycerol (LHG) from the CCP4 ligand library. Since the glycerophospholipid moieties of both PEF and LHG were positioned at the same region, the head groups were modelled by the alternate conformers of PEF and LHG with the common glycerophospholipid moiety. All crystallographic data and refinement statistics are summarized in Table 5. The atomic coordinates and structural factors of two Gip1 structures have been deposited in Worldwide Protein Data Bank under accession codes of 5Z1N (for Form I) and 5Z39 (for Form II). All molecular graphics were produced with PyMOL (The PyMOL Molecular Graphics System, Version 1.8.3.2. Schrödinger, LLC.). The surface electron potential was calculated with the APBS tool [Jurrus *et al.*, 2018].

Calculation of the structural features

I searched for residues 4 Å from a glycerophospholipid by using CONTACT program and described the closest distance between each residues and the glycerophospholipid. I calculated B-factors of each residue by using Baverage program. Both programs were implemented in CCP4 program suite [Winn *et al.*, 2011]. The surface areas and volumes of cavities were calculated with CASTp 3.0 server [Dundas *et al.*, 2006]. By using CASTp 3.0, I also found residues of which cavities were composed.

Structural alignment

I performed three-dimensional alignment using SUPERPOSE program implemented in the CCP4 program suite to compare the structural similarity. The r.m.s. deviation of each Cα atom was calculated from the corresponding Cα atom of the template model structure [Krissinel & Hnrick, 2004].

Determination of lipid extract from Gip1(146-310)

To determine the accommodated lipid inside the cavity, I extracted the lipids from purified Gip1(146-310) sample that was used for crystallization with the method described by Bligh and Dyer [Bligh & Dyer, 1959]. In this method, I first added the protein solution or buffer only with the mixture of chloroform and methanol in a glass tube at the final concentration of chloroform:methanol:water = 1:2:0.8 (v/v/v). Here, protein or buffer solutions were considered as water. The mixture was vortexed and incubated at room temperature for 10 min. After incubation, I sequentially added both a forth volumes of chloroform and Milli-Q water, and centrifuged the tube after mixing. The bottom organic solvent was collected in another fresh glass tube, and remaining aqueous solvent was further mixed with chloroform, whose volume was a forth of the earlier mixture. The bottom organic solvent was collected after the mixing and centrifugation, and added with the initially collected organic solvent. After dry up of the organic solvent, extracted lipids were dissolved with a small volume of chloroform and spotted on the lower edge of a HPTLC Silica gel 60 plate (Merck Millipore) where a developing solvent (chloroform:methanol:water = 65:25:4 (v/v/v)) did not touch. The plate was placed in a chamber containing the developing solvent and incubated until the running front of the solvent reached the upper edge of the plate. After air-dry, the sulfuric acid-sprayed plate was baked until lipids became visible. L-α-phosphatidylethanolamine from egg yolk (Sigma Al-

drich) and L-α-phosphatidyl-DL-glycerol from egg yolk (Sigma Aldrich) were developed on the same plate as standards.

Sequence homology of Gip1 and TNFAIP8 family proteins

Amino acid sequences were obtained from National Center for Biotechnology Information (NCBI), human TNFAIP8 for CAG33418.1, human TIPE1 for Q8WVP5.2, human TIPE2 for Q6P589.1, and human TIPE3 (isoform I) for NP_997264.2. Sequence alignment was performed with CLUSTALW server (http://www.genome.jp/tools-bin/clustalw) [Larkin *et al.,* 2007]. Similar amino acids were visualized with BoxShade program (https://embnet.vital-it.ch/software/BOX_form.html).

Cell growth and differentiation

As the parental strain, wild-type *Dictyostelium discoideum* AX2 was used. AX2, *gip1Δ*, *gγΔ*, and *gβΔ* cells were axenically grown in HL5 medium (Formedium, Norfolk) or on an SM plate (Formedium) with a *Klebsiella aerogenes* lawn at 22 °C. For preparing chemotactically competent cells, exponentially growing cells were collected and developed in developmental buffer (DB) comprising of 5 mM Na/KPO_4 (pH 6.5), 2 mM $MgSO_4$, and 0.2 mM $CaCl_2$ at 2 × 10^7 cells/ml after 1 hour of starvation, followed by the addition of 60 nM cAMP every 6 min for 4 hours. Phenotypes of cells were identified by observing the development on the SM plate with the *K. aerogenes* lawn or on a non-nutrient DB agar (1.5% agar in DB). Used cell strains are summarized in Table 3.

Immunoblotting

Proteins were subjected to sodium dodecyl sulphate-polyacrylamide gel electrophoresis (SDS-PAGE) and blotted onto a polyvinylidene difluoride membrane. Blotted proteins were probed using appropriate antibodies. Signals were visualized by chemiluminescence using

Western HRP Substrate (Merck Millipore), and images were obtained with ImageQuant LAS (GE Healthcare). A monoclonal anti-M2 antibody (A8592, Sigma-Aldrich, 1:25,000) was used to detect the Flag epitope. An anti-Ras antibody (#3965, Cell Signaling Technologies, 1:1,000) was used to detect several Ras. Rabbit polyclonal anti-Gβ (a.a. 35-51, 1:5,000) and anti-Gip1 (a.a. 96-110, 1:1,000) antibodies were made in-house [Kamimura *et al.,* 2016]. Rabbit polyclonal anti-Gα2 antibody (1:5,000) was kindly given by Dr. Hidekazu Kuwayama (Tsukuba University).

Identification of lipid modifications by mass spectrometry

Protein samples were subjected to SDS-PAGE and stained with Coomassie Brilliant Blue. The gels containing separated protein bands were excised, and the constituent Gγ and Gα2 were digested with Glu-C endoproteinase and trypsin, respectively. Peptides were separated by high-performance liquid chromatography and identified by tandem mass spectrometry.

Tryptophan scanning mutagenesis of Gip1

I systematically identified the residues consisting the hydrophobic cavity of Form I structure using CASTp 3.0 server with a spherical probe of 1.5 Å [Dundas *et al.*, 2006]. Among the identified 40 residues in the Form I structure, I selected 24 residues (leucine, isoleucine, and valine) for tryptophan mutagenesis. Gip1 mutants were created by the following method. Both forward and reverse primers were designated and synthesized to include a codon for tryptophan substitution. I also prepared the universal 5'-end forward primer and 3'-end reverse primer of the *gip1* gene, and amplified one mutated *gip1* gene into two DNA fragments by using these four primers. The produced two DNA fragments were further merged by fusion PCR using the universal 5' and 3'-end primers of the *gip1* gene, and cloned into a *Dictyostelim* expression vector (pJK1-GFPF). The expression plasmid was introduced into the *gip1Δ* cells expressing Gα2-Halo or Halo-Gγ. Used plasmids, primers, and cell strains are

summarized in Table 1-3.

Cells were pre-washed and starved in DB for 2 hours at 21 °C and followed by staining with tetramethyl rhodamine (TMR) ligands against Halo-tag for 30 min in the dark at room temperature. Stained cells were washed with DB three times, treated with 5 μM latrunculin A (LatA) for 15 min, and then observed with a confocal fluorescence microscope (FLUOVIEW FV1000, OLYMPUS). The fluorescence intensities of TMR and GFP were calculated by ImageJ software [Abràmoff *et al*., 2004]. The ratio of the fluorescence intensity of TMR at the plasma membrane and in the cytosol was calculated as relative fluorescence intensity of TMR, and the ratio (relative fluorescence intensity of TMR) was plotted against the fluorescence intensity of Gip1-GFPF. I chose cells expressing Gip1-GFPF with a fluorescence intensity between 4,000-6,000, and calculated the their mean and SD of the relative fluorescence intensity of Gα2-TMR and TMR-Gγ.

Pull-down assay

Cells expressing GFP-Flag-tagged proteins were pre-washed with DB and starved in phosphate magnesium (PM) buffer (5 mM Na/KPO_4 and 2 mM $MgSO_4$, pH 6.5) at a density of 2 × 10^7 cells/ml for 2 hours at 21 °C. The cells were lysed on ice with 1× CHAPS buffer (40 mM HEPES (pH 7.5), 120 mM NaCl, 20 mM NaF, 2 mM Na_3VO_4, 20 mM sodium pyrophosphate, 0.3% CHAPS, and complete EDTA-free protease inhibitor (Roche)) at a density of 4 × 10^7 cells/ml followed by centrifugation at 20,400 × *g* for 15 min at 4 °C to remove insoluble debris. The supernatants were incubated with anti-Flag M2 beads (Sigma-Aldrich), which were rinsed with 5 mg/ml BSA in advance, at 4 °C for 1.5 hours. After the wash with 1× CHAPS buffer, the beads were boiled in 1× SDS sample buffer at 95 °C for 5 min for the preparation of protein samples.

Competitive assay

I used cells expressing Gip1(WT)-GFPF and prepared beads-bound Gip1-GFPF in complex with G proteins as described in the method section of pull-down assay. Gip1-bound anti-Flag M2 beads were washed with 1× CHAPS buffer and incubated with 1× CHAPS buffer at 4 °C for 1 hour in the presence of 0, 10, 20, 40, and 100 μM of geranylgeranyl pyrophosphate (Sigma-Aldrich), 100 μM of farnesyl pyrophosphate (Sigma-Aldrich), or 100 μM of myristic acid (nacalai tesque) with 3.5% methanol and 1.5 μM NH_3. After the wash by 1× CHAPS buffer, protein samples were prepared by boiling the beads in 1× SDS sample buffer at 95 °C for 5 min. The amount of Gip1-GFPF bound to M2 beads was quantified by immunoblotting using an anti-Flag antibody in comparison to carboxy-terminal DYKDDDK-BAP (BAP-Flag, Wako) as a standard.

Fractionation assay

gγΔ cells expressing F_2G alone, F_2G-Gγ(WT), or F_2G-Gγ(ΔCAAX) were starved in PM buffer for 2 hours at 21 °C as described in the method section of pull-down assay. Afterwards, the cells were resuspended in PM buffer at a density of 8×10^7 cells/ml, mixed with the same volume of a basal buffer (20 mM Tris-HCl (pH 8.0) and 2 mM $MgSO_4$), and fractionated by passing through Nuclepore Track-Etched Membranes with a pore size of 5.0 μm (Whatman). The resulting cell lysate was centrifuged at 20,400 × *g* for 1 min at 4 °C to separate the supernatant and precipitant. The supernatant and precipitant were equalized in volume with 2 × CHAPS buffer and 1 × CHAPS buffer, respectively, followed by centrifugation at 20,400 × *g* for 15 min at 4 °C to remove insoluble debris. Prepared samples were used for pull-down assay as described above.

In vitro-binding assay for Gγ activity

6His-SUMO-tagged Gip1(1-310) was overproduced in Rosetta (DE3) *E. coli* cells as described in the method section of overproduction of Gip1(146-310). Harvested cells were frac-

tionated and passed through the 0.45 μm filter to remove debris before the purification by nickel-affinity chromatography with 5 ml volume of HisTrap HP (GE Healthcare) and size-exclusion chromatography with Superdex 200 Increase 10/300 GL (GE Healthcare). Fractions containing Gip1 were collected and mixed with SUMOstar protease (LifeSensors) for the cleavage of 6His-SUMO-tag overnight at 4 °C. Cleaved tag was trapped by nickel-affinity chromatography, and the flow-through fractions containing tag-free Gip1 were subjected to size-exclusion chromatography using Superdex 200 Increase 10/300 GL in 10 mM Tris-HCl (pH 8.0), 500 mM NaCl. The final proteins samples were enriched to 10 mg/ml, frozen with liquid nitrogen, and stored at -80 °C.

Dictyostelium cells expressing F_2G only or F_2G-Gγ(WT or ΔCAAX) were starved in PM buffer at a density of 2×10^7 cells/ml for 2 hours at 21 °C and lysed with NP40 buffer comprising 40 mM HEPES (pH 7.5), 300 mM NaCl, 1% NP40 and complete EDTA-free protease inhibitor (Roche) at a density of 4×10^7 cells/ml. After the centrifugation to remove insoluble debris, the supernatants were incubated with anti-Flag M2 beads, which were rinsed with 5 mg/ml BSA in advance, at 4 °C for 1 hour, washed with NP40 buffer and then rinsed with 1× CHAPS buffer. Rinsed M2 beads were incubated with recombinant Gip1 and BSA in 1× CHAPS buffer for 30 min on ice. After the wash with 1× CHAPS buffer, the beads were boiled in 1× SDS sample buffer at 95 °C for 5 min for the preparation of protein samples.

In vitro-binding assay for Gip1 activity

The *gip1* gene fragments encoding a.a. 1-310 (WT) and a.a. 1-303 (ΔC-tail) were amplified by PCR and cloned into pE-8HisSUMO-3C plasmid. Both Gip1 variants were overproduced using Rosetta (DE3) *E. coli* cells. Proteins were overproduced and purified as the same method as previously described in the section of overproduction and purification of Gip1(146-310). After the tag-cleavage, the flow-through of nickel-chelating resin was enriched to appropriate concentration, frozen with liquid nitrogen, and stored at -80 °C. These

proteins were used in in vitro-binding assay as described above but the bead-bound proteins were F_2G-Gγ(WT) or the F_2G-CAAX motif of RasG.

Quantification of endogenous Gβ and Gip1

Endogenous Gβ and Gip1 in *Dictyostelium* cells were quantified using purified His-tagged Gβ and full-length Gip1 as standards. His-tagged Gβ was overproduced in Rosetta (DE3) *E. coli*. Cells were cultivated until OD_{600} of 0.8-1.0 at 37 °C and harvested 2 hours after 0.1 mM IPTG induction. Collected cells were resuspended in PBS buffer and disrupted by sonication on ice. After centrifugation at 20,400 × *g* for 30 min at 4 °C, the precipitant was collected and boiled in 1× SDS sample buffer for 5 min at 4 °C. As a negative control, I used a sample from the same *E. coli* cells harvested before IPTG induction, subjected to the same His-tagged Gβ purification steps. Recombinant Gip1 was prepared as described in the method section of in vitro-binding assay for Gγ activity. Protein concentrations were approximately estimated in comparison with the known concentrations of BSA stained on the same polyacrylamide gel with Coomassie Brilliant Blue.

The wild-type *Dictyostelium* cells were starved in PM buffer for 6 hours at 21 °C, and fractionated into the supernatant and the precipitant as described in the method section of fractionation assay. The amounts of endogenous Gβ and Gip1 were estimated by comparing the known concentration of purified His-Gβ and Gip1 as standards.

Alanine scanning mutagenesis of Gip1

Mutant Gip1 was created as described in the method section of tryptophan mutagenesis above. Used plasmids, primers, and cell strains are summarized in Table 1-3.

Cells were starved in DB for 6 hours at 21 °C and stained with TMR in the presence of 4 mM caffeine for 30 min in the dark at room temperature. Stained cells were washed with DB three times, treated with 5 μM LatA for 10 min, and observed with a confocal fluo-

rescence microscope (A1, Nikon). To evaluate the binding ability of alanine substituted Gip1 mutants, I introduced the plasma membrane / cytosol (PM/Cyto) index as described following. The ratio of the fluorescence intensity of TMR at the plasma membrane and in the cytosol was calculated as relative fluorescence intensity of Gα2-TMR, and was plotted against the fluorescence intensity of Gip1-GFPF. The plots were fitted by a hyperbolic curve ($y = A/x + C$). Here, constant C was fixed by using the same value obtained from the results of wild-type Gip1-GFPF. The binding activity of Gip1 mutants was approximately estimated by A, which was used as PM/Cyto index. The index value was divided by that of wild-type, and relative PM/Cyto index was utilized to evaluate the binding ability of Gip1 alanine mutants.

Cells were also stimulated with cAMP in the presence of 5 μM LatA and 4 mM caffeine. A series of images were obtained with 4-sec interval. For the calculation, images were averaged before (-16 to 0 sec; -cAMP) and after (24 to 40 sec; +cAMP) the cAMP stimulation. The ratio of the fluorescent intensity of cytosolic Gα2-TMR in both images (±cAMP) was calculated and plotted against the cAMP concentration.

Small population chemotactic assay

Before the assay, cells were starved in DB for 6 hours at 21 °C. Approximately 3,000 cells were suspended in a 1-μl DB droplet and placed on a 0.7% agar plate (010-08725, Wako). For the hydrophobic treatment, the agar powder was washed with Milli-Q water ten times before dissolved in Milli-Q water containing 4 mM caffeine [Kamimura *et al*., 2009]. A cell droplet was observed 60 min after the start point of the experiment when a DB droplet containing cAMP was placed 2.5 mm apart from the center of the cell droplet at room temperature. A droplet is considered positive if more than half of the total cells migrated toward the cAMP drop side. The percentages of positive droplets were measured and plotted against the cAMP concetration.

Micropipette chemotactic assay

Dictyostelium cells were developed for 6 hours in DB at 21 °C, and approximately 1×10^5 cells in total were placed on a 27-mm glass-bottom dish (Iwaki). cAMP gradients were generated by a Femtotip microcapillary (Eppendorf) containing 100 μM cAMP and ATTO 633 (AD 633-21, ATTO-TEC GmbH) under a constant 10 hPa pressure using a FemtoJet (Eppendorf). The experiments were performed for 120 min and a series of images were obtained with 10-sec intervals using a confocal microscope (A1, Nikon). Separately moving cells were tracked by using G-Count software (g-angstrom). Each trajectory was divided into short 1-min trajectories as the data unit for the following analyses. The chemotaxis index was the cosine of the angle formed by the intersection of the two lines: a line connecting the start and end points of movement, and another line connecting the start point and the tip of micropipette. Motility speed was the total travelled distance during the short trajectory. The analysed values were plotted against the distance from the end point of each short trajectory to the tip of the micropipette.

Table 1 Plasmid list used in this study.

Name	Plasmid backbone / Encoding protein	Source or references
For *Escherichia coli*		
pE-SUMOstar	pE-SUMOstar / -	LifeSensors
pE-6HisSUMO-Gip1(1-310)	pE-SUMOstar / 6His-SUMO-Gip1(1-310)	This study
pE-8HisSUMO-3C	pE-8HisSUMO-3C / -	This study
pE-8HisSUMO-3C-Gip1(146-310)	pE-8HisSUMO-3C / 8His-SUMO-Gip1(146-310)	This study
pE-8HisSUMO-3C-Gip1(1-310)	pE-8HisSUMO-3C / 8His-SUMO-Gip1(1-310)	This study
pE-8HisSUMO-3C-Gip1(ΔC-tail)	pE-8HisSUMO-3C / 8His-SUMO-Gip1(1-303)	This study
pETDuet-1	pETDuet-1 / -	Novagen
pETDuet-1-(6His-Gβ, Gγ)	pETDuet-1 / 6His-Gβ, Gγ	This study
For *Dictyostelium discoideum*		
pJK1	pJK1 / -	From Dr. Devreotes
pJK1-Gα2-GFPF	pJK1 / Gα2-GFPF	Kamimura *et al.*, 2016
pJK1-Gα2(G2A,C4G)-GFPF	pJK1 / Gα2(G2A,C4G)-GFPF	This study
pJK1-Gip1-GFPF	pJK1 / Gip1(1-310)-GFPF	Kamimura *et al.*, 2016
pJK1-Gip1(ΔC-tail)-GFPF	pJK1 / Gip1(1-303)-GFPF	This study
pJK1-Gip1(4A)-GFPF	pJK1 / Gip1(K181A,K185A,K189A,R260A)-GFPF	This study
pJK1-Gip1(I152W)-GFPF	pJK1 / Gip1(I152W)-GFPF	This study
pJK1-Gip1(L159W)-GFPF	pJK1 / Gip1(L159W)-GFPF	This study
pJK1-Gip1(I160W)-GFPF	pJK1 / Gip1(I160W)-GFPF	This study
pJK1- Gip1(V163W)-GFPF	pJK1 / Gip1(V163W)-GFPF	This study
pJK1-Gip1(I166W)-GFPF	pJK1 / Gip1(I166W)-GFPF	This study
pJK1-Gip1(I183W)-GFPF	pJK1 / Gip1(I183W)-GFPF	This study
pJK1-Gip1(I186W)-GFPF	pJK1 / Gip1(I186W)-GFPF	This study
pJK1-Gip1(L187W)-GFPF	pJK1 / Gip1(L187W)-GFPF	This study
pJK1-Gip1(V190W)-GFPF	pJK1 / Gip1(V190W)-GFPF	This study
pJK1-Gip1(L204W)-GFPF	pJK1 / Gip1(L204W)-GFPF	This study
pJK1-Gip1(V207W)-GFPF	pJK1 / Gip1(V207W)-GFPF	This study
pJK1-Gip1(L211W)-GFPF	pJK1 / Gip1(L211W)-GFPF	This study
pJK1-Gip1(L218W)-GFPF	pJK1 / Gip1(L218W)-GFPF	This study
pJK1-Gip1(L244W)-GFPF	pJK1 / Gip1(L244W)-GFPF	This study
pJK1-Gip1(L254W)-GFPF	pJK1 / Gip1(L254W)-GFPF	This study
pJK1-Gip1(L274W)-GFPF	pJK1 / Gip1(L274W)-GFPF	This study

pJK1-Gip1(V283W)-GFPF	pJK1 / Gip1(V283W)-GFPF	This study
pJK1-Gip1(L293W)-GFPF	pJK1 / Gip1(L293W)-GFPF	This study
pJK1-Gip1(L296W)-GFPF	pJK1 / Gip1(L296W)-GFPF	This study
pJK1-Gip1(I297W)-GFPF	pJK1 / Gip1(I297W)-GFPF	This study
pJK1-Gip1(L300W)-GFPF	pJK1 / Gip1(L300W)-GFPF	This study
pJK1-Gip1(I306W)-GFPF	pJK1 / Gip1(I306W)-GFPF	This study
pJK1-Gip1(L308W)-GFPF	pJK1 / Gip1(L308W)-GFPF	This study
pJK1-Gip1(I309W)-GFPF	pJK1 / Gip1(I309W)-GFPF	This study
pJK1-Gip1(Ala-mutant)-GFPF	pJK1 / Gip1(Alanine-mutant)-GFPF	This study
pTX	pTX / -	Levi *et al*., 2000
pTX-F2G	pTX / F2G	Kamimura *et al*., 2016
pTX-F2G-Gγ(WT)	pTX / F2G-Gγ(WT)	Kamimura *et al*., 2016
pTX-F2G-Gγ(ΔCAAX)	pTX / F2G-Gγ(ΔCAAX)	This study
pTX-F2G-RasG	pTX / F2G-RasG(1-189)	This study
pTX-F2G-RasG(178-189)	pTX / F2G-RasG(178-189)	This study
pTX-F2G-Rac1A	pTX / F2G-Rac1A	This study
pTX-F2G-Rap1	pTX / F2G-Rap1	This study
pHK12	pHK12 / -	From lab stock
pHK12-Gα2-Halo	pHK12 / Gα2-Halo	Kamimura *et al*., 2016
pHK12-Halo-Gγ	pHK12 / Halo-Gγ	Kamimura *et al*., 2016

Table 2 Primer list used in this study.

Name	Plasmid	Direc-rec-tion	Sequence (5' to 3')	Comments
TM54	pE-6HisSUMO-3C-Gip1(1-310)	F	GAACAGATTGGAGGTCTG-GAAGTTCTGTTCCAGGGGCCC	
YK621	pE-6HisSUMO-3C-Gip1(1-310)	R	ATTCGGATCCTCTAGTTAA-TAAATCAATTCAATTTGAGTATATTTG	
TM55	pE-8HisSUMO-3C-Gip1(1-310)	R	ACCCATGGTATATCTCCTTCTTAAAGT	
TM57	pE-8HisSUMO-3C-Gip1(1-310)	F	CACCACCATCACCATCATCATCAC-GGGTCCCTGCAGGACTCAGAA	
TM109	pE-8HisSUMO-3C-Gip1(146-310)	F	TTCCAGGGGCCCCTGAGTGGTTTAAA-GAAATTGATTCCA	
TM110	pE-8HisSUMO-3C-Gip1(146-310)	R	ACGGAGCTCGAATTCTTAA-TAAATCAATTCAATTTGAGTATATTTGTT	
TM211	pE-8HisSUMO-3C-Gip1(146-303)	R	ACGGAGCTCGAATTCTTA ATATTTGTTAA-GAGCACTAATTAATAAGAATA	
TM212	pE-8HisSUMO-3C-Gip1(ΔC-tail)	F	TTCCAGGGGCCCCTG ATGGAGGCAATTACAATTGAAA	
YK383	pTX-F2G-Gγ (ΔCAAX)	F	AGGTGGTGGAG-GATCCGAATCACAATTAAAAAAAG	
YK819	pTX-F2G-Gγ (ΔCAAX)	R	ATCGTCTAGACTCGAG-TTATCCATTTCCTTTGAGTGGTTTAGTCC	
YK899	pTX-F2G-RasG(178-189)	F	AGGTGGTGGAGGATCCAAGAAGAAGA-GACCATTAAAAGCTT-GTACTCTTTTATAACTCGAGTCTAGACGAT	
YK900	pTX-F2G-RasG(178-189)	R	ATCGTCTAGACTCGAGTTATAAAAGAG-TACAAGCTTTTAATGGTCTCTTCTTCTT-GGATCCTCCACCACCT	
YK374	pTX-F2G-RasG	F	CCAGATCTGGTGGTGGAGGTGGTGGAG-GATCCATGACAGAATACAAATTAGTTA	
YK361	pTX-F2G-RasG	R	TCTAGATTATAAAAGAGTACAA-GCTTTTAATGGTCTC	
YK491	pTX-F2G-Rac1A	F	AGGTGGTGGAGGATCCATGCAA-GCAATTAAATGTGTCGTTGTCGGTGATGG	
YK492	pTX-F2G-Rac1A	R	ATCGTCTAGACTCGAGTTATAAAATGTT-GCAACCACCTGAAC	
YK485	pTX-F2G-Rap1	F	AGGTGGTGGAGGATCCATGCCTCTTAGA-GAATTCAAAATCGTCG	
YK486	pTX-F2G-Rap1	R	ATCGTCTAGACTCGAGTTACAATAAA-GCACATTTTGATTTAGC	
YK459	pJK1-Gip1(ΔC-tail)-GFPF	F	AATAAAAATCAGATCAAA-TAAAAATGGAGGCAATTACAATT-GAAATTAATC	
YK927	pJK1-Gip1(ΔC-tail)-GFPF	R	CACCACCTCCCTCGAGATATTTGTTAA-GAGCACTAATTAATAAG	
YK874	pJK1-Gα2(G2A, C4G)-GFPF	F	AATAAAAATCAGATCAAATAAAAATGGC-TATTGGTGCATCATCAATGG	
YK411	pJK1-Gα2(G2A, C4G)-GFPF	R	TACCTCTAGCAGATCTTAAGAATATAAAC-CAGCTTTCATAAC	
TM147	pJK1-Gip1(4A)-GFPF	F	AATATCCTAGCAATTTTAATCGCAG-TGTTTTTCTAC	
TM146	pJK1-Gip1(4A)-GFPF	R	GATTAAAATTGCTAGGATATTT-GCCTCCATTTC	
YK347	pETDuet-1-(6His-Gβ, Gγ)	F	GGTGGATCCGTCATCAGA-TATTTCAGAAAAAATTC	
YK348	pETDuet-1-(6His-Gβ, Gγ)	R	GGTGTCGACTTAAGCCCAAATCTTGAGGA-GAG	
YJ349	pETDuet-1-(6His-Gβ, Gγ)	F	CAT-ATGTCCGAATCACAATTAAAAAAAGTTTTAAAAG	
YK351	pETDuet-1-(6His-Gβ, Gγ)	R	CTCGAGTTATCCATTTCCTTTGAG-TGGTTTATGCC	

Ala/Trp mutaegnesis				
Name	pJK1-Gip1-GFPF			
YK259 (Universal Gip1-F)		F	AATAAAAATCAGATCAAA-TAAAAATGGAGGCAATTACAATTGAAATTAAT	The 5'-end primer
YK460 (Universal Gip1-R)		R	CACCACCTCCCTCGAGA-TAAATCAATTCAATTTGAGTATATTTG	The 3'-end primer
Extension Gip1-R		R	CCAAATCATCCCAAACTTTAGTG	The 3' primer of the N termial fragment for E288A, I289A, E290A, D291A, D292A, L293A, F294A, L295A, L296A.
S146A-F	S146A	F	GTTGGTAAGGCTGGTTTAAAGAAATTG	
S146A-R	S146A	R	CAATTTCTTTAAACCAGCCTTACCAAC	
G147A-F	G147A	F	GTTGGTAAGAGTGCTTTAAAGAAATTG	
G147A-R	G147A	R	CAATTTCTTTAAAGCACTCTTACCAAC	
L148A-F	L148A	F	GTTGGTAAGAGTGGTGCAAAGAAATTG	
L148A-R	L148A	R	CAATTTCTTTGCACCACTCTTACCAAC	
K149A-F	K149A	F	GGTAAGAGTGGTTTAGCAAAATTGAT-TCCAGAAG	
K149A-R	K149A	R	CTTCTGGAATCAATTTTGCTAAACCAC-TCTTACC	
K150A-F	K150A	F	GGTAAGAGTGGTTTAAAGGCATTG	
K150A-R	K150A	R	CAATGCCTTTAAACCACTCTTACC	
L151A-F	L151A	F	GGTTTAAAGAAAGCAATTCCAGAAGAG	
L151A-R	L151A	R	CTCTTCTGGAATTGCTTTCTTTAAACC	
I152A-F	I152A	F	GGTTTAAAGAAATTGGCTCCAGAAGAG	
I152A-R	I152A	R	CTCTTCTGGAGCCAATTTCTTTAAACC	
P153A-F	P153A	F	GGTTTAAAGAAATTGATTGCAGAAGAG	
P153A-R	P153A	R	CTCTTCTGCAATCAATTTCTTTAAACC	
E154A-F	E154A	F	CCAGCAGAGGGTCGTGAATTG	
E154A-R	E154A	R	CAATTCACGACCCTCTGCTGG	
E155A-F	E155A	F	CCAGAAGCAGGTCGTGAATTG	
E155A-R	E155A	R	CAATTCACGACCTGCTTCTGG	
G156A-F	G156A	F	CCAGAAGAGGCTCGTGAATTG	
G156A-R	G156A	R	CAATTCACGAGCCTCTTCTGG	
R157A-F	R157A	F	CCAGAAGAGGGTGCTGAATTG	
R157A-R	R157A	R	CAATTCAGCACCCTCTTCTGG	
E158A-F	E158A	F	CCAGAAGAGGGTCGTGCATTG	
E158A-R	E158A	R	CAATGCACGACCCTCTTCTGG	

L159A-F	L159A	F	CGTGAAGCAATTGGATCAGTTAAAAAG	
L159A-R	L159A	R	CTTTTTAACTGATCCAATTGCTTCACG	
I160A-F	I160A	F	CGTGAATTGGCTGGATCAGTTAAAAAG	
I160A-R	I160A	R	CTTTTTAACTGATCCAGCCAATTCACG	
G161A-F	G161A	F	CGTGAATTGATTGCATCAGTTAAAAAG	
G161A-R	G161A	R	CTTTTTAACTGATGCAATCAATTCACG	
S162A-F	S162A	F	CGTGAATTGATTGGAGCAGTTAAAAAG	
S162A-R	S162A	R	CTTTTTAACTGCTCCAATCAATTCACG	
V163A-F	V163A	F	CGTGAATTGATTGGATCAGCTAAAAAG	
V163A-R	V163A	R	CTTTTTAGCTGATCCAATCAATTCACG	
K164A-F	K164A	F	CAGTTGCAAAGATCATTAAGAGAGTC	
K164A-R	K164A	R	GACTCTCTTAATGATCTTTGCAACTG	
K165A-F	K165A	F	CAGTTAAAGCAATCATTAAGAGAGTC	
K165A-R	K165A	R	GACTCTCTTAATGATTGCTTTAACTG	
I166A-F	I166A	F	CAGTTAAAAAGGCAATTAAGAGAGTC	
I166A-R	I166A	R	GACTCTCTTAATTGCCTTTTTAACTG	
I167A-F	I167A	F	CAGTTAAAAAGATCGCTAAGAGAGTC	
I167A-R	I167A	R	GACTCTCTTAGCGATCTTTTTAACTG	
K168A-F	K168A	F	CAGTTAAAAAGATCATTGCAAGAGTC	
K168A-R	K168A	R	GACTCTTGCAATGATCTTTTTAACTG	
R169A-F	R169A	F	CAGTTAAAAAGATCATTAAGGCAGTC	
R169A-R	R169A	R	GACTGCCTTAATGATCTTTTTAACTG	
V170A-F	V170A	F	CATTAAGAGAGCATCAAATGAAGAG	
V170A-R	V170A	R	CTCTTCATTTGATGCTCTCTTAATG	
S171A-F	S171A	F	CATTAAGAGAGTCGCAAATGAAGAG	
S171A-R	S171A	R	CTCTTCATTTGCGACTCTCTTAATG	
N172A-F	N172A	F	CATTAAGAGAGTCTCAGCTGAAGAG	
N172A-R	N172A	R	CTCTTCAGCTGAGACTCTCTTAATG	
E173A-F	E173A	F	GAGTCTCAAATGCAGAGAAAGC	
E173A-R	E173A	R	GCTTTCTCTGCATTTGAGACTC	
E174A-F	E174	F	GAGTCTCAAATGAAGCAAAAGC	
E174A-R	E174A	R	GCTTTTGCTTCATTTGAGACTC	
K175A-F	K175A	F	GAGTCTCAAATGAAGAGGCAGCAAATG	
K175A-R	K175A	R	CATTTGCTGCCTCTTCATTTGAGACTC	
N177A-F	N177A	F	GAGAAAGCAGCTGAAATGGAG	
N177A-R	N177A	R	CTCCATTTCAGCTGCTTTCTC	

E178A-F	E178A	F	GCAAATGCAATGGAGAAGAATATCC	
E178A-R	E178A	R	GGATATTCTTCTCCATTGCATTTGC	
M179A-F	M179A	F	GCAAATGAAGCAGAGAAGAATATCC	
M179A-R	M179A	R	GGATATTCTTCTCTGCTTCATTTGC	
E180A-F	E180A	F	GCAAATGAAATGGCAAAGAATATCC	
E180A-R	E180A	R	GGATATTCTTTGCCATTTCATTTGC	
K181A-F	K181A	F	GCAAATGAAATGGAGGCAAA-TATCCTAAAGATTTTAATC	
K181A-R	K181A	R	GATTAAAATCTTTAGGATATTT-GCCTCCATTTCATTTGC	
N182A-F	N182A	F	GGAGAAGGCTATCCTAAAGATTTTAATC	
N182A-R	N182A	R	GATTAAAATCTTTAGGATAGCCTTCTCC	
I183A-F	I183A	F	GGAGAAGAATGCACTAAAGATTTTAATC	
I183A-R	I183A	R	GATTAAAATCTTTAGTGCATTCTTCTCC	
L184A-F	L184A	F	GGAGAAGAATATCGCAAAGATTTTAATC	
L184A-R	L184A	R	GATTAAAATCTTTGCGATATTCTTCTCC	
K185A-F	K185A	F	GGAGAAGAATATCCTAG-CAATTTTAATCAAAGTG	
K185A-R	K185A	R	CACTTTGATTAAAATTGCTAGGA-TATTCTTCTCC	
I186A-F	I186A	F	GGAGAAGAATATCCTAAAGGCTTTAATC	
I186A-R	I186A	R	GATTAAAGCCTTTAGGATATTCTTCTCC	
L187A-F	L187A	F	CCTAAAGATTGCAATCAAAGTG	
L187A-R	L187A	R	CACTTTGATTGCAATCTTTAGG	
I188A-F	I188A	F	CCTAAAGATTTTAGCAAAAGTG	
I188A-R	I188A	R	CACTTTTGCTAAAATCTTTAGG	
K189A-F	K189A	F	CCTAAAGATTTTAATCGCAGTGTTTTTC-TACATTG	
K189A-R	K189A	R	CAATGTAGAAAAACACTGCGAT-TAAAATCTTTAGG	
V190A-F	V190A	F	GATTTTAATCAAAGCATTTTTCTAC	
V190A-R	V190A	R	GTAGAAAAATGCTTTGATTAAAATC	
F191A-F	F191A	F	GATTTTAATCAAAGTGGCTTTCTAC	
F191A-R	F191A	R	GTAGAAAGCCACTTTGATTAAAATC	
F192A-F	F192A	F	CAAAGTGTTTGCATACATTGATTC	
F192A-R	F192A	R	GAATCAATGTATGCAAACACTTTG	
Y193A-F	Y193A	F	CAAAGTGTTTTTCGCAATTGATTC	
Y193A-R	Y193A	R	GAATCAATTGCGAAAAACACTTTG	
I194A-F	I194A	F	CAAAGTGTTTTTCTACGCTGATTC	
I194A-R	I194A	R	GAATCAGCGTAGAAAAACACTTTG	
D195A-F	D195A	F	CTACATTGCTTCTAAAGCAATTC	
D195A-R	D195A	R	GAATTGCTTTAGAAGCAATGTAG	

S196A-F	S196A	F	CATTGATGCTAAAGCAATTC	
S196A-R	S196A	R	GAATTGCTTTAGCATCAATG	
K197A-F	K197A	F	CTACATTGATTCTGCAGCAATTC	
K197A-R	K197A	R	GAATTGCTGCAGAATCAATGTAG	
I199A-F	I199A	F	CTAAAGCAGCTCAAATTGGTG	
I199A-R	I199A	R	CACCAATTTGAGCTGCTTTAG	
Q200A-F	Q200A	F	CTAAAGCAATTGCAATTGGTG	
Q200A-R	Q200A	R	CACCAATTGCAATTGCTTTAG	
I201A-F	I201A	F	GCAATTCAAGCTGGTGATTTGGC	
I201A-R	I201A	R	GCCAAATCACCAGCTTGAATTGC	
G202A-F	G202A	F	GCAATTCAAATTGCTGATTTGGC	
G202A-R	G202A	R	GCCAAATCAGCAATTTGAATTGC	
D203A-F	D203A	F	GGTGCTTTGGCAAAGGTTG	
D203A-R	D203A	R	CAACCTTTGCCAAAGCACC	
L204A-F	L204A	F	GCAATTCAAATTGGTGATGCAGCAAAGG	
L204A-R	L204A	R	CCTTTGCTGCATCACCAATTTGAATTGC	
K206A-F	K206A	F	GGTGATTTGGCAGCAGTTGATAG	
K206A-R	K206A	R	CTATCAACTGCTGCCAAATCACC	
V207A-F	V207A	F	GATTTGGCAAAGGCTGATAGAGC	
V207A-R	V207A	R	GCTCTATCAGCCTTTGCCAAATC	
D208A-F	D208A	F	GGTTGCTAGAGCTTTACGTGACGG	
D208A-R	D208A	R	CCGTCACGTAAAGCTCTAGCAACC	
R209A-F	R209A	F	GGTTGATGCAGCTTTACGTGACGG	
R209A-R	R209A	R	CCGTCACGTAAAGCTGCATCAACC	
L211A-F	L211A	F	GGTTGATAGAGCTGCACGTGACGG	
L211A-R	L211A	R	CCGTCACGTGCAGCTCTATCAACC	
R212A-F	R212A	F	GGTTGATAGAGCTTTAGCTGACGG	
R212A-R	R212A	R	CCGTCAGCTAAAGCTCTATCAACC	
D213A-F	D213A	F	GATAGAGCTTTACGTGCAGGTTTC	
D213A-R	D213A	R	GAAACCTGCACGTAAAGCTCTATC	
G214A-F	G214A	F	GCTTTACGTGACGCTTTCAATCATTTAG	
G214A-R	G214A	R	CTAAATGATTGAAAGCGTCACGTAAAGC	
F215A-F	F215A	F	GCTTTACGTGACGGTGCAAATCATTTAG	
F215A-R	F215A	R	CTAAATGATTTGCACCGTCACGTAAAGC	
N216A-F	N216A	F	GCTTTACGTGACGGTTTCGCTCATTTAG	
N216A-R	N216A	R	CTAAATGAGCGAAACCGTCACGTAAAGC	

H217A-F	H217A	F	GACGGTTTCAATGCTTTAGATCGTGC	
H217A-R	H217A	R	GCACGATCTAAAGCATTGAAACCGTC	
L218A-F	L218A	F	GACGGTTTCAATCATGCAGATCGTGC	
L218A-R	L218A	R	GCACGATCTGCATGATTGAAACCGTC	
D219A-F	D219A	F	CATTTAGCTCGTGCTTTCAG	
D219A-R	D219A	R	CTGAAAGCACGAGCTAAATG	
R220A-F	R220A	F	CATTTAGATGCTGCTTTCAG	
R220A-R	R220A	R	CTGAAAGCAGCATCTAAATG	
F222A-F	F222A	F	GATCGTGCTGCAAGATACTATGG	
F222A-R	F222A	R	CCATAGTATCTTGCAGCACGATC	
R223A-F	R223A	F	CGTGCTTTCGCATACTATGG	
R223A-R	R223A	R	CCATAGTATGCGAAAGCACG	
Y224A-F	Y224A	F	GCTTTCAGAGCATATGGTGTAAAG	
Y224A-R	Y224A	R	CTTTACACCATATGCTCTGAAAGC	
Y225A-F	Y225A	F	GCTTTCAGATACGCTGGTGTAAAG	
Y225A-R	Y225A	R	CTTTACACCAGCGTATCTGAAAGC	
G226A-F	G226A	F	GCTTTCAGATACTATGCTGTAAAG	
G226A-R	G226A	R	CTTTACAGCATAGTATCTGAAAGC	
V227A-F	V227A	F	GATACTATGGTGCAAAGAAAGCCGC	
V227A-R	V227A	R	GCGGCTTTCTTTGCACCATAGTATC	
K228A-F	K228A	F	GGTGTAGCAAAAGCCGCTGATCTCG	
K228A-R	K228A	R	CGAGATCAGCGGCTTTTGCTACACC	
K229A-F	K229A	F	GGTGTAAAGGCAGCCGCTGATCTCG	
K229A-R	K229A	R	CGAGATCAGCGGCTGCCTTTACACC	
D232A-F	D232A	F	GGTGTAAAGAAAGCCGCTGCTCTCG	
D232A-R	D232A	R	CGAGAGCAGCGGCTTTCTTTACACC	
L233A-F	L233A	F	GCCGCTGATGCAGTTGTAATCTTGGAG	
L233A-R	L233A	R	CTCCAAGATTACAACTGCATCAGCGGC	
V234A-F	V234A	F	GCCGCTGATCTCGCTGTAATCTTGGAG	
V234A-R	V234A	R	CTCCAAGATTACAGCGAGATCAGCGGC	
V235A-F	V235A	F	GCCGCTGATCTCGTTGCAATCTTGGAG	
V235A-R	V235A	R	CTCCAAGATTGCAACGAGATCAGCGGC	
I236A-F	I236A	F	GCCGCTGATCTCGTTGTAGCATTGGAG	
I236A-R	I236A	R	CTCCAATGCTACAACGAGATCAGCGGC	
L237A-F	L237A	F	GCTGATCTCGTTGTAATCGCAGAGAAG	
L237A-R	L237A	R	CTTCTCTGCGATTACAACGAGATCAGC	

E238A-F	E238A	F	CTTGGCAAAGGCTTCTACTGCC	
E238A-R	E238A	R	GGCAGTAGAAGCCTTTGCCAAG	
K239A-F	K239A	F	CTTGGAGGCAGCTTCTACTGCC	
K239A-R	K239A	R	GGCAGTAGAAGCTGCCTCCAAG	
S241A-F	S241A	F	GAAGGCTGCTACTGCCTTGAAAGAAGC	
S241A-R	S241A	R	GCTTCTTTCAAGGCAGTAGCAGCCTTC	
T242A-F	T242A	F	GAAGGCTTCTGCTGCCTTGAAAGAAGC	
T242A-R	T242A	R	GCTTCTTTCAAGGCAGCAGAAGCCTTC	
L244A-F	L244A	F	GAAGGCTTCTACTGCCGCAAAAGAAGC	
L244A-R	L244A	R	GCTTCTTTTGCGGCAGTAGAAGCCTTC	
K245A-F	K245A	F	GCCTTGGCAGAAGCTGAACAAG	
K245A-R	K245A	R	CTTGTTCAGCTTCTGCCAAGGC	
E246A-F	E246A	F	GCCTTGAAAGCAGCTGAACAAG	
E246A-R	E246A	R	CTTGTTCAGCTGCTTTCAAGGC	
E248A-F	E248A	F	GCCTTGAAAGAAGCTGCACAAG	
E248A-R	E248A	R	CTTGTGCAGCTTCTTTCAAGGC	
Q249A-F	Q249A	F	GCTGAAGCAGAAACTGTAACC	
Q249A-R	Q249A	R	GGTTACAGTTTCTGCTTCAGC	
E250A-F	E250A	F	GCTGAACAAGCAACTGTAACC	
E250A-R	E250A	R	GGTTACAGTTGCTTGTTCAGC	
T251A-F	T251A	F	CAAGAAGCTGTAACCTTACTCACTCCTTTC	
T251A-R	T251A	R	GAAAGGAGTGAGTAAGGTTACAGCTTCTTG	
V252A-F	V252A	F	CAAGAAACTGCAACCTTACTCACTCCTTTC	
V252A-R	V252A	R	GAAAGGAGTGAGTAAGGTTGCAGTTTCTTG	
T253A-F	T253A	F	CAAGAAACTGTAGCATTACTCACTCCTTTC	
T253A-R	T253A	R	GAAAGGAGTGAGTAATGCTACAGTTTCTTG	
L254A-F	L254A	F	CAAGAAACTGTAACCGCACTCACTCCTTTC	
L254A-R	L254A	R	GAAAGGAGTGAGTGCGGTTACAGTTTCTTG	
L255A-F	L255A	F	CAAGAAACTGTAACCTTAGCAACTCCTTTC	
L255A-R	L255A	R	GAAAGGAGTTGCTAAGGTTACAGTTTCTTG	
T256A-F	T256A	F	CAAGAAACTGTAACCTTACTCGCTCCTTTC	
T256A-R	T256A	R	GAAAGGAGCGAGTAAGGTTACAGTTTCTTG	
P257A-F	P257A	F	CTCACTGCTTTCTTTAGACCAC	
P257A-R	P257A	R	GTGGTCTAAAGAAAGCAGTGAG	
F258A-F	F258A	F	CTCACTCCTGCATTTAGACCAC	
F258A-R	F258A	R	GTGGTCTAAATGCAGGAGTGAG	

F259A-F	F259A	F	CTCACTCCTTTCGCTAGACCAC	
F259A-R	F259A	R	GTGGTCTAGCGAAAGGAGTGAG	
R260A-F	R260A	F	CTCCTTTCTTTGCACCACAC	
R260A-R	R260A	R	GTGTGGTGCAAAGAAAGGAG	
P261A-F	P261A	F	CTTTAGAGCACACAATATTCAACTC	
P261A-R	P261A	R	GAGTTGAATATTGTGTGCTCTAAAG	
H262A-F	H262A	F	CTTTAGACCAGCAAATATTCAACTC	
H262A-R	H262A	R	GAGTTGAATATTTGCTGGTCTAAAG	
N263A-F	N263A	F	CTTTAGACCACACGCTATTCAACTC	
N263A-R	N263A	R	GAGTTGAATAGCGTGTGGTCTAAAG	
I264A-F	I264A	F	CTTTAGACCACACAATGCTCAACTC	
I264A-R	I264A	R	GAGTTGAGCATTGTGTGGTCTAAAG	
Q265A-F	Q265A	F	CACAATATTGCACTCATTCGTAATAC	
Q265A-R	Q265A	R	GTATTACGAATGAGTGCAATATTGTG	
L266A-F	L266A	F	CACAATATTCAAGCAATTCGTAATAC	
L266A-R	L266A	R	GTATTACGAATTGCTTGAATATTGTG	
I267A-F	I267A	F	CACAATATTCAACTCGCTCGTAATAC	
I267A-R	I267A	R	GTATTACGAGCGAGTTGAATATTGTG	
R268A-F	R268A	F	CTCATTGCTAATACTTTTGC	
R268A-R	R268A	R	GCAAAAGTATTAGCAATGAG	
N269A-F	N269A	F	CTCATTCGTGCTACTTTTGC	
N269A-R	N269A	R	GCAAAAGTAGCACGAATGAG	
T270A-F	T270A	F	CTCATTCGTAATGCTTTTGC	
T270A-R	T270A	R	GCAAAAGCATTACGAATGAG	
F271A-F	F271A	F	CGTAATACTGCTGCATTTTTGGG	
F271A-R	F271A	R	CCCAAAAATGCAGCAGTATTACG	
F273A-F	F273A	F	CGTAATACTTTTGCAGCTTTGGGTTC	
F273A-R	F273A	R	GAACCCAAAGCTGCAAAAGTATTACG	
L274A-F	L274A	F	CTTTTGCATTTGCAGGTTCTTTAGAC	
L274A-R	L274A	R	GTCTAAAGAACCTGCAAATGCAAAAG	
G275A-F	G275A	F	GCATTTTTGGCTTCTTTAGACTTTTTC	
G275A-R	G275A	R	GAAAAAGTCTAAAGAAGCCAAAAATGC	
S276A-F	S276A	F	GCATTTTTGGGTGCTTTAGACTTTTTC	
S276A-R	S276A	R	GAAAAAGTCTAAAGCACCCAAAAATGC	
L277A-F	L277A	F	GCATTTTTGGGTTCTGCAGACTTTTTCAC	
L277A-R	L277A	R	GTGAAAAAGTCTGCAGAACCCAAAAATGC	

D278A-F	D278A	F	GGTTCTTTAGCATTTTTCAC	
D278A-R	D278A	R	GTGAAAAATGCTAAAGAACC	
F279A-F	F279A	F	CTTTAGACGCTTTCACTAAAGTTTGG	
F279A-R	F279A	R	CCAAACTTTAGTGAAAGCGTCTAAAG	
F280A-F	F280A	F	CTTTAGACTTTGCAACTAAAGTTTGG	
F280A-R	F280A	R	CCAAACTTTAGTTGCAAAGTCTAAAG	
T281A-F	T281A	F	CTTTAGACTTTTTCGCTAAAGTTTGG	
T281A-R	T281A	R	CCAAACTTTAGCGAAAAAGTCTAAAG	
K282A-F	K282A	F	CACTGCAGTTTGGGATGATTTGG	
K282A-R	K282A	R	CCAAATCATCCCAAACTGCAGTG	
V283A-F	V283A	F	CTTTTTCACTAAAGCTTGGGATGATTTG	
V283A-R	V283A	R	CAAATCATCCCAAGCTTTAGTGAAAAAG	
W284A-F	W284A	F	CACTAAAGTTGCAGATGATTTGG	
W284A-R	W284A	R	CCAAATCATCTGCAACTTTAGTG	
D285A-F	D285A	F	CACTAAAGTTTGGGCTGATTTGG	
D285A-R	D285A	R	CCAAATCAGCCCAAACTTTAGTG	
D286A-F	D286A	F	CACTAAAGTTTGGGATGCTTTGG	
D286A-R	D286A	R	CCAAAGCATCCCAAACTTTAGTG	
L287A-F	L287A	F	GTTTGGGATGATGCAGAAATTGAAG	
L287A-R	L287A	R	CTTCAATTTCTGCATCATCCCAAAC	
E288A-F	E288A	F	CACTAAAGTTTGGGATGATTTGGCAATTG	
I289A-F	I289A	F	CACTAAAGTTTGGGATGATTTGGAA-GCTGAAGATGATTTATTC	
E290A-F	E290A	F	CACTAAAGTTTGGGATGATTTGGAAATT-GCAGATG	
D291A-F	D291A	F	CACTAAAGTTTGGGATGATTTGGAAATT-GAAGCTGATTTATTC	
D292A-F	D292A	F	CACTAAAGTTTGGGATGATTTGGAAATT-GAAGATGCTTTATTC	
L293A-F	L293A	F	CACTAAAGTTTGGGATGATTTGGAAATT-GAAGATGATGCATTCTTATTAATTAGTGC	
F294A-F	F294A	F	CACTAAAGTTTGGGATGATTTGGAAATT-GAAGATGATTTAGCTTTATTAATTAGTGC	
L295A-F	L295A	F	CACTAAAGTTTGGGATGATTTGGAAATT-GAAGATGATTTATTCGCATTAATTAGTGC	
L296A-F	L296A	F	CACTAAAGTTTGGGATGATTTGGAAATT-GAAGATGATTTATTCTTAGCAATTAGTGC	
I297A-R	I297A	R	CACCACCTCCCTCGAGA-TAAATCAATTCAATTTGAGTATATTT-GTTAAGAGCACTAGCTAATAAG	
S298A-R	S298A	R	CACCACCTCCCTCGAGA-TAAATCAATTCAATTTGAGTATATTT-GTTAAGAGCAGCAATTAATAAG	
L300A-R	L300A	R	CACCACCTCCCTCGAGA-TAAATCAATTCAATTTGAGTATATTT-GTTAGCAGCACTAATTAATAAG	
N301A-R	N301A	R	CACCACCTCCCTCGAGA-TAAATCAATTCAATTTGAGTATATTTAG-CAAGAGCACTAATTAATAAG	

K302A-R	K302A	R	CACCACCTCCCTCGAGA-TAAATCAATTCAATTTGAG-TATATGCGTTAAGAGCAC	
Y303A-R	Y303A	R	CACCACCTCCCTCGAGA-TAAATCAATTCAATTTGAGTAGCTTT-GTTAAGAGCAC	
T304A-R	T304A	R	CACCACCTCCCTCGAGA-TAAATCAATTCAATTTGAGCATATTT-GTTAAGAGCAC	
Q305A-R	Q305A	R	CACCACCTCCCTCGAGA-TAAATCAATTCAATTGCAGTATATTT-GTTAAGAGCAC	
I306A-R	I306A	R	CACCACCTCCCTCGAGA-TAAATCAATTCAGCTTGAGTATATTT-GTTAAGAGCAC	
E307A-R	E307A	R	CACCACCTCCCTCGAGA-TAAATCAATGCAATTTGAG	
L308A-R	L308A	R	CACCACCTCCCTCGAGATAAA-TAGCTTCAATTTGAGTATATTTG	
I309A-R	I309A	R	CACCACCTCCCTCGAGATAA-GCCAATTCAATTTGAGTATATTTG	
Y310A-R	Y310A	R	CACCACCTCCCTCGAGAG-CAATCAATTCAATTTGAGTATATTTG	
V163W-R	V163W	R	CTTTTTCCATGATCCAATCAATTCAC-GACCCTC	
V163W-F	V163W	F	GGATCATGGAAAAAGATCATTAAGAGAG-TCTCAA	
I183W-R	I183W	R	CTTTAGCCAATTCTTCTCCATTTCATTT-GCTTTC	
I183W-F	I183W	F	AAGAATTGGCTAAAGAT-TTTAATCAAAGTGTTTTTC	
L187W-R	L187W	R	TTGATCCAAATCTTTAGGA-TATTCTTCTCCATTTC	
L187W-F	L187W	F	AAAGATTTGGATCAAAGTGTTTTTC-TACATTGATTC	
L211W-R	L211W	R	GTCACGCCAAGCTCTATCAACCTTTGC	
L211W-F	L211W	F	AGAGCTTGGCGTGACGGTTTCAAT	
L296W-R	L296W	R	ACTAATCCATAAGAA-TAAATCATCTTCAATTTCCAAATCAT	
L296W-F	L296W	F	TTCTTATGGATTAGTGCTCTTAACAAA-TATACTC	
L300W-R	L300W	R	CACCACCTCCCTCGAGA-TAAATCAATTCAATTTGAGTATATTT-GTTCCAAGCACT	
I309W-R	I309W	R	CACCACCTCCCTCGAGATAC-CACAATTCAATTTGAGTATATTTGTT	
I152W-F	I152W	F	GGTTTAAAGAAATTGTGGCCAGAAGAG	
I152W-R	I152W	R	CTCTTCTGGCCACAATTTCTTTAAACC	
L159W-F	L159W	F	CGTGAATGGATTGGATCAGTTAAAAAG	
L159W-R	L159W	R	CTTTTTAACTGATCCAATCCATTCACG	
I160W-F	I160W	F	CGTGAATTGTGGGGATCAGTTAAAAAG	
I160W-R	I160W	R	CTTTTTAACTGATCCCCACAATTCACG	
I166W-F	I166W	F	CAGTTAAAAAGTGGATTAAGAGAGTC	
I166W-R	I166W	R	GACTCTCTTAATCCACTTTTTAACTG	
I186W-F	I186W	F	GGAGAAGAATATCCTAAAGTGGTTAATC	
I186W-R	I186W	R	GATTAACCACTTTAGGATATTCTTCTCC	

V190W-F	V190W	F	GATTTTAATCAAATGGTTTTTCTAC	
V190W-R	V190W	R	GTAGAAAAACCATTTGATTAAAATC	
L204W-F	L204W	F	GCAATTCAAATTGGTGATTGGGCAAAGG	
L204W-R	L204W	R	CCTTTGCCCAATCACCAATTTGAATTGC	
V207W-F	V207W	F	GATTTGGCAAAGTGGGATAGAGC	
V207W-R	V207W	R	GCTCTATCCCACTTTGCCAAATC	
L218W-F	L218W	F	GACGGTTTCAATCATTGGGATCGTGC	
L218W-R	L218W	R	GCACGATCCCAATGATTGAAACCGTC	
L244W-F	L244W	F	GAAGGCTTCTACTGCCTGGAAAGAAGC	
L244W-R	L244W	R	GCTTCTTTCCAGGCAGTAGAAGCCTTC	
L254W-F	L254W	F	CAAGAAACTGTAACCTGGCTCACTCCTTTC	
L254W-R	L254W	R	GAAAGGAGTGAGCCAGGTTACAGTTTCTTG	
L274W-F	L274W	F	CTTTTGCATTTTGGGGTTCTTTAGAC	
L274W-R	L274W	R	GTCTAAAGAACCCCAAAATGCAAAAG	
V283W-F	V283W	F	CTTTTTCACTAAATGGTGGGATGATTTG	
V283W-R	V283W	R	CAAATCATCCCACCATTTAGTGAAAAAG	
L293W-F	L293W	F	CACTAAAGTTTGGGATGATTTGGAAATT-GAAGATGATTGGTTCTTATTAATTAGTGC	
I297W-R	I297W	R	CACCACCTCCCTCGAGA-TAAATCAATTCAATTTGAGTATATTT-GTTAAGAGCACTCCATAATAAG	
I306W-R	I306W	R	CACCACCTCCCTCGAGA-TAAATCAATTCCCATTGAGTATATTT-GTTAAGAGCAC	
L308W-R	L308W	R	CACCACCTCCCTCGAGA-TAAATCCATTCAATTTGAGTATATTTG	
L293W-R	L293W	R	TCCAAATCATCCCAAACTTTAG-TGAAAAAGTCTAAAG	

Table 3 Cell strain list used in this study.

Strains	Plasmid	Source or references
Escherichia coli		
Rosetta(DE3)	-	Novagen
Rosetta(DE3)pLysS	-	Novagen
Rosetta(DE3)	pE- 6His-SUMO-Gip1(1-310)	This study
Rosetta(DE3)	pE-8HisSUMO-3C-Gip1(146-310)	This study
Rosetta(DE3)	pE-8HisSUMO-3C-Gip1(1-310)	This study
Rosetta(DE3)	pE-8HisSUMO-3C-Gip1(ΔC-tail)	This study
Rosetta(DE3)pLysS	pETDuet-1-(6His-Gβ, Gγ)	This study
Dictyostelium discoideum		
AX2	-	From lab stock
gβΔ	-	From lab stock
gγΔ	-	From lab stock
gip1Δ	-	Kamimura *et al.*, 2016
AX2	pTX-F2G	Kamimura *et al.*, 2016
AX2	pTX-F2G-Gγ(WT)	Kamimura *et al.*, 2016
AX2	pTX-F2G-Gγ(ΔCAAX)	This study
AX2	pJK1-Gα2-GFPF	Kamimura *et al.*, 2016
AX2	pJK1-Gα2(G2A,C4G)-GFPF	This study
AX2	pTX-F2G-RasG	This study
AX2	pTX-F2G-RasG(178-189)	This study
AX2	pTX-F2G-Rac1A	This study
AX2	pTX-F2G-Rap1	This study
AX2	pHK12-Gα2-Halo	Kamimura *et al.*, 2016
gβΔ	pHK12-Gα2-Halo	This study
gγΔ	pTX-F2G	This study
gγΔ	pTX-F2G-Gγ(WT)	This study
gγΔ	pTX-F2G-Gγ(ΔCAAX)	This study
gip1Δ	pJK1-Gip1-GFPF	Kamimura *et al.*, 2016
gip1Δ	pHK12-Gα2-Halo	Kamimura *et al.*, 2016
gip1Δ	pHK12-Halo-Gγ	Kamimura *et al.*, 2016
gip1Δ	pJK1, pHK12-Gα2-Halo	Kamimura *et al.*, 2016
gip1Δ	pJK1-Gip1(WT)-GFPF, pHK12-Gα2-Halo	Kamimura *et al.*, 2016
gip1Δ	pJK1-Gip1(4A)-GFPF, pHK12 / Gα2-Halo	This study
gip1Δ	pJK1-Gip1(I152W)-GFPF, pHK12-Gα2-Halo	This study
gip1Δ	pJK1-Gip1(L159W)-GFPF, pHK12-Gα2-Halo	This study
gip1Δ	pJK1-Gip1(I160W)-GFPF, pHK12-Gα2-Halo	This study
gip1Δ	pJK1-Gip1(V163W)-GFPF, pHK12-Gα2-Halo	This study

gip1Δ	pJK1-Gip1(I166W)-GFPF, pHK12-Gα2-Halo	This study
gip1Δ	pJK1-Gip1(I183W)-GFPF, pHK12-Gα2-Halo	This study
gip1Δ	pJK1-Gip1(I186W)-GFPF, pHK12-Gα2-Halo	This study
gip1Δ	pJK1-Gip1(L187W)-GFPF, pHK12-Gα2-Halo	This study
gip1Δ	pJK1-Gip1(V190W)-GFPF, pHK12-Gα2-Halo	This study
gip1Δ	pJK1-Gip1(L204W)-GFPF, pHK12-Gα2-Halo	This study
gip1Δ	pJK1-Gip1(V207W)-GFPF, pHK12-Gα2-Halo	This study
gip1Δ	pJK1-Gip1(L211W)-GFPF, pHK12-Gα2-Halo	This study
gip1Δ	pJK1-Gip1(L218W)-GFPF, pHK12-Gα2-Halo	This study
gip1Δ	pJK1-Gip1(L244W)-GFPF, pHK12-Gα2-Halo	This study
gip1Δ	pJK1-Gip1(L254W)-GFPF, pHK12-Gα2-Halo	This study
gip1Δ	pJK1-Gip1(L274W)-GFPF, pHK12-Gα2-Halo	This study
gip1Δ	pJK1-Gip1(V283W)-GFPF, pHK12-Gα2-Halo	This study
gip1Δ	pJK1-Gip1(L293W)-GFPF, pHK12-Gα2-Halo	This study
gip1Δ	pJK1-Gip1(L296W)-GFPF, pHK12-Gα2-Halo	This study
gip1Δ	pJK1-Gip1(I297W)-GFPF, pHK12-Gα2-Halo	This study
gip1Δ	pJK1-Gip1(L300W)-GFPF, pHK12-Gα2-Halo	This study
gip1Δ	pJK1-Gip1(I306W)-GFPF, pHK12-Gα2-Halo	This study
gip1Δ	pJK1-Gip1(L308W)-GFPF, pHK12-Gα2-Halo	This study
gip1Δ	pJK1-Gip1(I309W)-GFPF, pHK12-Gα2-Halo	This study
gip1Δ	pJK1-Gip1(ΔC-tail)-GFPF, pHK12-Gα2-Halo	This study
gip1Δ	pJK1-Gip1(Ala-mutant)-GFPF, pHK12-Gα2-Halo	This study
gip1Δ	pJK1, pHK12-Halo-Gγ	Kamimura *et al.*, 2016
gip1Δ	pJK1-Gip1(WT)-GFPF, pHK12-Halo-Gγ	Kamimura *et al.*, 2016
gip1Δ	pJK1-Gip1(I166W)-GFPF, pHK12-Halo-Gγ	This study
gip1Δ	pJK1-Gip1(V190W)-GFPF, pHK12-Halo-Gγ	This study
gip1Δ	pJK1-Gip1(L211W)-GFPF, pHK12-Halo-Gγ	This study
gip1Δ	pJK1-Gip1(L300W)-GFPF, pHK12-Halo-Gγ	This study
gip1Δ	pJK1-Gip1(I306W)-GFPF, pHK12-Halo-Gγ	This study
gip1Δ	pJK1-Gip1(D208A)-GFPF, pHK12-Halo-Gγ	This study
gip1Δ	pJK1-Gip1(ΔC-tail)-GFPF, pHK12-Gα2-Halo	This study

III. Results

III-1. Structural determination of the G protein binding region of Gip1

Gip1 is a newly identified binding partner of heterotrimeric G proteins. Gip1 has three molecular functions to extend chemotactic dynamic range: sequestration of G proteins in the cytosol, regulation of G protein shuttling in the cAMP dependent manner, and biased redistribution of G proteins to the plasma membrane along the cAMP gradient. Among these functions, cytosolic sequestration of G proteins requires C terminal region of Gip1. The region is also essential for interacting with G proteins, specifically with Gβγ subunit. To reveal how Gip1 sequesters G proteins in the cytosol, I first determined the crystal structure of Gip1 by X-ray crystallography.

III-1-1 Purification and crystallization of Gip1(146-310)

To determine the crystal structure of Gip1, I first designed the Gip1 construct suitable for crystallization using GlobPlot 2.3 server (http://globplot.embl.de/) [Linding *et al.,* 2003]. GlobPlot revealed that Gip1 has three potential disordered regions: two at the N-terminal PH domain and one at C-terminal DUF758 domain, respectively (Fig. 8). Because disordered regions were unsuitable for crystallization, I decided to remove the potential disordered regions and constructed the His-SUMO-tagged Gip1 construct (a.a. 146-310; Gip1(146-310)) (Fig. 9a). Gip1(146-310) was overproduced with the bacterial expression system and purified through nickel-affinity purification and size exclusion chromatography steps (Fig. 9b). Corresponding to the result of SDS-PAGE, the chamoratogram of final size-exclusion chromatography showed the single peak, indicating that almost all contaminants were removed through the purification steps (Fig. 9c). Compared to a full-length Gip1 construct, the C-terminal Gip1 construct showed less contaminants after first nickel-affinity purification (Fig. 9d). Furthermore, the purified Gip1(146-310) sample showed monodispersity with dynamic light scattering (Fig. 10), suggesting that almost all Gip1 molecules were uniform in

size. These results supported that Gip1(146-310) was suitable for crystallization.

At the first crystal screening step, tiny crystals were formed in one day at 20 °C in some conditions (Table 4). Since tiny crystals were illuminated on the UV light and revealed to be plausible protein crystals (Fig. 11a), the conditions were further optimized to grow large crystals. At the optimized conditions, some crystals appeared in about three days at 20 °C and got larger in over one week (Fig. 11b).

Through the refinement process for building a structural model, I found that there were unexpected electron densities inside the cavity (Fig. 12a,b). The shape of electron densities was tetrahedron followed by two long tails. I suspected that the electron densities were derived from phospholipids from host *E. coli* cells used for overexpressing proteins. Previous reports say that the composition of bacterial membrane was mainly occupied by 70% of PE and 20% of PG [Ames, 1968]. Furthermore, extracted lipids from Gip1(146-310) sample used for crystallization were revealed to be mixture of PE and PG by thin layer chromatography (Fig. 12c). Taken together, I decided that the unexpected electron densities were mixture of PE and PG. I then put lipid derivatives as model structures, finished a structural model refinement, and consequently determined the Gip1(146-310) structure. Through the study, I obtained two forms of Gip1 structures, and named Form I (PDB 5Z1N) and Form II (PDB 5Z39) (Table 5).

III-1-2 Overall structures of two forms of Gip1

Both structures of Gip1(146-310) were composed of seven α-helices and designated as α0 to α6 from N terminus (Fig. 13). Among them, six α-helices from α1 to α6 formed a cylinder-like structure with a central cavity as a structural hallmark. The cavity was mainly comprised of hydrophobic amino acids (Table 6) and accommodated a bacterial phospholipid (Fig. 14). Contrary to the hydrophobicity inside the cavity, the surface of water-exposed side was relatively charged (described in detail in the section III-1-3) (Fig. 15). The overall struc-

tures between Form I and Form II were very similar, while r.m.s. deviations were relatively high at loop regions between helices (Fig. 16a). The r.m.s. deviations of each residue between two forms of Gip1 were relatively similar to B-factor of each residue (Fig. 16b). Large differences in r.m.s. deviations were observed around α1 and α6 helices. α6 helix was partially uncoiled near its N terminus in Form I resulting from the insertion of water molecules, while the helix made coordination bonds with a sodium ion in Form II (Fig. 16c). The other differences were observed in α1 and C terminus of α6. These regions were located around the rim of the entrance of the cavity in the Gip1 structure (Fig. 17a). Here, both α1 and α6 displayed rotational movements (Fig. 17b). In addition, a hydrogen bonding network between C-terminal tail region and α3 was rearranged (Fig. 17c). These structural differences between two forms of Gip1 affected to many aspects: the direction of the side chain of Glu307 (Fig. 18a), the shape and the size of the cavity (Fig. 18b,c), and the position of the phospholipid inside the cavity (Fig. 18d). Superposed with asymmetric Form II molecules, Form I molecule did not crash with asymmetric Form II molecule except for Gln305 (Fig. 18e).

III-1-3 Structural comparison of Gip1 with TNFAIP8 family proteins

C-terminal region of Gip1, whose structure was determined in this study, showed weak sequence homology with TNFAIP8 family proteins in mammal (Fig. 19) [Kamimura *et al.*, 2016]. Because of such a weak homology, Gip1 did not completely share some important residues reported in previous studies [Fayngerts *et al.,* 2014; Kim *et al.,* 2017]. TNFAIP8 family proteins include TNFAIP8, TIPE1, TIPE2 and TIPE3, and structures of TNFAIP8, TIPE2 and TIPE3 have already been solved in mouse (TNFAIP8) and human (TIPE2 and TIPE3) [Zhang *et al.,* 2009; Fayngerts *et al.,* 2014; Kim *et al.,* 2017]. They are sylinder-like structures composed of six α-helices and have a central hydrophobic cavity. Despite the weak homology in primary sequence, the overall structures of TNFAIP8 family were similar to that of Gip1 with r.m.s. deviations at 2.0, 2.7 and 2.1 Å for 88 amino acids (a.a. 173-196, 205-221,

236-256, 261-286 from Gip1 Form I), respectively. Gip1 had a positively charged patch between α2- and α5-helices. Focused on TIPE3 as a representative of TNFAIP8 family proteins, the similar charged area was also observed (Fig. 20a). Interestingly, the charged area was comprised of conserved lysines (Fig. 20b). Substitution of these charged residues to alanine (Gip1(K181A,K185A,K189A,R260A) or Gip1(4A)) severely impaired the interaction between Gip1 and G proteins (Fig. 20c). In addition, Gip1 was negatively charged around the cavity entrance and region between α1- and α6-helices. TIPE3 also showed the similar structural feature, although the charge was weaker than Gip1. On the other hand, there are some structural differences between Gip1 and TNFAIP8 family. Regarding to the electrostatic surface potential, Gip1 showed a positively charged area between α3- and α4-helices, although TIPE3 did not (Fig. 20d). This charge was attributed to His217, Arg220, and Lys239. Remarkably, Gip1 extended its α0 and C-terminal tail to different directions from those of TIPE3. α0-helix bent at a sharp angle from α1. This was caused by the hydrogen bonds connecting α0 and α1 helices in Gip1, but not in TIPE3 (Fig. 20d). The C-terminal tail region elongated to the outside from the cavity in Gip1, while the tail region directed to the cavity in TIPE3 (Fig. 20d). Although physiological and molecular functions of TNFAIP8 family proteins remain controversial, these structural features should reflect the common or distinct functions of Gip1 and TNFAIP8 family proteins.

III-1-4 Structural comparison of Gip1 with solubilization factors

From a structural viewpoint, solubilization factors are roughly categorized into two groups: immunoglobulin-like fold proteins and REP-like fold proteins. Both folds form a hydrophobic cavity or pocket for conveying lipid-modified cargo proteins (e.g. Rho, Ras, Rab). Although their molecular functions, carrying lipid-modified proteins, were similar to that of Gip1, their structural features were totally different. Compared with solubilization factors, Gip1 had the larger cavity (Table 7). Gip1 changed its cavity approximately 26% between

two forms. On the other hand, PDEδ reduced its cavity about 90% by interacting with-Arl2-GTP.

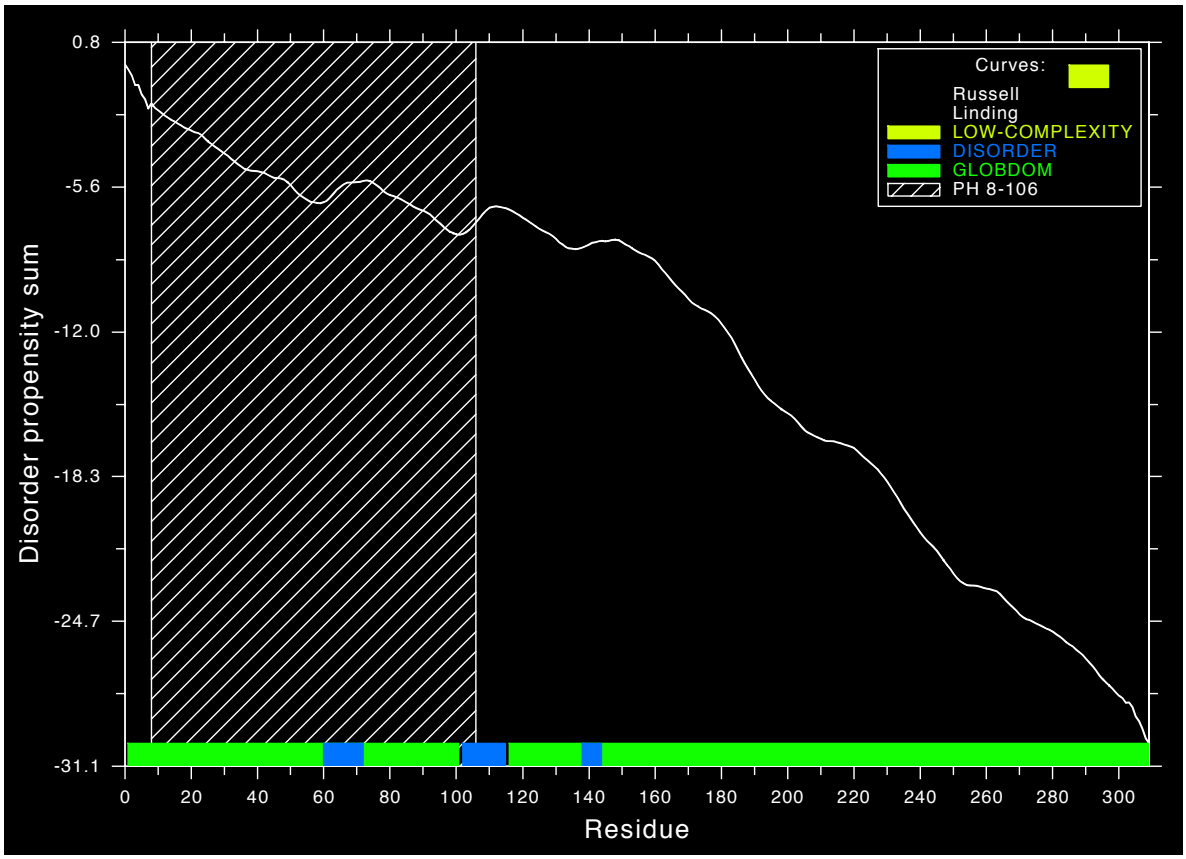

Fig. 8 Prediction of intrinsic disordered regions.

Structural prediction for the construct design suitable for crystallization. GlobPlot server predicted the disordered region from the primary sequence of Gip1. Disordered and globular regions are shown in blue and green, respectively. Slash lined area indicates PH domain.

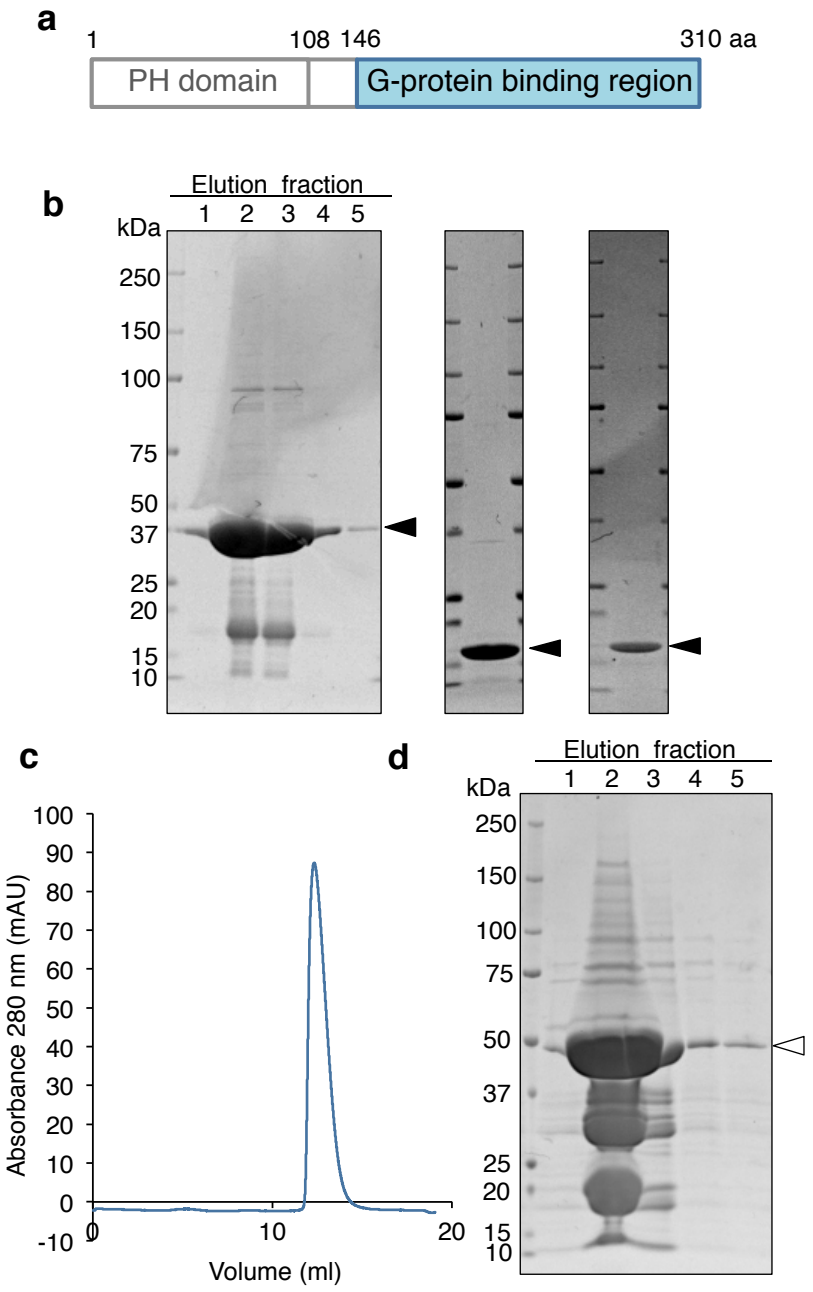

Fig. 9 Purification profiles of Gip1(146-310).

(a) Schematic view of C-terminal Gip1 for crystallization. Used region is colored in blue. **(b)** Purification process of Gip1(146-310). Gip1(146-310) was subjected to nickel-affinity purification (left), second nickel-affinity purification after His-SUMO-tag cleavage (middle), and size-exclusion chromatography (right). Second and third elution fractions were collected at the first nickel-affinity purification step. Gip1 is shown by black arrow heads. **(c)** Chromatogram of Gip1(146-310) in size-exclusion chromatography. **(d)** Nickel-affinity purification of full-length Gip1. Gip1 included disordered regions were purified with the same purification method shown in Fig. 9b. Gip1 is shown by a white arrow head.

Temperature (℃):	20.0	**Meas Date & Time:**	2016年8月24日 13:50:12
Derived Count Rate (kcps...	263.8	**Solvent:**	Water
Intercept:	0.874	**Measurement quality:**	Good

Hydrodynamic Radius

Z-Average (± SD) (d.nm): 9.085 ± 3.906

Polydispersity Index: 0.185

Estimated MW (± SD) (KDa): 116 ± 49.9

%Polydispersity: 43.0

Sample Polydispersity: Polydisperse

Distribution Results

	Mean ± SD (nm)	%Pd	Est. MW (KDa) (Mean ± SD)*	% Intensity	% Mass	Peak Polydispersity
Peak 1	8.604 1.237	14.4	102.3 ± 14.7	100.0	100.0	Monodisperse
Peak 2	0.000 ± 0.000	0	0.0 ± 0.0	0.0	0.0	
Peak 3:	0.000 ± 0.000	0	0.0 ± 0.0	0.0	0.0	

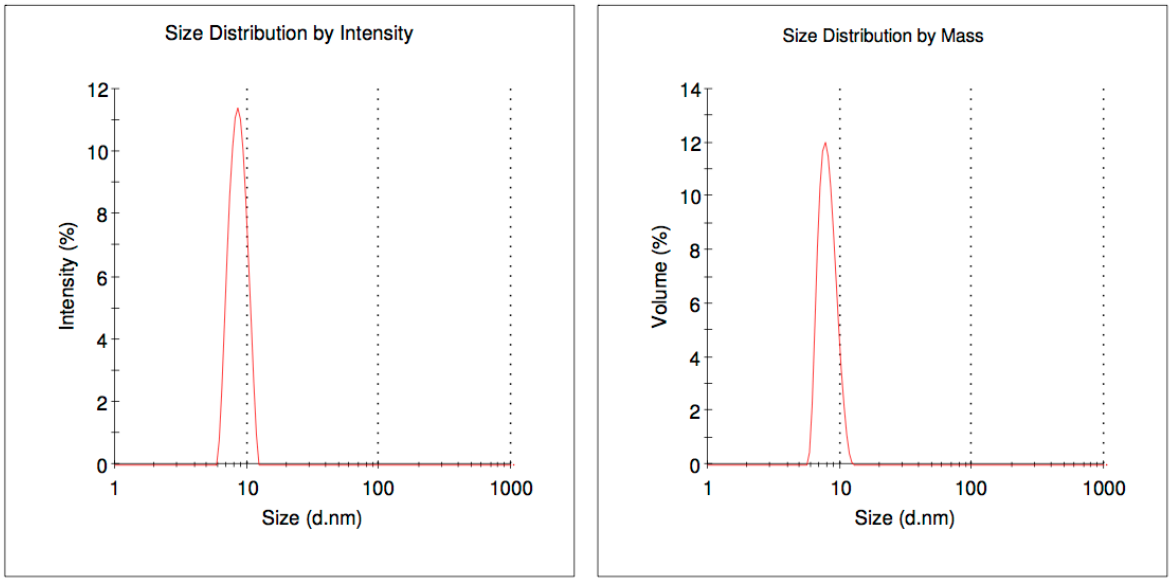

Fig. 10 Result of dynamic light scattering.

Purified Gip1(146-310) shows monodispersity with a single peak in both graphs of size distribution by intensity and mass.

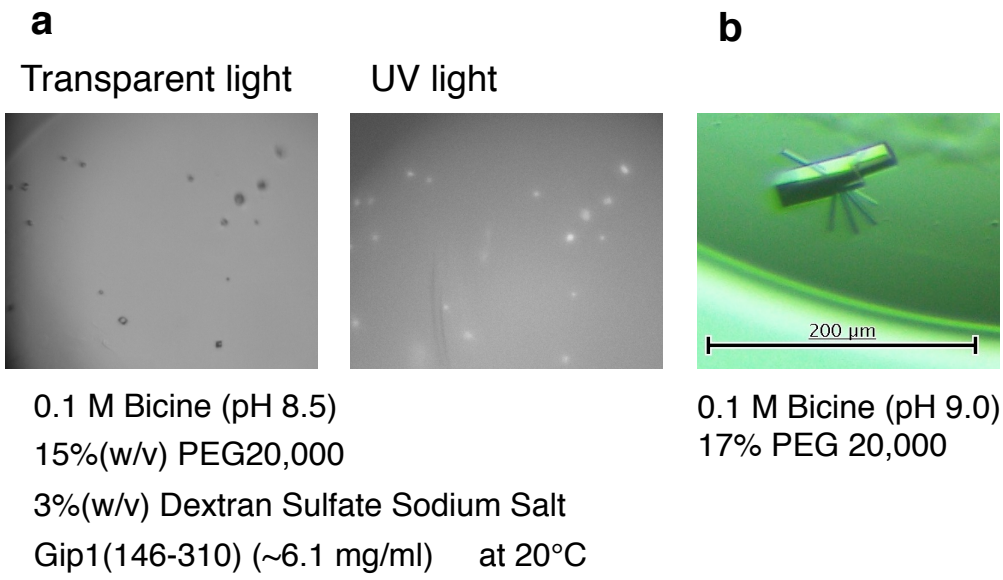

Fig. 11 Crystal formation and simplified authentication.

(a) Tiny crystal formations at the first crystal screening. Crystals are bright on the illumination of ultraviolet light. **(b)** Grown crystal in the optimized condition.

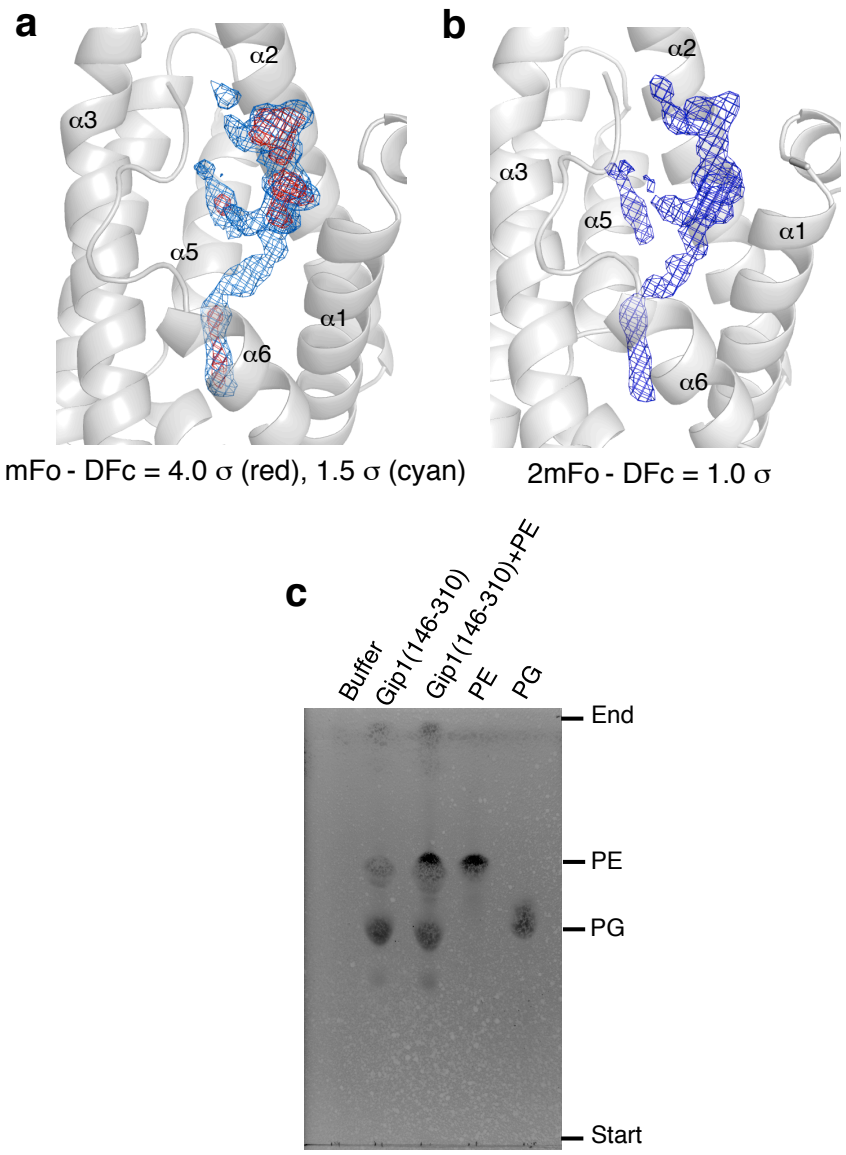

Fig. 12 Electron density in the hydrophobic cavity.

(a) The structure of Gip1(146-310) with a possible glycerophospholipid. The mFo-DFc omit electron density map is contoured at 4.0 σ (red mesh) and 1.5 σ (cyan mesh). **(b)** The model structure of PE and PG with Gip1(146-310). The 2mFo-DFc electron density map of the phospholipid is contoured at 1.0 σ (blue mesh). **(c)** Determination of phospholipids in Gip1(146-310) by thin layer chromatography. Lipid extracts from buffer, Gip1(146-310) samples, PE and PG were separated and visualized on a silica plate. Two major spots on the Gip1(146-310) lane were determined to be PE (upper) and PG (bottom) based on comparison with standards.

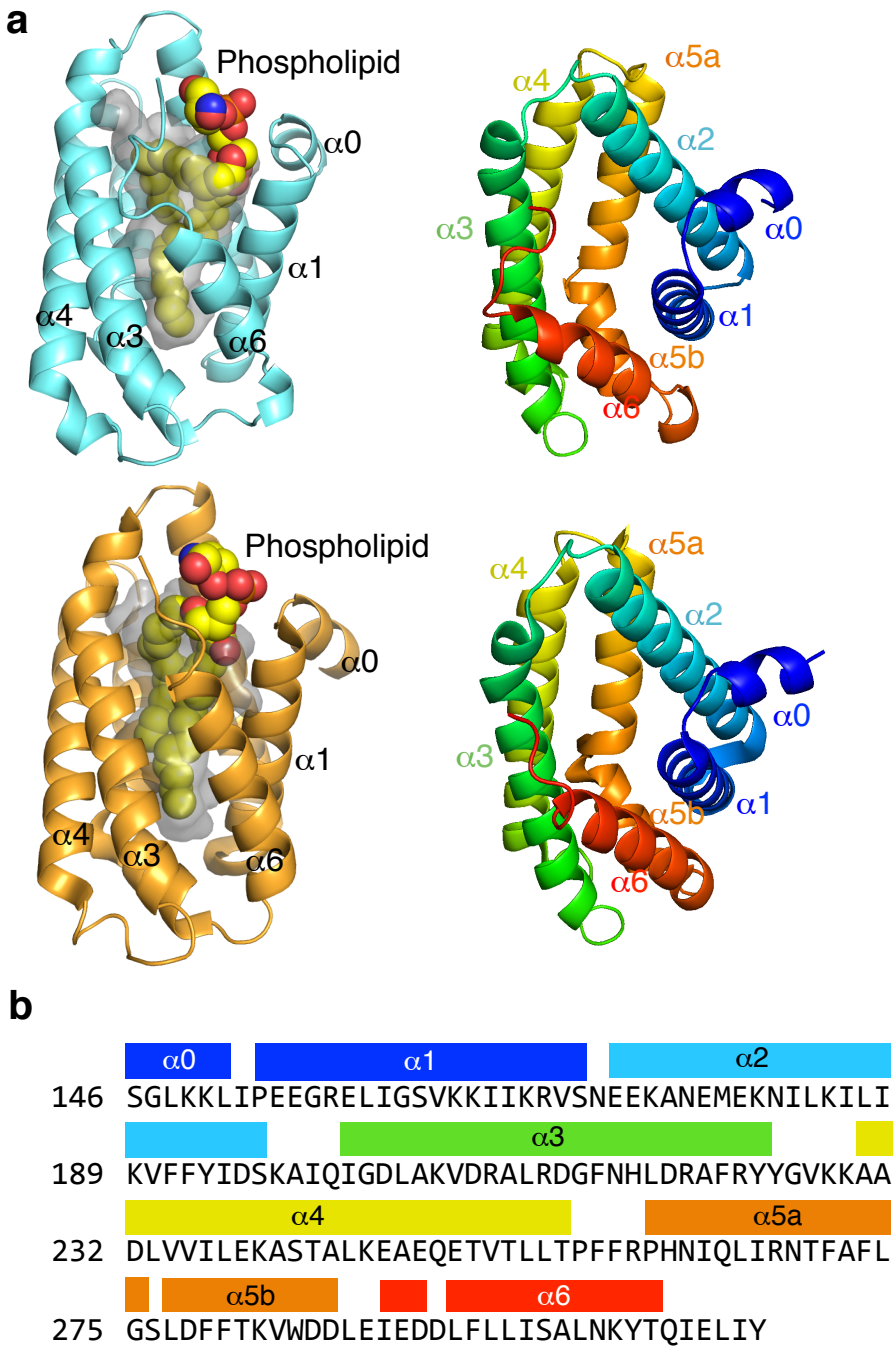

Fig. 13 Crystal structures of the G protein binding region of Gip1.

(a) Overall structure of Gip1(146-310) and a phospholipid represented by a cartoon and ball model. The surface of the cavity is shown in gray. Form I is in cyan (top) and Form II is in orange (bottom). Secondary structure of Gip1(146-310) is indicated in rainbow (right). **(b)** Secondary structure assignment of the sequence of Gip1(146-310). The color corresponds to the color of Form I shown in Fig. 13a.

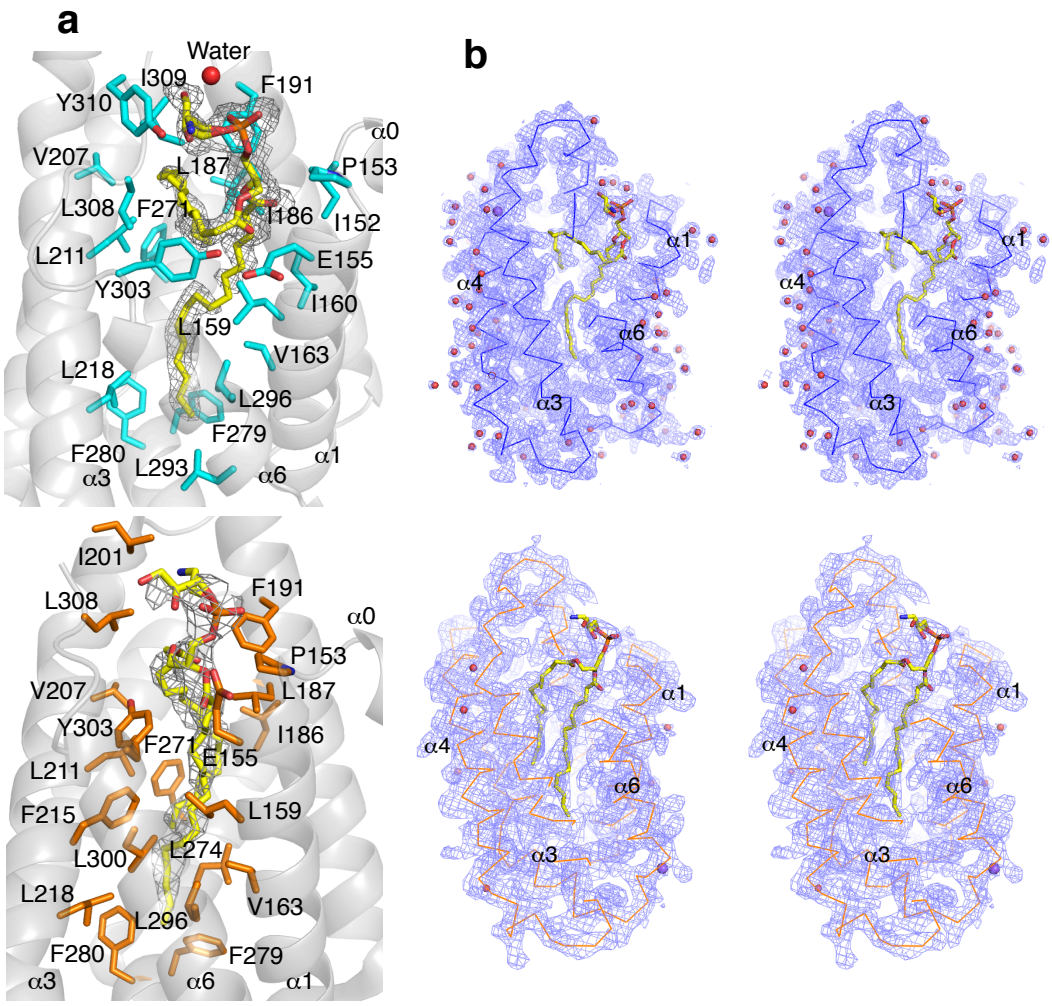

Fig. 14 Structural features around a phospholipid.

(a) Residues and water within van der Waals distance from the phospholipid. The phospholipid is shown with the 2mFo-DFc electron density map contoured at 1.0 σ. Residues within 4 Å from the lipid are shown as sticks (Form in cyan (top); Form II in orange (bottom)). Water molecule is shown as a red ball. **(b)** Stereo views of Gip1(146-319). Overall structures were shown by a ribbon and stick model with the 2mFo-DFc electron density map contoured at 1.0 σ. Water molecules and a sodium ion are shown as red and purple balls, respectively. Form I was in upper and Form II was in bottom.

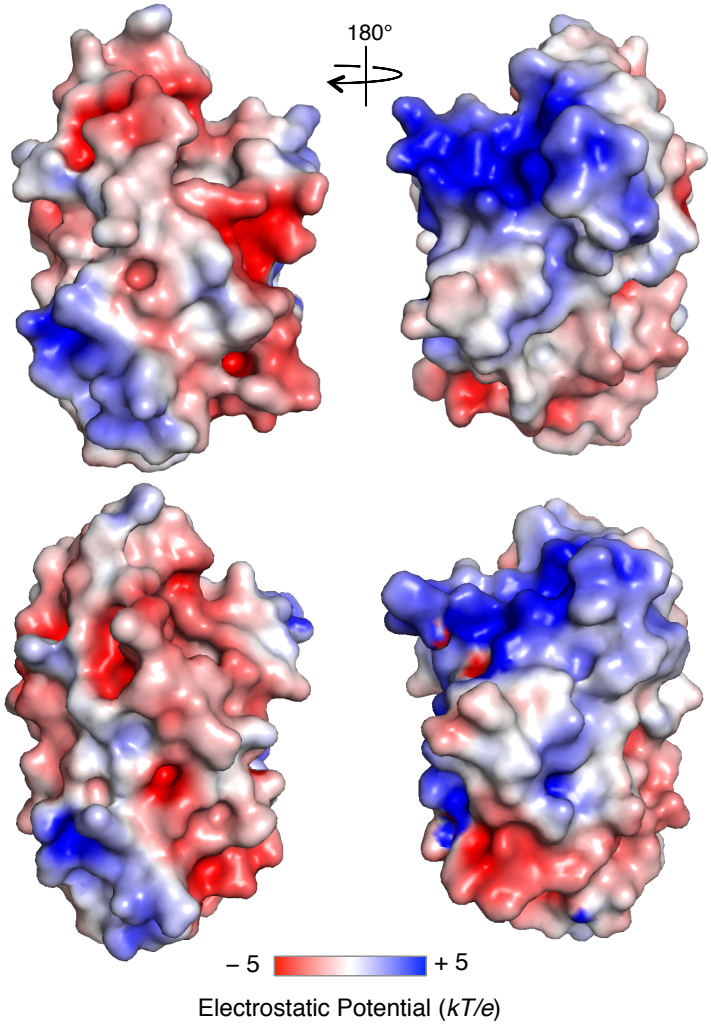

Fig. 15 Surface electrostatic potential of Gip1(146-310).

The potentials range from blue (+ 5 *kT/e*) to red (− 5 *kT/e*). Form I is in upper and Form II is in bottom. The structures are shown as surface models, left of which are depicted from the same viewpoint of the left structures in Fig. 13.

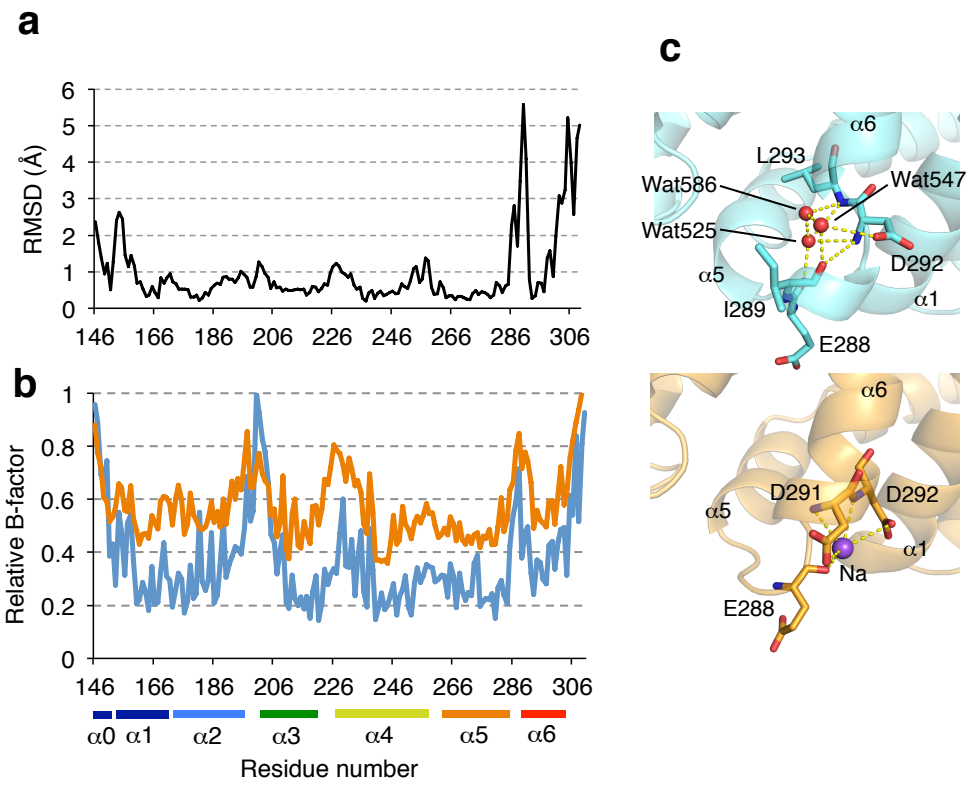

Fig. 16 R.m.s. deviations and B-factors of two forms of Gip1.

(a) R.m.s. deviations between Form I and Form II. The r.m.s. deviations (RMSD) of Cα atoms between Form I and Form II are plotted for each amino acid. **(b)** Relative B-factors of Form I (cyan) and Form II (orange). Secondary structure is aligned under the horizontal line colored in rainbow as Fig. 13b. **(c)** Structural difference between the two forms of Gip1 in the region between the α5 to α6 helices (a.a. 286-291) with a cartoon model (cyan; Form I, light orange; Form II). In Form I, the α6 helix is partially kinked by water molecules (red balls). On the other hand, α6 helix is tightly folded in Form II, which interacts with a sodium ion (purple ball). Hydrogen bonds and coordination bonds are represented by yellow dashed lines.

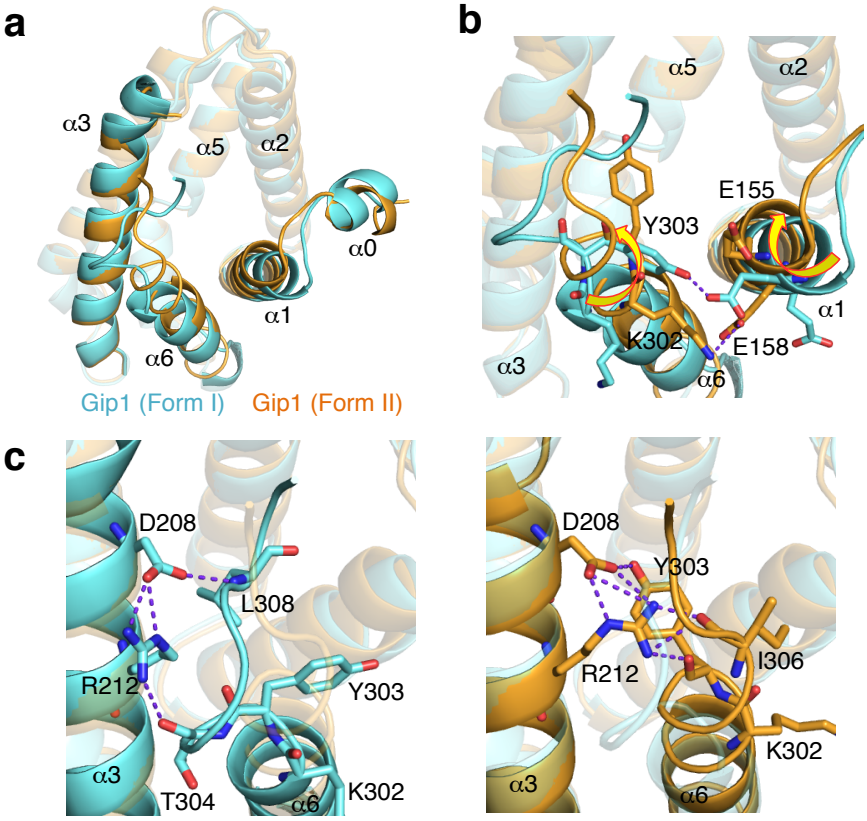

Fig. 17 Structural comparison of two forms of Gip1.

(a) Comparison of two crystal structures of Gip1(146-310). Two forms of Gip1 (Form I in cyan and Form II in light orange) are superimposed. **(b)** Rotational movements around α1- and α6-helices. The movements reconstruct a hydrogen bond between α1 and α6. Hydrogen bonds are shown as purple dashed lines. **(c)** Rearrangement of the hydrogen bonding network at α3 and the C-terminal tail region. Structural change induces the rearrangement of the hydrogen bonding network, including Asp208 as a hub of the network. Hydrogen bonds are shown as purple dashed lines.

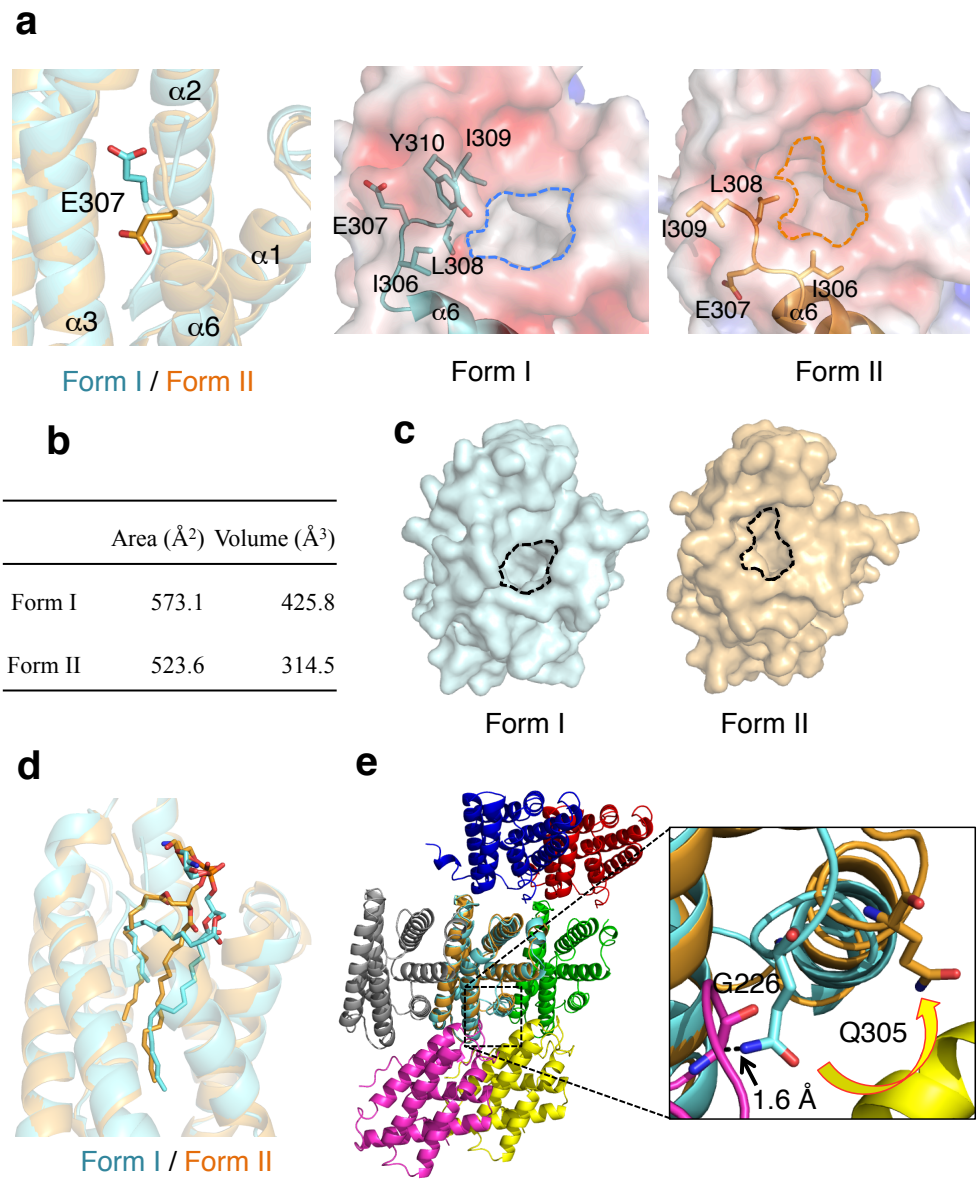

	Area (Å²)	Volume (Å³)
Form I	573.1	425.8
Form II	523.6	314.5

Fig. 18 Structural comparison of the cavity between two forms of Gip1.

(a) Directional difference of Glu307 between Form I and Form II. The two forms (cyan; Form I, light orange; Form II) are superimposed in cartoon representation with the side chains of Glu307 shown as stick models (left). Surface representation around the entrance of the cavity. The surface electrostatic potential is shown with the side chains depicted as stick models (Form I; middle, Form II, right). **(b)** Comparison of the size of the hydrophobic cavity. The data were calculated with the CASTp 3.0 server. **(c)** Rearrangement of cavity entrance. The structures of the two forms are shown in surface representation from the same viewpoint (Form I; left, Form II; right). The entrance of the cavity is surrounded by a dashed line. **(d)** Structural comparison of accommodated lipids. The structures of the two forms are superimposed in cartoon representation with the accommodated phospholipids shown as stick

models (Form I; cyan, Form II; light orange). **(e)** Investigation of the molecular packing in two crystals. Symmetry-related molecules of Gip1 (Form II) are shown in various colors other than cyan. Gip1 (Form I; cyan) is superimposed on the central Gip1 (Form II) on the left. The contact region between the α6 helix and a symmetry-related molecule is surrounded by the dashed square. The right figure shows a magnified view of the contact region. The residues shown as stick models represent clashes with an adjacent molecule. For example, the distance between Gln305 of Form I (cyan) and Gly226 of the symmetry-related Form II (magenta) is too close (1.6 Å).

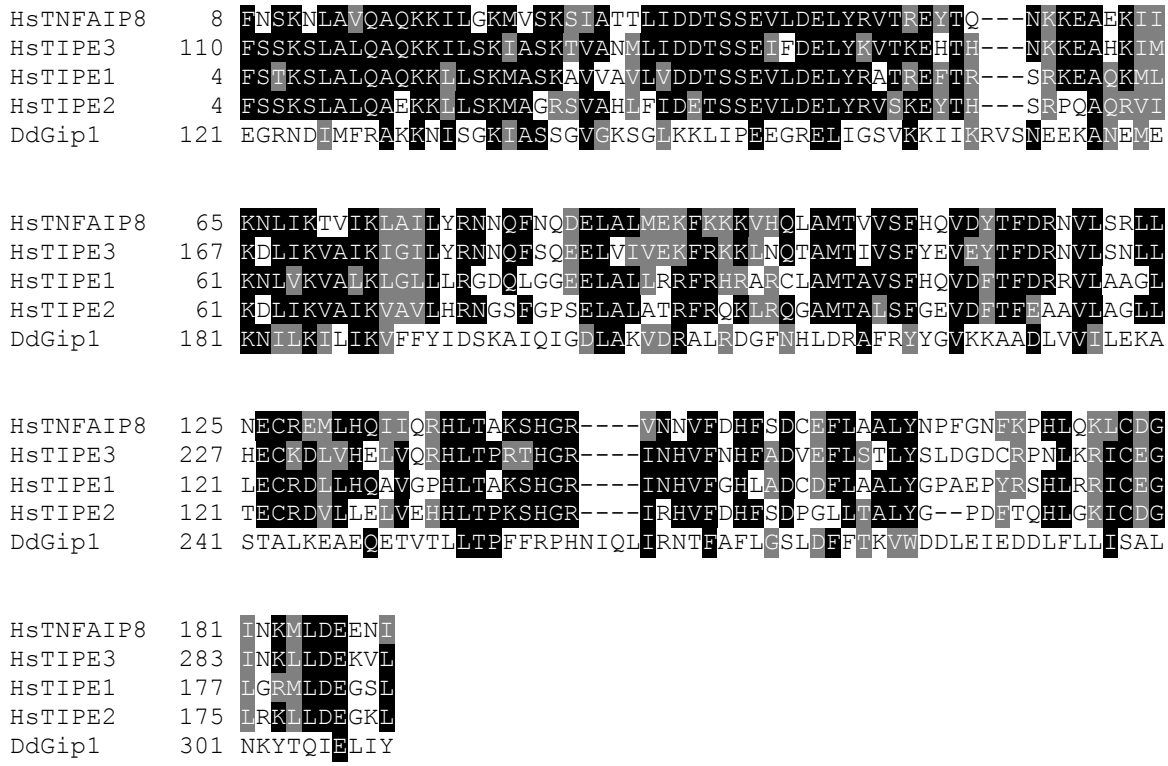

Fig. 19 Sequence comparison of Gip1 and TNFAIP8 family proteins.

Sequence alignment of Gip1 and human TNFAIP8 family proteins. Alignment was generated by CLUSTALW. Identical residues and similar residues are highlighted in black and gray, respectively. The alignment scores between Gip1 and TNFAIP8 (CAG33418.1), TIPE1 (sp|Q8WVP5.2), TIPE2 (sp|Q6P589.1), and TIPE3 (NP_997264.2) are 13.7, 14.5, 14.7, and 14.0, respectively. Hs, *Homo sapiens*; Dd, *Dictyostelium discoideum*.

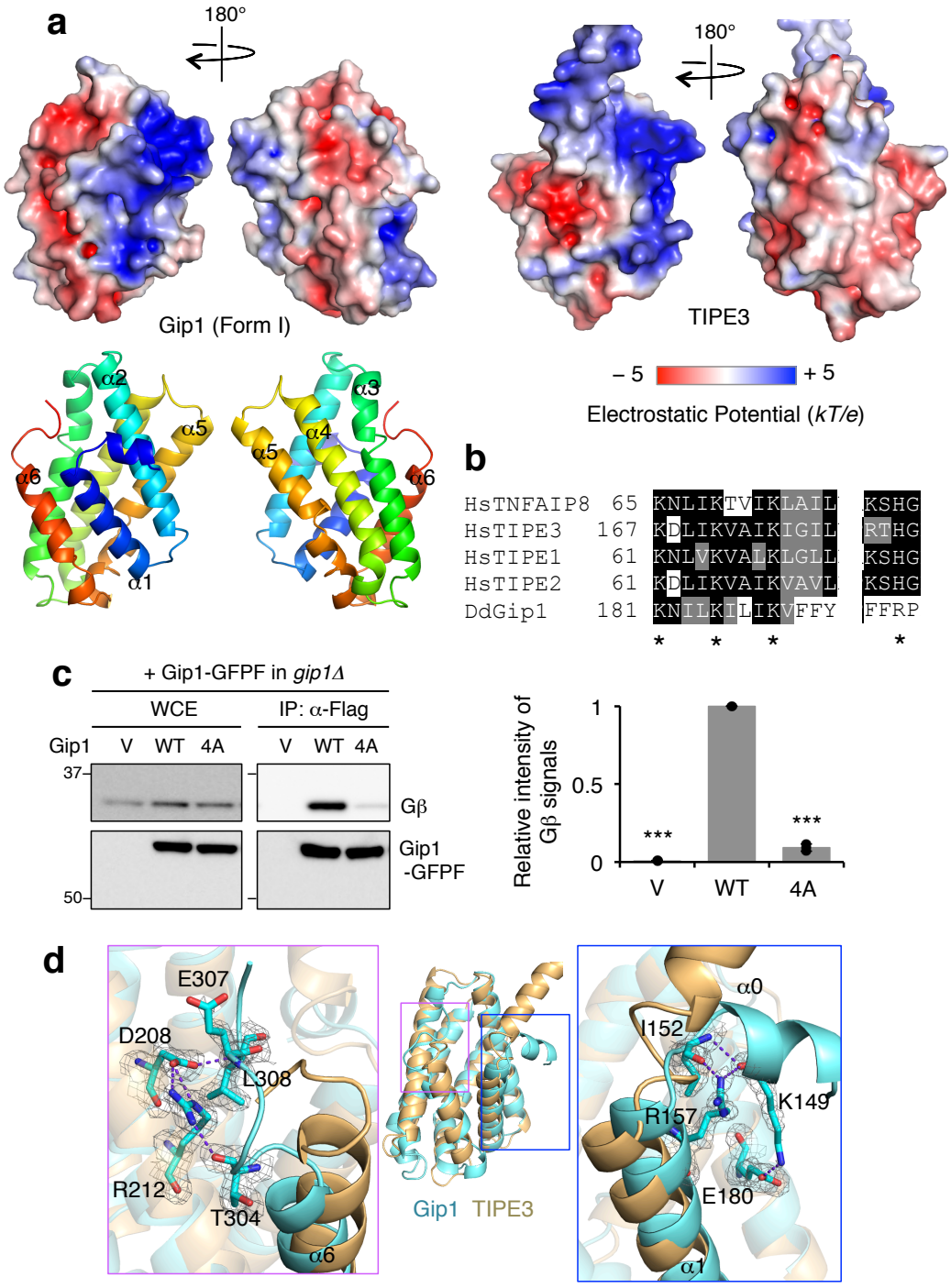

Fig. 20 Structural comparison of Gip1(146-310) and TIPE3.

(a) Structural comparison of charged areas in Gip1 and TIPE3. The potentials range from blue (+ 5 *kT/e*) to red (− 5 *kT/e*). Gip1 is displayed in not only surface model, but also cartoon model colored as same as Fig. 13. **(b)** Alignment of primary sequence. Mutated residues for Gip1(4A) are shown with asterisks (Lys181, Lys185, Lys189, and Arg260). **(c)** Physiological significance of a conserved positively charged patch on G protein binding. The data

were normalized relative to wild-type Gip1 and presented as the mean ± SD of three independent experiments (n = 3, ***P < 0.001 versus wild-type, two-tailed unpaired Student's t-test). **(d)** Structural differences between Gip1 and TIPE3. Hydrogen-bonded residues of Gip1 are shown as stick models with the 2mFo-DFc electron density map contoured at 1.0 σ. Hydrogen bonds are shown as dashed lines. Gip1 and TIPE3 are depicted in cyan and tint, respectively.

Table 4 Crystallization conditions at the first screening.

Screening Kit	Kit No.	Composition
INDEX	12	0.1 M Tris pH 8.5; 3.0 M Sodium Chroride
INDEX	31	0.1 M Tris pH 8.5; 0.5% PEG MME 5,000; 0.8 M Potassium sodium tartrate tetrahydrate
PEGRx2	48	0.1 M BICINE pH 8.5; 15% PEG 20,000; 3% w/v Dextran sulfate sodium salt

Table 5 Crystallographic statistics for Gip1(146-310).

Structure	Native (Form I)	Native (Form II)
Data collection		
Space group	$P2_12_12_1$	$P2_12_12_1$
a, b, c (Å)	33.32, 44.14, 96.64	33.47, 43.62, 101.69
Wavelength	1.0000	1.7000
Total reflections	41,315	57,793
Unique reflections	10,906	4,277
Resolution (Å)	50.00 - 1.95 (1.98 - 1.95)	43.62 - 2.74 (2.87 - 2.74)
R_{merge}*	9.0 (35.3)	11.9 (59.3)
$I / \sigma(I)$#	17.7 (2.9)	18.9 (4.8)
Completeness (%)	98.3 (66.2)	100.0 (100.0)
Redundancy	3.8 (3.2)	13.5 (13.9)
Refinement		
Resolution (Å)	48.32 - 1.95	43.62 - 2.74
No. reflections	10,864	4,242
R_{work} / R_{free}	0.18 / 0.23	0.21 / 0.27
No. atoms		
Protein	1,373	1,356
Ligand/ion	53	53
Water	110	7
B-factors	18.34	47.35
R.m.s deviations		
Bond lengths (Å)	0.003	0.002
Bond angles (°)	0.602	0.456
Ramachandran outlier	0.61	0.61

Values in parentheses are for the highest-resolution shell.

*$R_{merge} = \Sigma_{hkl} |I(hkl) - \langle I(hkl)\rangle| / \Sigma_{hkl} I(hkl)$, where $\langle I(hkl)\rangle$ is the mean of the symmetry-equivalent reflections of $I(hkl)$.

#$I / \sigma(I) = \langle I\rangle / \langle \sigma(I)\rangle$ for Form I (processed with HKL2000) and $= \langle I / \sigma(I)\rangle$ for Form II (processed with XDS).

Table 6 Residues within Van der Waals distance from the phospholipid.

Residue number	Residues within 4 Å from the phospholipid (Å)	
	Form I	Form II
I152	3.8	
P153	3.6	3.1
E155	3.6	3.5
G156	3.3	
L159	3.7	3.6
I160	3.8	
V163	3.6	3.7
I186	3.9	3.7
L187	3.7	3.7
F191	3.6	3.3
I201		3.9
V207	3.9	3.9
L211	3.6	3.8
F215		3.6
L218	3.8	3.9
F271	3.5	3.5
L274		3.6
F279	3.9	3.7
F280	3.9	3.6
L293	4	
L296	3.8	3.7
L300		4
Y303	3.3	3.6
L308	3.3	3.4
I309	3.4	
Y310	3.1	
Total residues	22	20

Colors of the table correspond to the colors of α-helices shown in Fig. 13. Blanks indicate that no atoms were selected at the corresponding residues in the structure.

Table 7 Structural comparison of lipid-binding proteins based on PDB structures.

	PDB ID	Fold /Binding site	Ligand in PDB	Lipid[*1]	Surface (Å^2)	Volume (Å^3)	References
Gip1 (Form I)	5Z1N	cylinder-like /cavity	PE/PG	-	573.1	425.8	This study
Gip1 (Form II)	5Z39	cylinder-like /cavity	PE/PG	-	523.6	314.5	This study
RhoGDI1	1RHO	Ig-like /cavity	Free	-	128.3	99.2	Keep *et al*., 1997
RhoGDI1	1DOA	Ig-like /cavity	Cdc42 (GDP)	GG	329.9	218.2	Hoffman *et al*., 2000
RhoGDI1	1HH4	Ig-like /cavity	Rac1 (GDP)	GG	250.4	115.0	Grizot *et al.*, 2001
RhoGDI1	4F38	Ig-like /cavity	RhoA (GppNHp)	GG	446.2	250.4	Tnimov *et al*., 2012
RhoGDI2	1DS6	Ig-like /cavity	Rac2 (GDP)	-	239.0	171.8	Scheffzek *et al.*, 2000
PDEδ	1KSG	Ig-like /cavity	Arl2 (GTP)	-	58.9	31.8	Hanzal-Bayer *et al.*, 2002
PDEδ	3T5G	Ig-like /cavity	RheB (GDP)	Far	383.4	207.2	Ismail *et al*., 2011
PDEδ	4JHP	Ig-like /cavity	RPGR RCC1 -like domain	-	422.4	214.1	Wätzlich *et al*., 2013
PDEδ	5TAR	Ig-like /cavity	KRas4B (GDP)	Far	464.4	309.3	Dharmaiah *et al*., 2016
PDEδ	5TB5	Ig-like /cavity	KRas4B (GDP)	Far	498.0	311.4	Dharmaiah *et al*., 2016
PDEδ	5F2U	Ig-like /cavity	INPP5E pep-tide	Far	458.6	299.5	Fansa *et al*., 2016
PDEδ	5T4X	Ig-like /cavity	Free	-	411.2	310.5	Qureshi *et al*., 2018
UNC119a	3GQQ	Ig-like /cavity	Free	-	515.9	344.1	Zhang *et al.*, 2011
UNC119a	3RBQ	Ig-like /cavity	Gαt mimic peptide	Lau	459.0	307.9	Zhang *et al*., 2011
UNC119a	4GOJ	Ig-like /cavity	Arl3 (GppNHp)	-	442.5	212.3	Ismail *et al.*, 2012
UNC119a	4GOK	Ig-like /cavity	Arl2 (GppNHp)	-	N.D. [*2]	N.D. [*2]	Ismail *et al*., 2012
UNC119a	5L7K	Ig-like /cavity	NPHP3 pep-tide	Myr	283.4	133.3	Jaiswal *et al*., 2016
RabGDI	1GND	REP[*3]-like /pocket	Free	-	29.5	6.2	Schalk *et al.*, 1996
RabGDI	1LV0	REP[*3]-like /pocket	GG-peptide	GG[*4]	24.6	4.2	An *et al.,* 2003
RabGDI	1UKV	REP[*3]-like /pocket	Ypt1 (GDP)	GG (×1)	360.0	336.9	Rak *et al*., 2003
RabGDI	2BCG	REP[*3]-like	Ypt1	GG	366.8	364.9	Pylypenko *et al*.,

		/pocket	(GDP)	(×2)			2006
TIPE2	3F4M	cylinder-like /cavity	-	-	N.D. *2	N.D. *2	Zhang *et al*., 2009
TIPE3	4Q9V	cylinder-like /cavity	-	-	604.4	385.3	Fayngerts *et al*., 2014
Tnfaip8	5JXD	cylinder-like /cavity	PE	-	518.6	349.8	Kim *et al.*, 2017

The size of the cavity was calculated with the CASTp 3.0 server.

*1) Lipid indicates the lipid modification of ligands in PDB structures. GG, Far, Lau, and Myr are geranylgeranyl, farnesyl, lauryl, and myristoyl groups, respectively.

*2) The hydrophobic cavity was not precisely determined due to partially lacking the structural information.

*3) REP is Rab escort protein.

*4) This geranylgeranyl peptide binds to different sites from those in 1UKV and 2BCG.

III-2. Molecular mechanism underlying complex formation

Gip1 had the central hydrophobic cavity at the C-terminal G protein binding region. This cavity accommodated a phospholipid that might be derived from *E. coli*. Although it was not clear whether Gip1 bound to the lipid compounds in physiological conditions, the data reminded me the hypothesis that Gip1 contains a lipid-modified moiety into its hydrophobic cavity. Since it has already been revealed that Gip1 preferentially binds to Gβγ subunits, I next focused on the lipid modification on the Gγ subunit.

III-2-1 Prenyl-modification on Gγ for the interaction with Gip1

Heterotrimeric G proteins localize on the plasma membrane by tethering with lipid-modification on Gα and Gγ subunits. As I unveiled that Gip1 had a hydrophobic cavity at its G protein binding region, I supposed that Gip1 accommodates lipid-modified moiety on G proteins, specifically on Gβγ subunit. To examine this hypothesis, I first identified what kinds of lipid modification are attached to Gα2Gβγ. Based on the genomic information in dictyBase (http://dictybase.org/) [Fey *et al.*, 2013], Gγ (DDB_G0274125) has CSVL sequence at its C terminus and Gα2 (DDB_G0276267) has MGIC sequence at its N terminus. Previous studies show that cysteine of C-terminal CAAL motif on Gγ subunit is subjected to geranylgeranylation [Jiang *et al*., 2018]. On the other hand, it is possible that second glycine and fourth cysteine of N-terminal MGIC on Gα2 are subjected to myristoylation and palmitoylation, respectively [Resh, 2006]. According to the mass spectrometric studies, I determined that Cys66 at C-terminal Gγ and Gly2 at N-terminal Gα2 were subjected to geranylgeranyltion and myristoylation, respectively (Fig. 21). However, Gly4 on Gα2 was not palmitoylated.

Since Gip1 preferentially interacts with Gβγ subunit [Kaminura *et al.,* 2016], I specifically focused on the geranylgeranylation on C-terminal Gγ. I constructed the lipid-modification-deficient Gγ mutant by removing CAAX motif (Gγ(ΔCAAX)), which is es-

sential sequence for the modification, and introduced the Gγ mutant into *gγΔ Dictyostelium* cells. Gγ(ΔCAAX) failed to localize on the plasma membrane and uniformly existed in the cytosol, although wild-type Gγ was able to concentrate on the plasma membrane (Fig. 22a). In addition, cells expressing Gγ(ΔCAAX) were not able to appropriately develop and to form fruiting bodies (Fig. 22b). Regarding the interacting ability, both wild-type Gγ and Gγ(ΔCAAX) complexed with Gβ subunit (Fig. 22c). However, Gβγ comprising Gγ(ΔCAAX) was not able to bind with Gip1. Significance of lipid-modification on Gγ was further evaluated with in vitro-binding assay. Without Gα subunit, Gβγ comprising wild-type Gγ was able to interact with bacterially purified Gip1, but Gβγ comprising Gγ(ΔCAAX) was not (Fig. 22d). Correspondingly, Gα2Gβγ was competitively dissociated from Gip1 in the presence of geranylgeranyl pyrophosphate (Fig. 23a). In this experimental setting, beads-bound Gip1 was estimated as 4 pmol (Fig. 23b). So, 2 nmol of geranylgeranyl pyrophosphates (indicated as 1% GG-pyroP) began to effect on the 4 pmol of beads-bound Gip1. Compared with some lipid derivatives, geranylgeranyl pyrophosphate showed the great effects on the complex formation rather than farnesyl pyrophosphate and myristic acid, although farnesyl pyrophosphate showed a little effect (Fig. 23c). These results strongly suggest that geranylgeranyl modification on Gγ subunit is essential for the complex formation with Gip1.

Next, I assessed where Gip1 interacts with G proteins in a cell. It was previously reported that Gip1 sequesters G proteins in the cytosol [Kamimura *et al.,* 2016]. Indeed, Gip1 formed complex with wild-type G proteins only in the cytosolic fraction (Fig. 24a). By using purified Gβ and Gip1 (Fig. 24b), I quantified the stoichiometric relationship between Gip1 and G proteins. The numbers of Gβ molecule in total and in the cytosol were estimated as 240,000 and 60,000, respectively. On the other hand, the number of Gip1 molecule in the cytosol was calculated as 157,000 (Fig. 24c). Since Gβ is unstable in *gγΔ* cells (Fig. 22c), the amount of Gβ can be equivalent to that of Gγ. These data suggest that almost all cytosolic Gβγ are bound to Gip1.

I then investigated the binding specificity of Gip1 with some lipid-modified proteins. Gip1 interacted with Gβγ but not with Ras proteins at the same conditions (Fig. 25a). *Dictyostelium* encodes some Ras superfamily proteins. Among them, RasG, Rac1A, and Rap1 were predicted as geranylgeranyl-modified proteins because of their CAAX motifs [Jiang *et al*., 2018], although Rac1A and Rap1 predominantly localized in the cytosol (Fig. 25b). All of the three Ras subfamily proteins were hardly bound to Gip1 compared with Gβγ (Fig. 25c). These data indicate that Gip1 preferentially binds to Gβγ, and lipid-modification is necessary but not sufficient factor for determining Gip1 binding partner.

III-2-2 Induction of steric block inside the cavity

It was unveiled that lipid-modification on Gγ subunit was indispensable for complex formation between Gip1 and G proteins. However, it was not clear whether the lipid-modified moiety actually inserts into the hydrophobic cavity. So, I conducted the tryptophan mutagenesis to hinder the cavity by introducing balky tryptophan as a blockade. I used CASTp 3.0 server to comprehensively select the amino acids of which the cavity was composed [Dundas *et al.*, 2006]. The server selected 40 residues containing 24 leucine, isoleucine, and valine residues as candidates for tryptophan substitution (Table 8). The effects of the tryptophan substitution were evaluated by observing the localization of subcellular Gα2 and Gγ in the presence of latrunculin A. As results, approximately 80% of total replaced residues (19 of 24 residues) significantly impaired the cytosolic localization of Gα2 (Fig. 26a,b,c). The results were corresponding with the Gγ localization (Fig. 26d). Besides, Gα2 was very weekly expressed in the cytosolic fraction in the absence of Gγ (Fig. 26e). Mapped on the crystal structure, these mutation-affected residues were broadly distributed on the cavity surface (Fig. 26f). Moreover, these substitutions severely decreased the Gip1 binding ability with Gβγ (Fig. 27). These results indicate that the whole interior side of the cavity is important to form cytosolic fractions of G proteins by interacting with G proteins.

III-2-3 Hydrogen bonding network at the cavity entrance

In addition to the tryptophan mutagenesis, I conducted the comprehensive alanine scanning mutagenesis to find out other significant residues. The effects of alanine mutagenesis were evaluated by observing the cytosolic localization of Gα2 and mapped on the crystal structure of Gip1 (Fig. 28). Alanine substitution affected both polarized and non-polarized amino acids. Especially, the highly affected residues by alanine substitution were summarized and compared with corresponding residues of TNFAIP8 family proteins (Table 9,10). Among the negatively affected residues whose substitution impaired the cytosolic Gα2 localization, Glu307 was highly conserved in Gip1 and TNFAIP8 (Table 9). On the other hand, Asp219, Lys239, and Tyr303 were totally different in their charges between Gip1 and TNFAIP8 family proteins. The side chains of polarized residues formed hydrogen bonds with other intramolecular residues, except for Lys239 and Glu307. Negatively affected residues seemed to be biased on α3-, α4-, and α6-helices (Fig. 29a). Among the positively affected residues whose substitution increased the cytosolic Gα2 localization, it seemed that Arg260 was conserved but the others were not (Table 10). Contrary to the negatively affected polarized residues, positively affected Arg233, Arg260, and Asp291 did not form hydrogen bonds with intramolecular residues, although the side chain of Arg233 formed a hydrogen bond with its main chain (Fig. 29b). Interestingly, positively affected residues seemed to reside near the loop regions.

Asp208 formed hydrogen bonds with Arg212 and Leu308 at the rim of the cavity entrance connecting α3 helix and C-terminal tail region (Fig. 17c). The C-terminal tail region contained Glu307, which was largely affected by alanine mutagenesis. The side chain of Glu307 directed to the solvent and did not form hydrogen bonds with any intramolecular atoms. The importance of the C-terminal tail region was assessed as follows. Subcellular localization of Gα2 and Gγ were impaired in cells expressing C-terminal deleted Gip1 (a.a.

304-310; Gip1(ΔC-tail)) as well as Gip1(D208A) (Fig. 30a). Both of these two Gip1 mutants were not interact with Gβγ (Fig. 30b). To evaluate whether C-terminal tail interact with the lipid-modified moiety of target proteins, I performed an in vitro-binding assay. Full-length and C-terminal deleted Gip1 were purified and mixed with wild-type Gβγ and CAAX box from *Dictyostelium* RasG. Surprisingly, purified Gip1 was able to bind with both wild-type Gβγ and CAAX region regardless of C-terminal tail region (Fig. 30c). This result demonstrates that the proper location and configuration of the Gip1 C-terminal tail is necessary for Gip1 function at least in vivo.

a

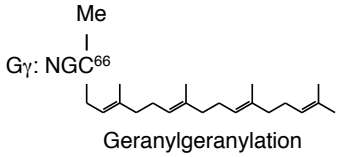

Geranylgeranylation

b

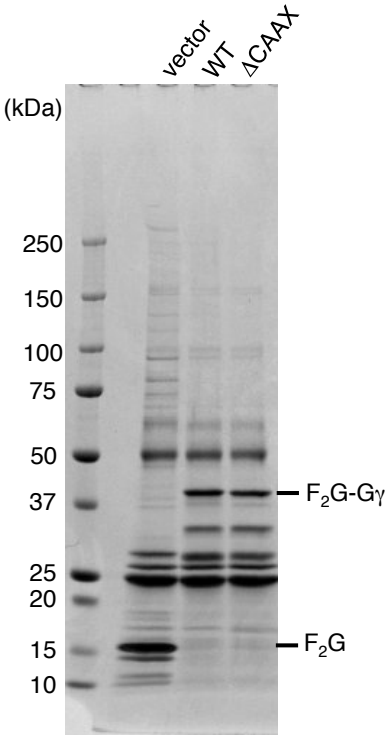

CBB staining

c

Gγ(WT)

MSESQLKKVL KENETLKAQL EKSTTILKVS EACESLQDYC
TKTSDPFIPG WSGENEWTKP LKGNGCSVL

Score	Expect	Peptide
13	0.046	E.NEWTKPLKGNGC.- + GG+Met (C)
13	0.045	E.WTKPLKGNGC.-
1	0.71	E.WTKPLKGNGC.- + GG (C)
5	0.33	E.WTKPLKGNGC.- + GG+Met (C)
2	0.67	E.WTKPLKGNGC.- + GG+Met (C)
2	0.69	E.WTKPLKGNGC.- + GG+Met (C)

Gγ(ΔCAAX)

MSESQLKKVL KENETLKAQL EKSTTILKVS EACESLQDYC
TKTSDPFIPG WSGENEWTKP LKGNG

Score	Expect	Peptide
26	0.0028	E.NEWTKPLKGNG.-
11	0.089	E.NEWTKPLKGNG.-
13	0.052	E.WTKPLKGNG.-
12	0.067	E.WTKPLKGNG.-
14	0.038	E.WTKPLKGNG.-
12	0.063	E.WTKPLKGNG.-
24	0.0043	E.WTKPLKGNG.-
12	0.067	E.WTKPLKGNG.-
8	0.14	E.WTKPLKGNG.-
35	0.00033	E.WTKPLKGNG.-
22	0.0062	E.WTKPLKGNG.-

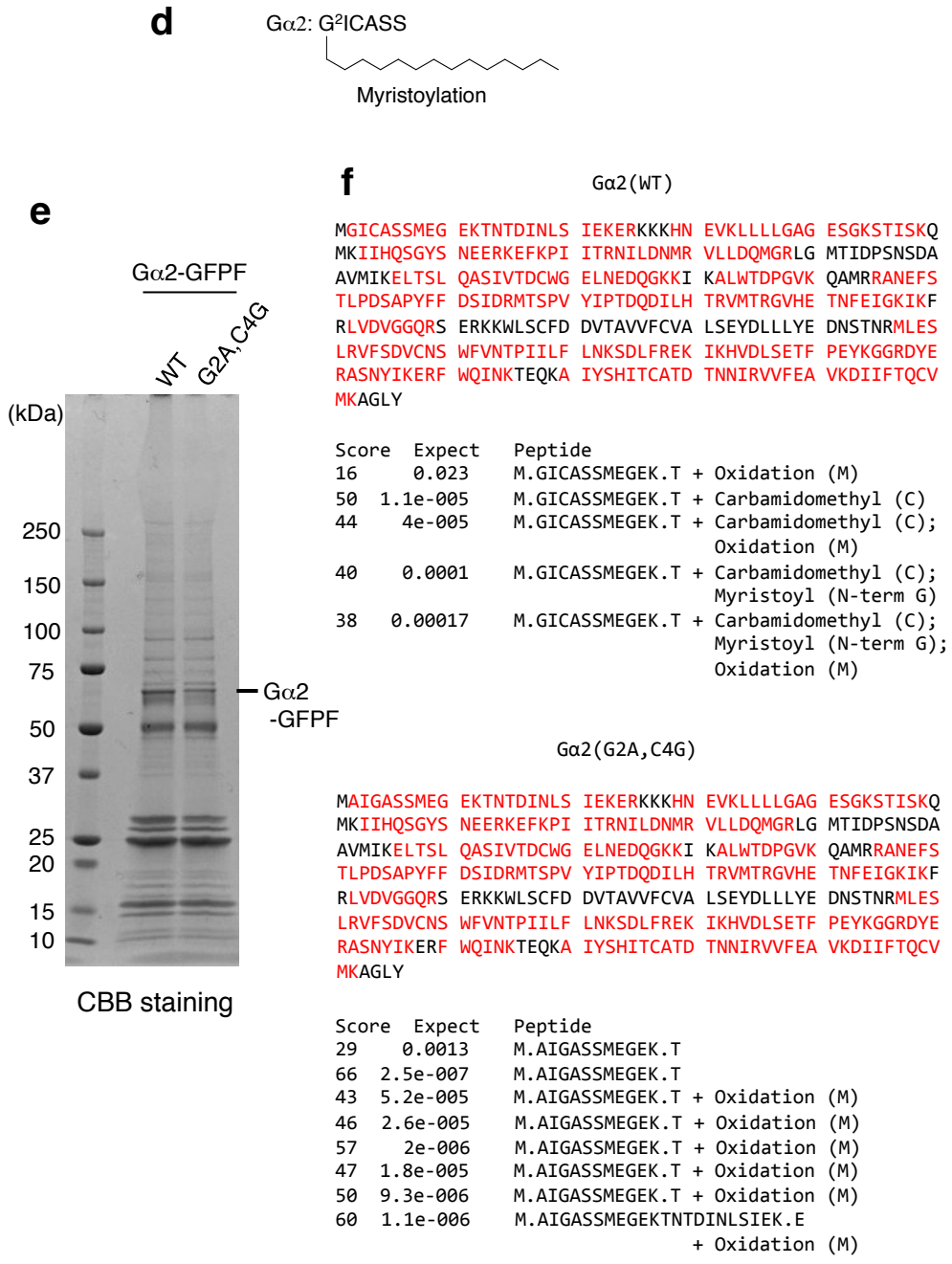

Fig. 21 Mass spectrometric identification of prenyl modification of Gγ and myristoylation of Gα2.

(a) Schematic diagram of Gγ modification. C-terminal cysteine (C^{66}) is geranylgeranylated and methylated (Me). **(b)** Preparation for mass spectrometric analysis of Gγ. The indicated proteins were purified by anti-Flag beads and separated. **(c)** Identification of chemical modifications on Gγ. The identified peptides of Gγ(WT) and Gγ(ΔCAAX) are shown in red. The geranylgeranylated and methylated peptide was identified only in Gγ(WT) and not in Gγ(ΔCAAX). **(d)** Schematic diagram of Gα2 modification. N-terminal glycine (G^2) is

myristoylated. **(e)** Preparation for mass spectrometric analysis of Gα2. **(f)** Identification of chemical modifications on Gα2. The identified peptides of Gα2(WT) and Gα2(G2A,C4G) are shown in red. The myristoylated peptide was identified only in Gα2(WT) and not in Gα2(G2A,C4G).

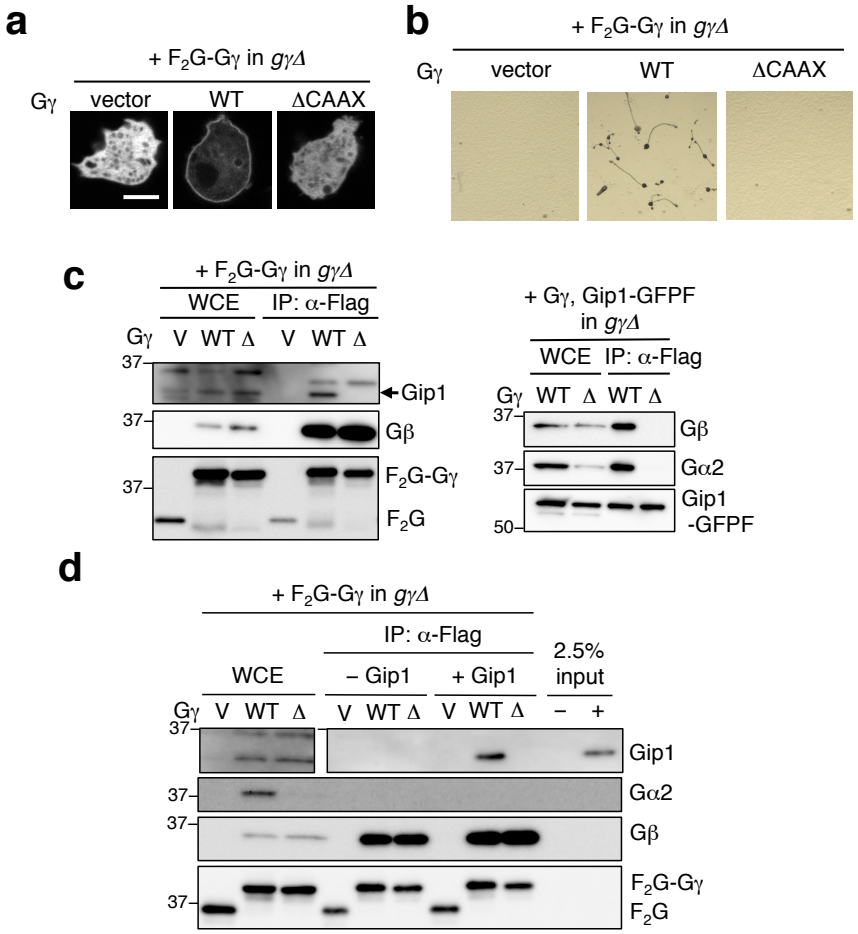

Fig. 22 Recognition of the prenyl-moiety on Gγ through the hydrophobic cavity of Gip1. **(a)** Subcellular localization of Gγ in a living cell. Flag-Flag-GFP (F_2G) tag alone (vector) or F_2G-tagged Gγ(WT) or Gγ(ΔCAAX) were expressed in *gγΔ* cells. Scale bar, 5 μm. **(b)** Developmental phenotypes of Gγ mutant cells upon starvation. Used cells are the same as shown in Fig. 22a. Cells were developed on non-nutrient agar overnight and observed whether they formed into fruiting bodies. **(c)** Co-immunoprecipitation of Gγ or Gip1. F_2G-Gγ(WT) or F_2G-Gγ(ΔCAAX) was expressed in *gγΔ* cells (left). GFP-Flag-tagged Gip1 (Gip1-GFPF) was coexpressed with Gγ(WT) or Gγ(ΔCAAX) in *gγΔ* cells (right). **(d)** Complex formation of Gβγ and purified Gip1 in vitro. Gβγ subunits were bound to beads via F_2G tag and incubated with purified full-length Gip1.

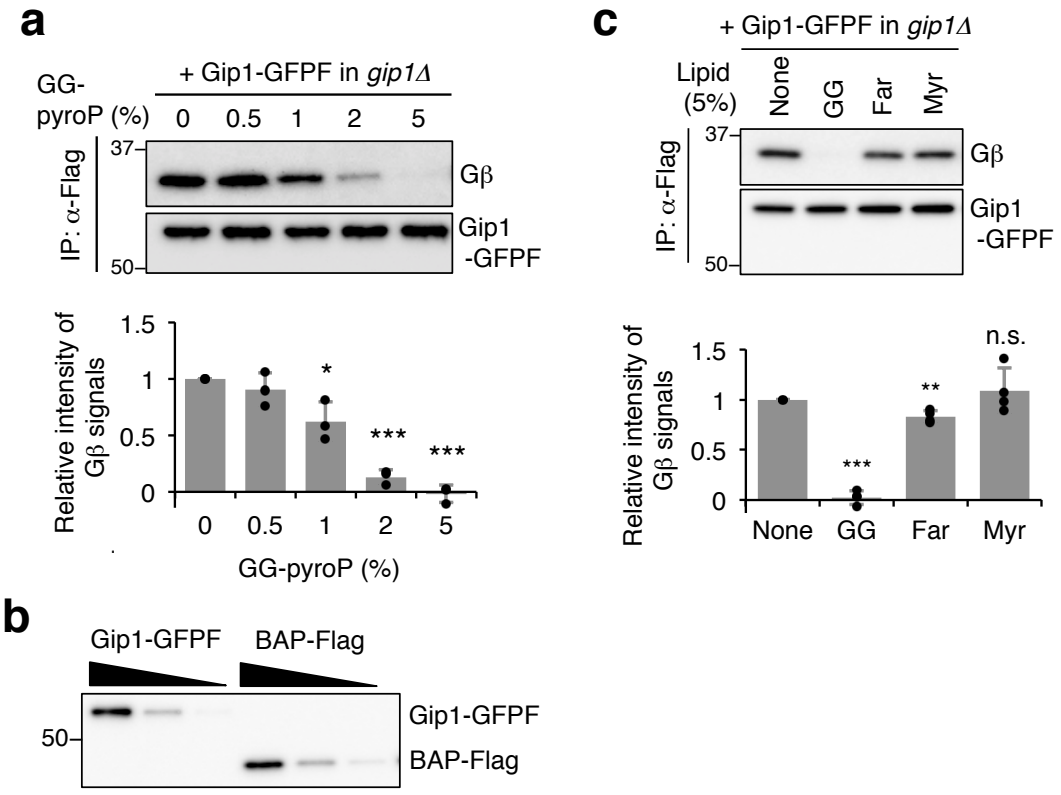

Fig. 23 Competitive inhibition of complex formation by lipid derivatives.

(a) Competitive dissociation of G proteins from Gip1 with geranylgeranyl pyrophosphate (GG-pyroP). The data were normalized relative to the band intensities of Gβ against 0% GG-pyroP, and shown as the mean ± SD of three independent experiments ($n = 3$, $^{*}P < 0.05$, $^{***}P < 0.001$ versus 0% GG-pyroP, two-tailed unpaired Student's *t*-test). **(b)** Quantification of the amount of Gip1-GFPF bound to anti-Flag beads used for the competitive assay shown in Fig. 23a. For this purpose, 0.5, 0.17, and 0.05% of a sample containing Gip1-GFPF were immunoblotted with an anti-Flag antibody together with 1, 0.33, and 0.1 ng of BAP-Flag as a standard. **(c)** Competitive dissociation of G proteins from Gip1 by the same concentration (100 μM) of geranylgeranyl pyrophosphate (GG), farnesyl pyrophosphate (Far), and myristic acid (Myr). The data were normalized relative to the band intensities of Gβ without lipid and shown as the mean ± SD of four independent experiments ($n = 4$, $^{**}P < 0.01$, $^{***}P < 0.001$ versus 0% lipid, two-tailed unpaired Student's *t*-test).

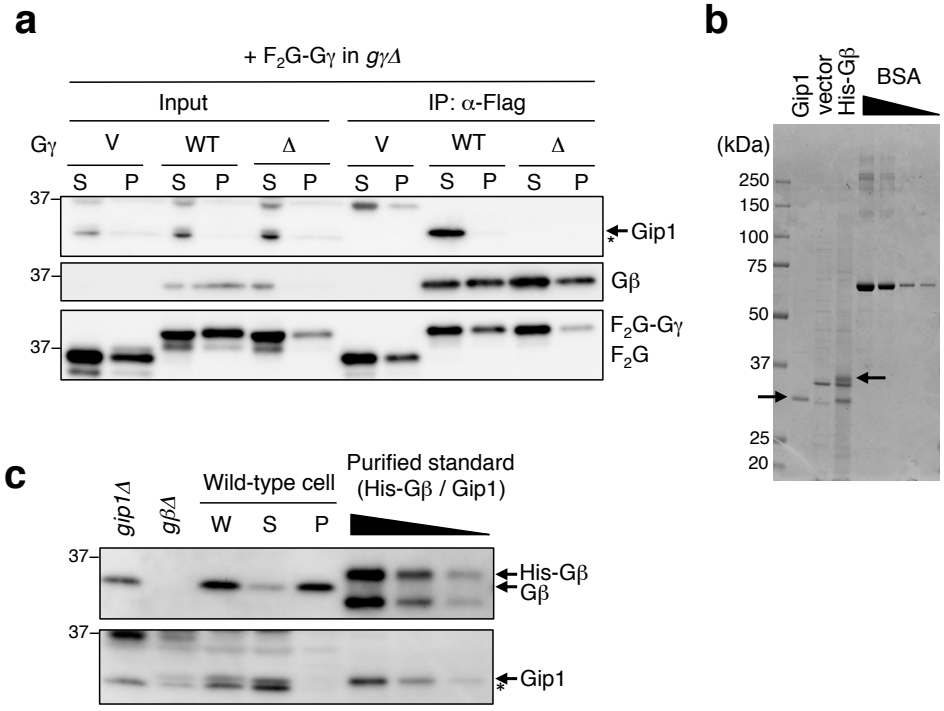

Fig. 24 Subcellular localization of endogenous Gip1 and Gβ.

(a) Complex formation between G proteins and Gip1 in each cell fractions. Cells were fractionated, and each fraction was used for the immunoprecipitation of F_2G or F_2G-Gγ. The indicated proteins were visualized by immunoblotting using anti-Gip1, Gβ, and Flag antibodies. **(b)** Quantification of His-Gβ and full-length Gip1. Both proteins were bacterially expressed and purified, as shown by the arrows. These proteins, along with 500, 200, 50, and 20 ng of BSA, were separated on a polyacrylamide gel and visualized by Coomassie Brilliant Blue. **(c)** Quantification of the amount of endogenous Gβ and Gip1. Cells were fractionated into whole cell extract (W), supernatant (S), and precipitant (P). Proteins in each fraction were estimated in comparison to purified protein standards (His-Gβ or full-length Gip1) shown in Fig. 24b. The bands indicated by arrows represent His-Gβ, Gβ, and Gip1. Bands with an asterisk denote nonspecific bands.

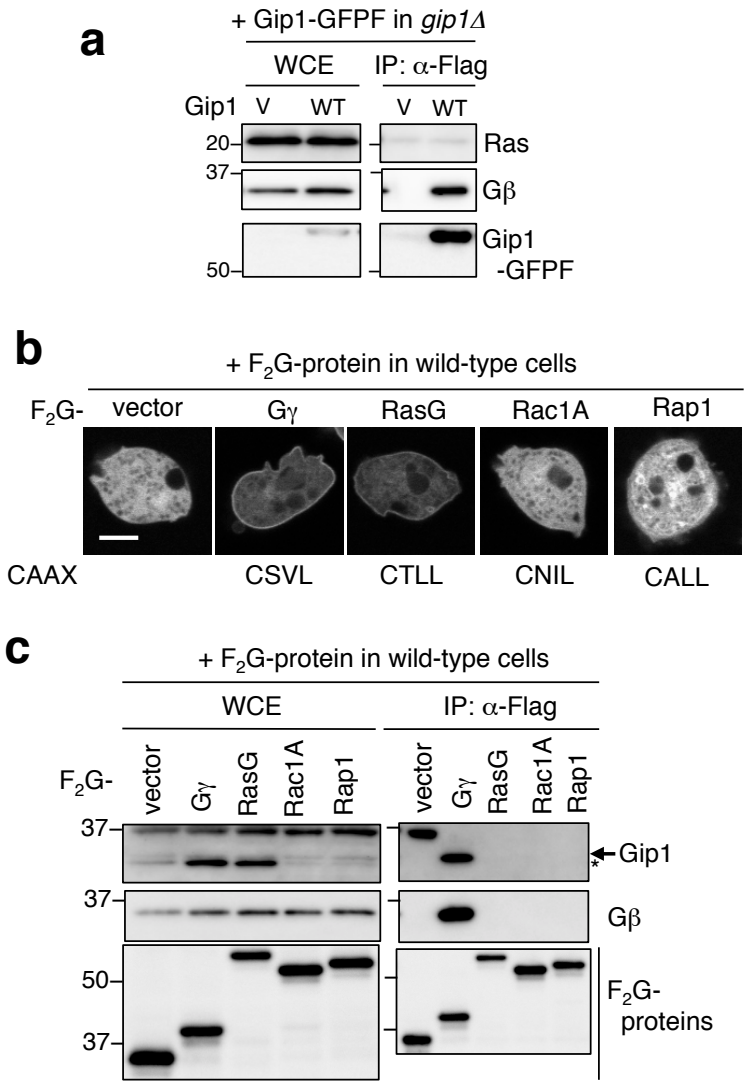

Fig. 25 Binding specificity of Gip1 to small G proteins.

(a) Binding specificity for Ras subfamily proteins. Gip1-GFPF proteins were pulled down, followed by immunoblotting with anti-Ras, anti-Gβ, and anti-Flag antibodies. **(b)** Subcellular localization of proteins with a CAAX motif. The indicated proteins with GFP were observed by confocal microscopy. The amino acid sequences of each CAAX motif are shown under micrographs. Scale bar, 5 μm. **(c)** Binding of Gip1 to proteins with a CAAX motif. F_2G tagged proteins were pulled down, followed by immunoblotting with anti-Gip1, anti-Gβ, and anti-Flag antibodies.

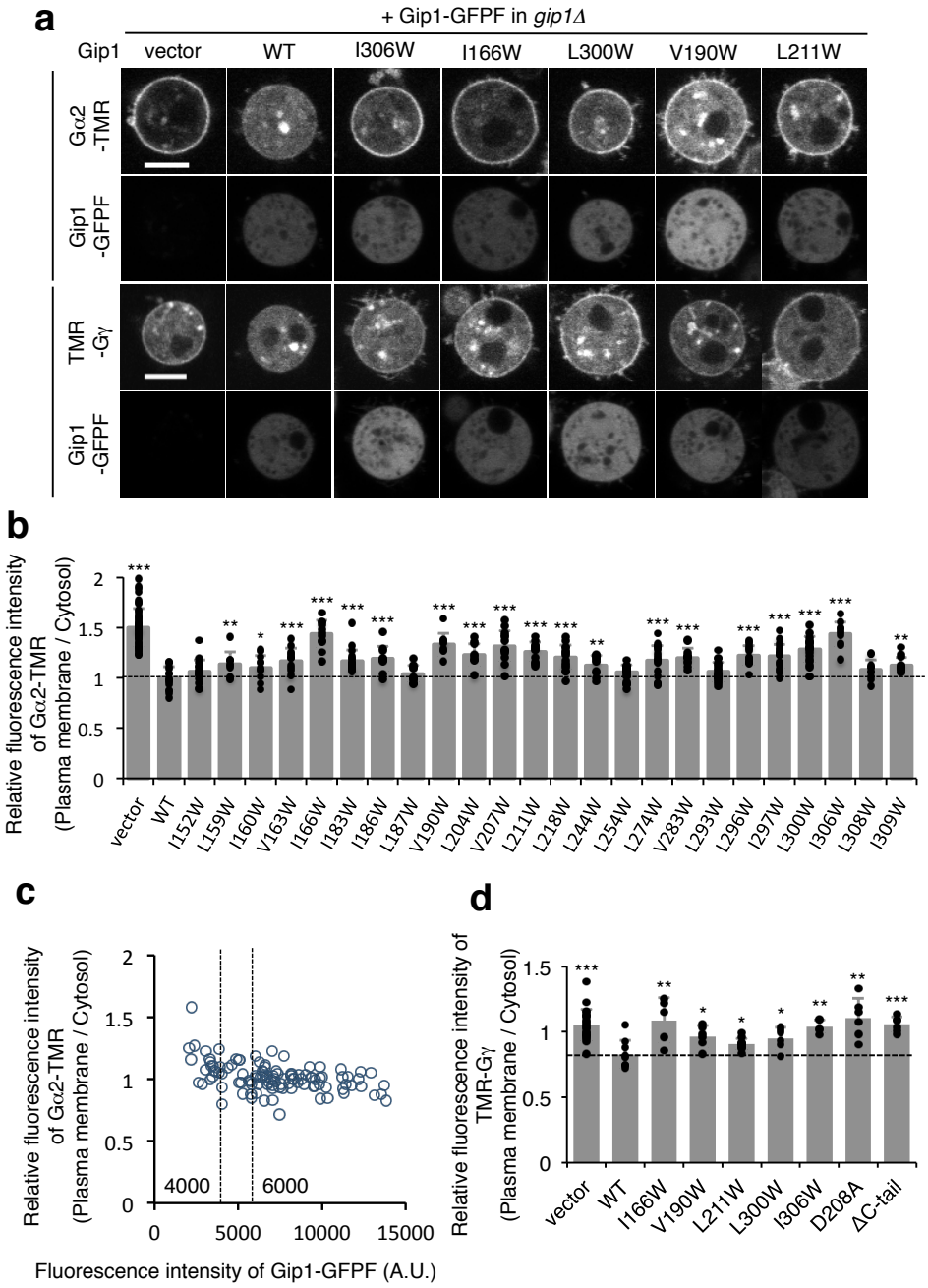

Fig. 26 Tryptophan mutagenesis to induce steric hindrance inside the cavity.

Subcellular localization of Gα2 and Gγ labelled with TMR and Gip1-GFPF in a living cell in the presence of LatA. Representative images of the severely impaired top five mutants are shown. Scale bar, 5 μm. **(b)** Evaluations of tryptophan scanning mutagenesis. The data represent the mean ± SD ($n \geq 10$ cells, $^{*}P < 0.05$, $^{**}P < 0.01$, $^{***}P < 0.001$ versus wild type, two-tailed unpaired Student's *t*-test). **(c)** Scatter plot of the fluorescence intensities of Gα2-Halo and Gip1-GFPF. The plot is depicted from wild-type as the representative of examinations. To evaluate the effect of tryptophan substitution, data plots between Gip1-GFPF intensity of 4,000 and 6,000 (shown as dashed lines) are selected. **(d)** Evaluations of the

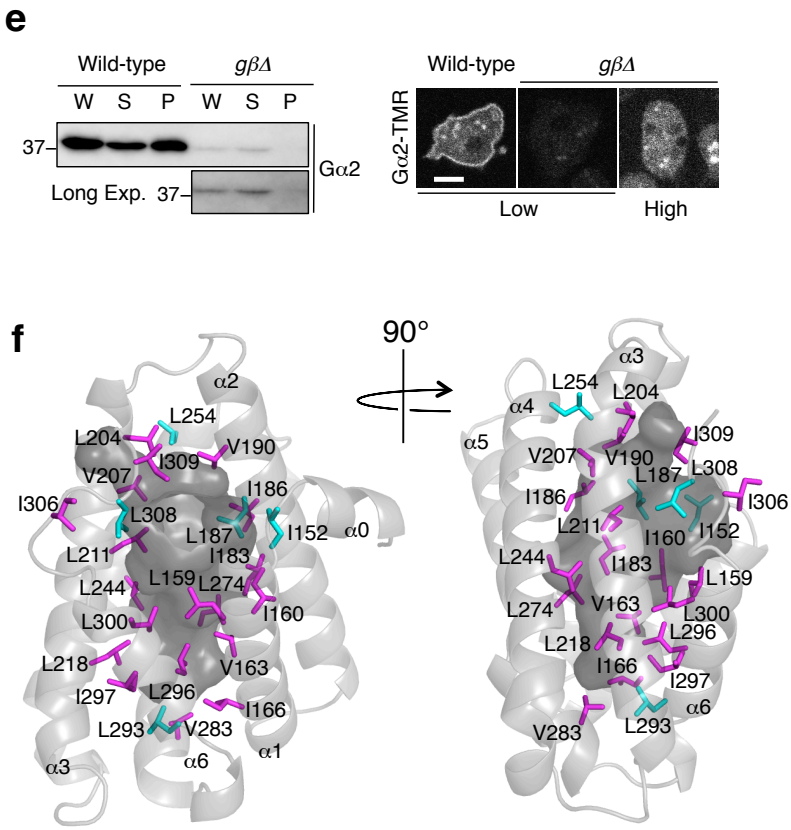

tryptophan scanning mutagenesis, D208A, and ΔC-tail, assessed by TMR-Gγ instead of Gα2-TMR. The data represent the mean ± SD ($n \geq 5$ cells, $^{*}P < 0.05$, $^{**}P < 0.01$, $^{***}P < 0.001$ versus wild type, two-tailed unpaired Student's *t*-test). **(e)** Gα2 localization in wild-type or *gβΔ* cells. The cells were fractionated as in Fig. 24. Protein samples were immunoblotted with an anti-Gα2 antibody (upper panel). Confocal micrographs of Gα2-TMR are shown in a wild-type or *gβΔ* cell (bottom panel). For a *gβΔ* cell, a representative image at high-laser-power values is shown due to its weak signals. Scale bar, 5 μm. **(f)** Representation of tryptophan-substituted residues. Mutated residues are depicted as stick models. Residues in magenta and cyan show the residues that reduced the cytosolic Gα2 and the residues with no effects, respectively. The surface of the cavity is colored in dark gray.

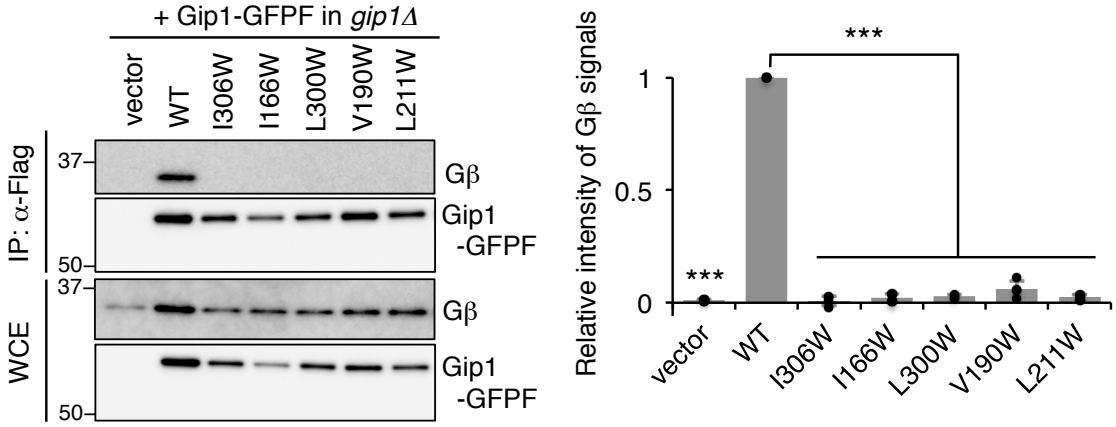

Fig. 27 Binding ability of cavity-blocked Gip1 to Gβγ.

Co-immunoprecipitation of Gip1 with Gβγ. The used mutants are as the same as cells shown in Fig. 26a. The data were normalized relative to the band intensities of Gβ against wild-type Gip1 and are presented as the mean ± SD of at least three independent experiments (n = 5 (vector, WT), 4 (I306W, I166W, V190W), and 3 (L300W, L211W), ***P < 0.001 versus wild-type, two-tailed unpaired Student's t-test).

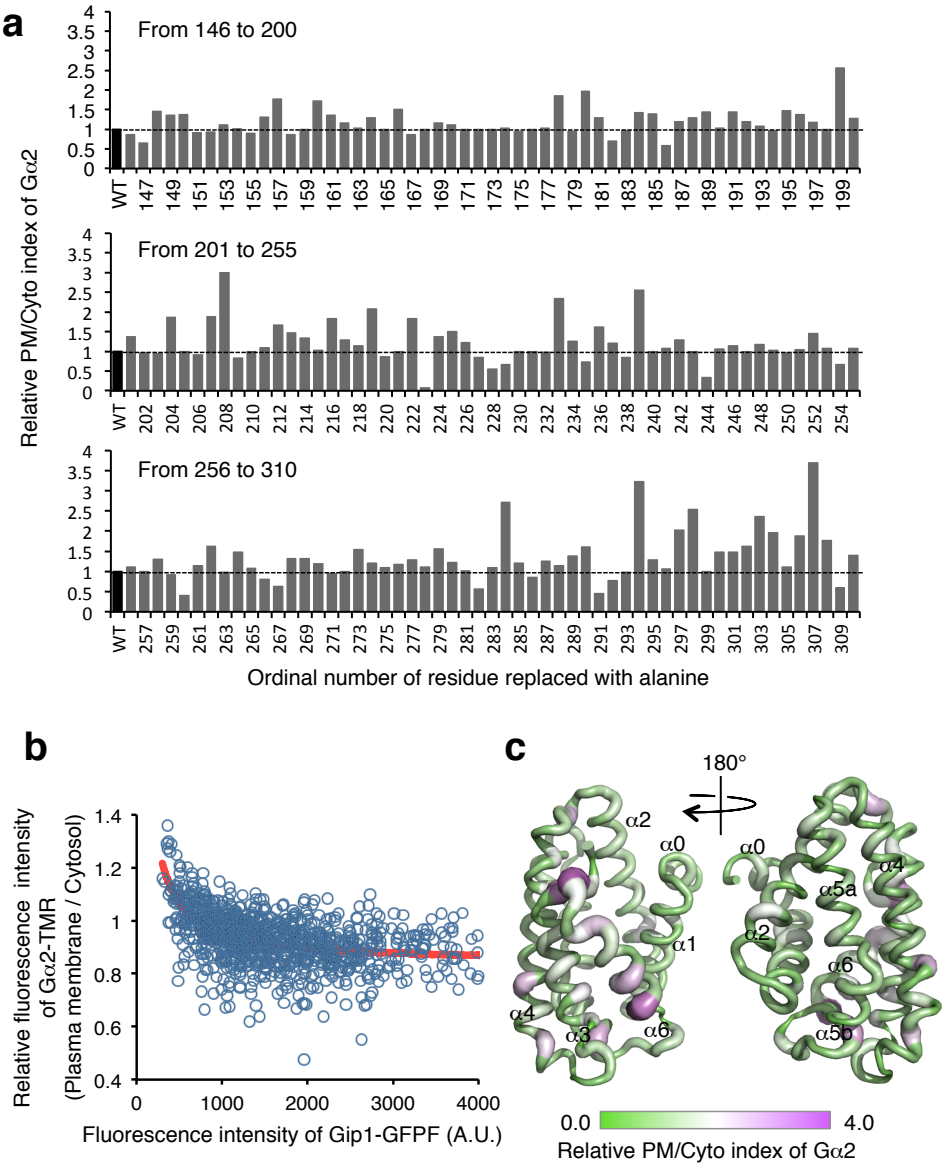

Fig. 28 Comprehensive alanine mutagenesis.

(a) Effects of the alanine mutagenesis scan. The data are the obtained A values ($n \geq 50$ cells). **(b)** Scatter plot of the fluorescence intensities of Gα2-Halo and Gip1-GFPF. The plot is depicted from wild-type as the representative of examinations. To evaluate the effect of alanine substitution, data plots were fitted with a hyperbolic curve colored in red ($y = A/x + C$). A is used as a PM/Cyto index. **(c)** Structural mapping of the alanine scanning mutagenesis of Gip1(146-310). Relative plasma membrane / cytosol (PM/Cyto) indexes were normalized by the value of wild-type and mapped onto the structure. The values range from purple (strong) to green (weak), represented by both the color and the thickness of the ribbon diagram.

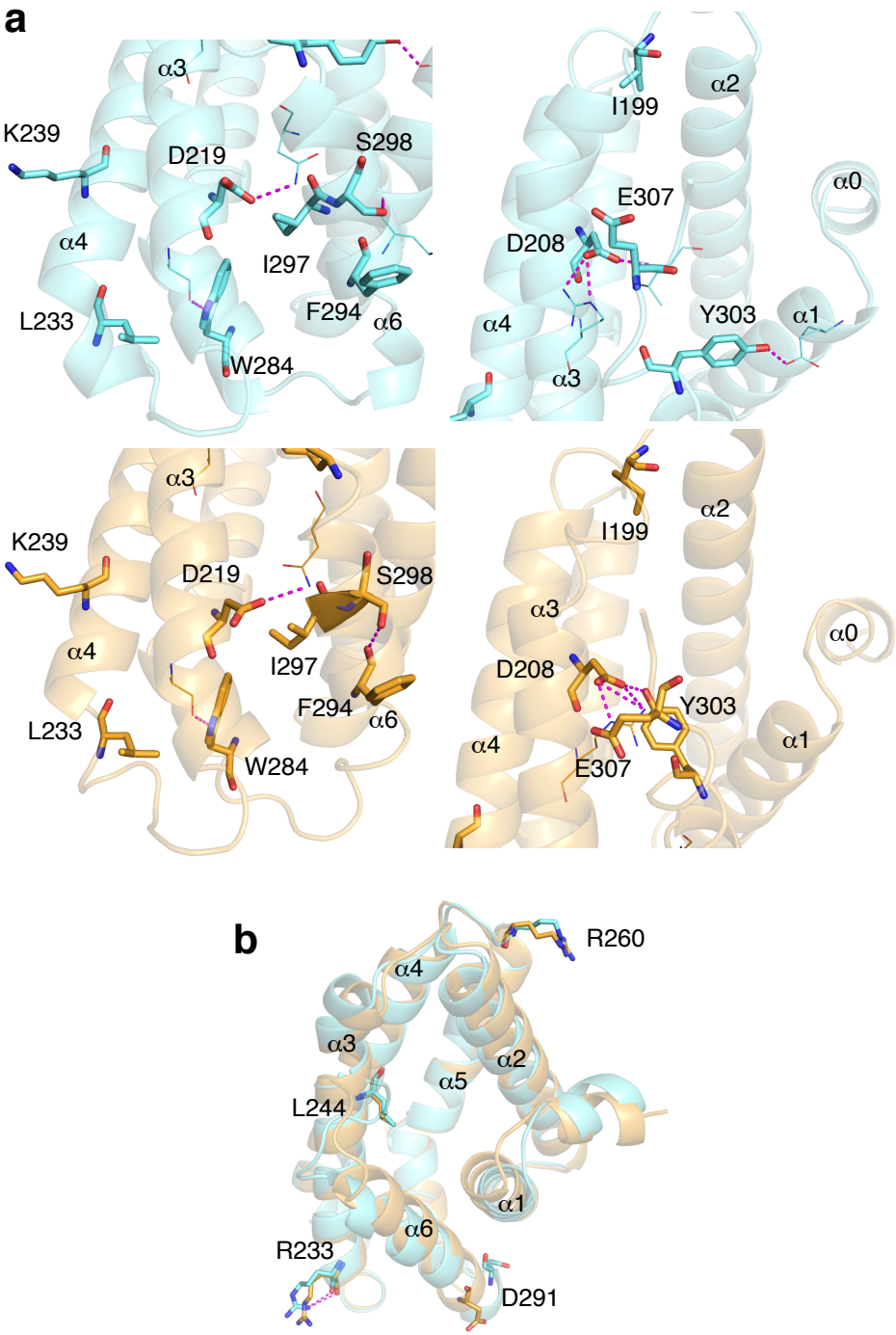

Fig. 29 Notably affected residues by alanine scanning mutagenesis.

(a) Negatively affected residues. Residues listed in Table 9 are depicted as stick models. Form I and Form II are shown in cyan and light orange, respectively. Hydrogen bonds are shown as dashed lines colored in magenta. **(b)** Positively affected residues. Residues are listed in Table 10. Hydrogen bonds are shown as dashed lines, colored in magenta**.**

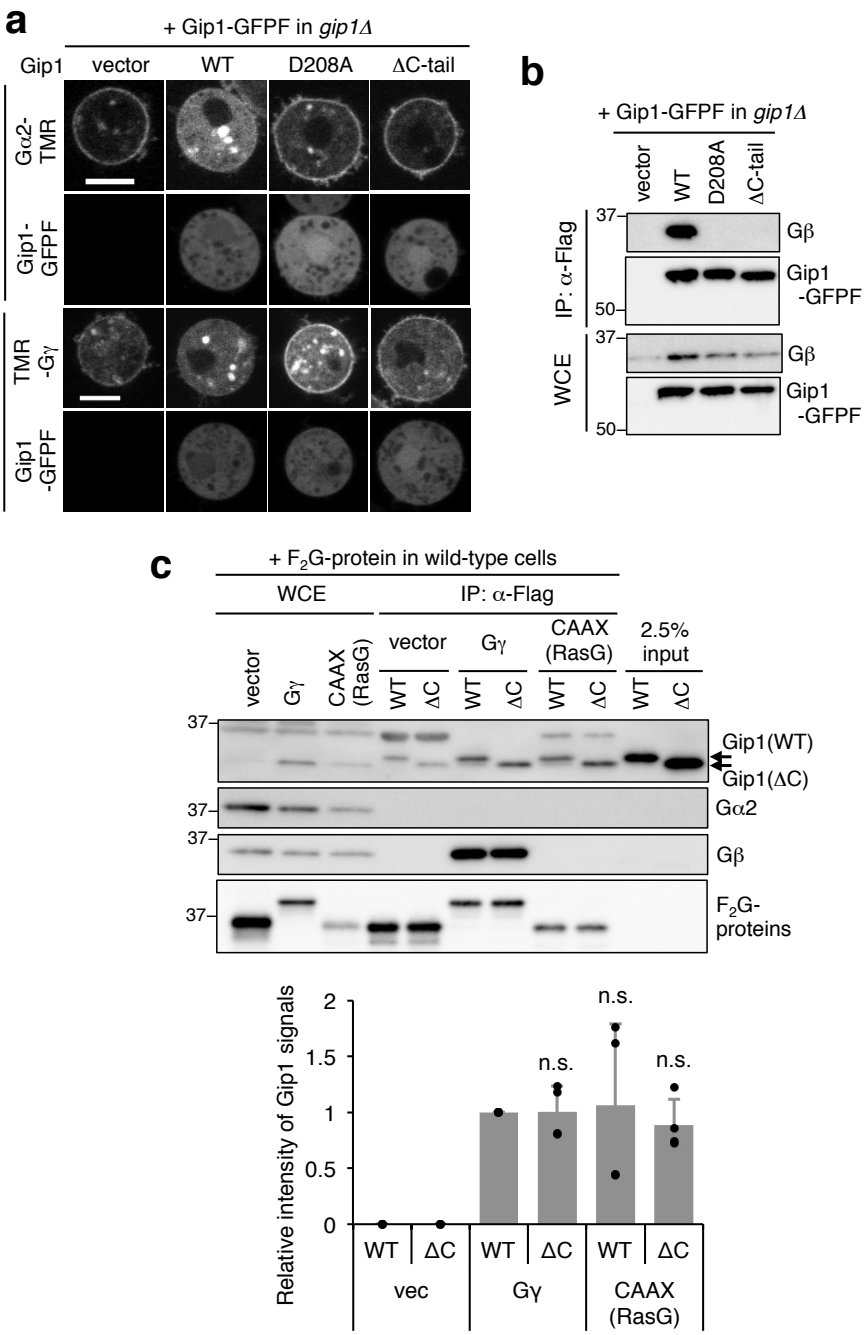

Fig. 30 Important residues found through alanine scanning.

(a) Subcellular localization of Gα2 and Gγ labelled with TMR and Gip1-GFPF in a living cell in the presence of LatA. Representative images of a cell expressing Gip1(D208A) and Gip1(1-303; ΔC-tail) are shown. Scale bar, 5 μm. **(b)** Co-immunoprecipitation of Gip1 with Gβγ. **(c)** In vitro complex formation of purified Gip1. Flag-Flag-GFP (F_2G) as a vector (V), F_2G-Gβγ, and F_2G-tagged CAAX box (a.a. 178-189 from RasG) were bound to beads and incubated with purified full-length Gip1 (WT) or C terminus-deleted Gip1(a.a. 1-303; ΔC). The results are indicated in bar graphs (bottom). Purified Gip1 proteins were wild-type (a.a. 1-310) and ΔC-tail (a.a. 1-303). Prenyl-modified proteins were F_2G, F_2G-Gγ, and

F_2G-RasG(178-189). The results are normalized relative to the band intensities of wild-type Gip1 bound to F_2G-Gγ and represent the mean ± SD of four independent experiments (n = 4, two-tailed unpaired Student's t-test versus Gip1(WT) to F_2G-Gγ).

Table 8 Selected residues for tryptophan substitution.

	Selected with CASTp	Substituted to tryptophan	Residues within 4 Å from the phospholipid (Å)
α1	I152	○	3.8
	P153		3.6
	E155		3.6
	G156		3.3
	L159	○	3.7
	I160	○	3.8
	V163	○	3.6
	I166	○	
α2	I183	○	
	I186	○	3.9
	L187	○	3.7
	V190	○	
	F191		3.6
α3	L204	○	
	V207	○	3.9
	D208		
	L211	○	3.6
	F215		
	L218	○	3.8
α4	L244	○	
	T251		
	L254	○	
α5	T270		
	F271		3.5
	L274	○	
	G275		
	F279		3.9
	F280		3.9
α6	V283	○	
	W284		
	L293	○	4.0
	L296	○	3.8
	I297	○	
	L300	○	
	Y303		3.3
	I306	○	
	E307		
	L308	○	3.3
	I309	○	3.4
	Y310		3.1

Colors of the table correspond to the colors of α-helices shown in Fig. 13. Blanks indicate that no atoms were selected at the corresponding residues in the structure. Right column is the result of Form I shown in Table 6.

Table 9 Negatively affected residues by alanine mutagenesis and sequence alignment.

	DdGip1	HsTNFAIP8	HsTIPE1	HsTIPE2	HsTIPE3
I199	I	F	L	F	F
D208	D	E	R	T	E
D219	D	M	M	M	M
L233	L	R	R	A	R
K239	K	L	G	L	L
W284	W	Y	Y	Y	Y
F294	F	L	L	L	L
I297	I	L	I	I	I
S298	S	C	C	C	C
Y303	Y	K	R	K	K
E307	E	E	E	E	E

Residues in the DdGip1 column increased the PM/Cyto index over two-fold by alanine mutagenesis. The affected residues were compared with corresponding residues of TNFAIP8 family proteins. Colored residues indicate the electrostatic charge: red and blue for positive and negative, respectively.

Table 10 Positively affected residues by alanine mutagenesis and sequence alignment.

	DdGip1	HsTNFAIP8	HsTIPE1	HsTIPE2	HsTIPE3
R233	R	S	S	S	S
L244	L	R	R	R	K
R260	R	H	H	H	H
D291	D	K	R	T	R

Residues in the DdGip1 column decreased the PM/Cyto index less than half by alanine mutagenesis. The affected residues were compared with corresponding residues of TNFAIP8 family proteins. Colored residues indicate the electrostatic charge: red and blue for positive and negative, respectively.

III-3. Significance of the hydrophobic cavity for eukaryotic chemotaxis

I revealed that interior side and the entrance of the hydrophobic cavity of Gip1 including the C-terminal tail were significant for complex formation with G proteins and hence proper localization of G proteins. Finally, I explored the relationship between the hydrophobic cavity and chemotactic behaviors.

III-3-1 Effects of cavity mutations on chemotactic behaviors

To unveil the relationship between the complex formation and chemotactic ability, chemotactic behaviors were measured using *gip1Δ Dictyostelium* cells expressing wild-type or mutated Gip1, which did not complex with G proteins. Cells expressing wild-type Gip1 were able to migrate toward a source of cAMP. On the other hand, cells expressing vector, Gip1(D208A), and Gip1(ΔC-tail) were not able to chemotax to near the source of cAMP (Fig. 31a). Compared to wild-type cells, mutated cells exhibited low chemotactic ability (chemotaxis index) when cells were close to the cAMP source (Fig. 31b). The mean motility speeds were not so different between Gip1 variants (Fig. 31c). Taken together, the defects of chemotactic behaviors are supposed to be resulted from the impairment of sensing ability. The cells were also provided to another chemotactic experiment, small population assay. Cells expressing wild-type Gip1 exhibited chemotactic ability over broad range (from 0.1 μM to 100 μM) of cAMP concentration. While, cells expressing vector, mutant Gip1 were impaired in chemotaxis at the relatively high (approximately over 10 μM) cAMP concentration (Fig. 31c). These results were not only in Gip1(D208A) and Gip1(ΔC-tail), but also in some tryptophan substituted Gip1 mutants (Fig. 31d). Finally, I observed the translocation of Gα2 subunit inside the cells. Wild-type Gip1 sequestered Gα2 at the cytosolic pool and translocated Gα2 to the plasma membrane in the cAMP stimulation-dependent manner consistent with previous data (Fig. 31e) [Kamimura *et al.,* 2016]. However, Gip1(D208A) and Gip1(ΔC-tail) did not sequester Gα2 in the cytosol even in the resting state because these mutants were not able to

interact with G proteins (Fig. 31e). Therefore, it was obvious that the rate of cytosolic Gα2 did not change in the cells expressing mutated Gip1 regardless of the cAMP stimulation (Fig. 31f).

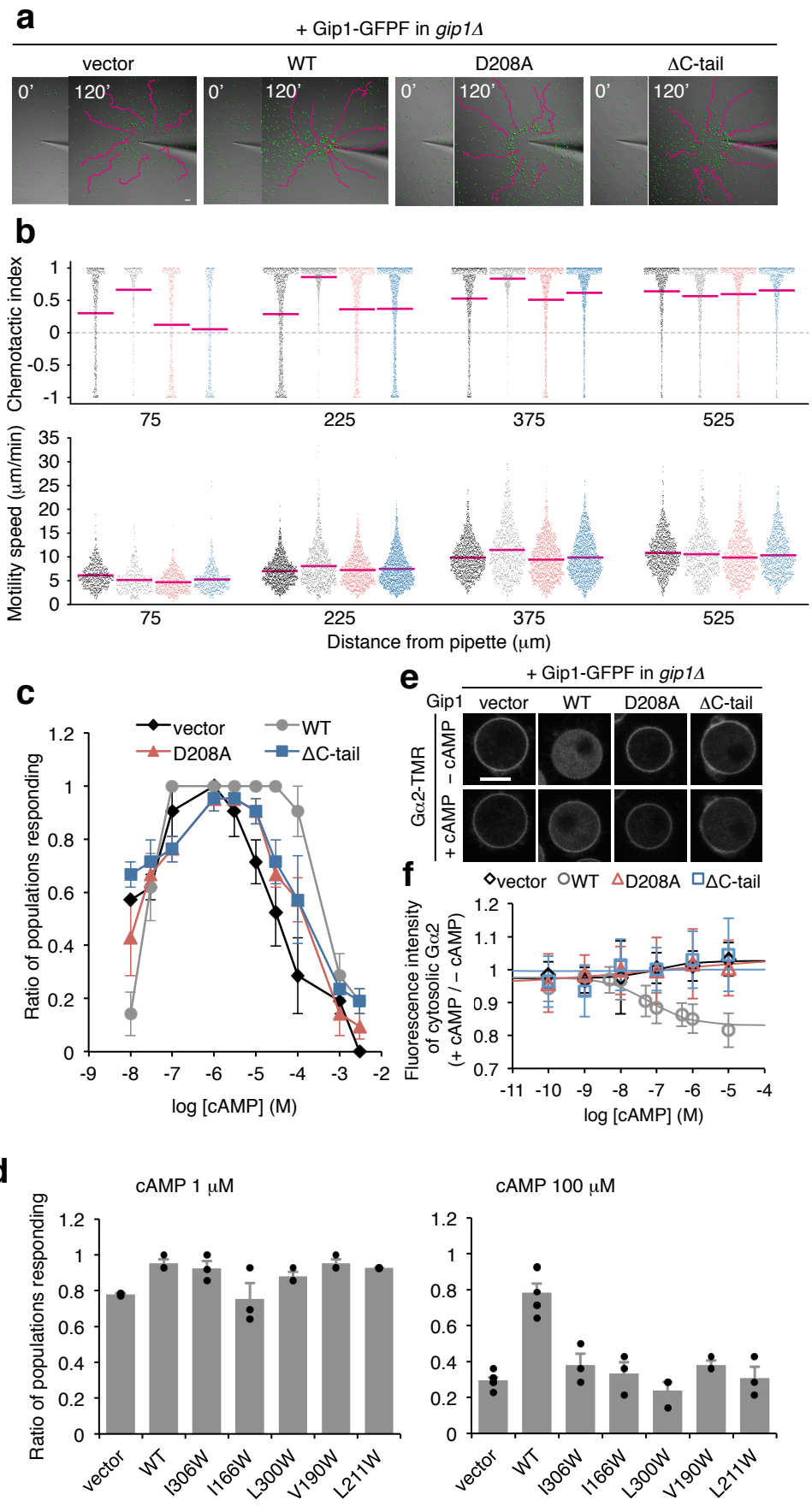
a
+ Gip1-GFPF in gip1Δ
vector
WT
D208A
ΔC-tail
0'
120'
b
Chemotactic index
Motility speed (μm/min)
Distance from pipette (μm)
c
vector
WT
D208A
ΔC-tail
Ratio of populations responding
log [cAMP] (M)
e
+ Gip1-GFPF in gip1Δ
Gip1
Gα2-TMR
– cAMP
+ cAMP
f
Fluorescence intensity of cytosolic Gα2 (+ cAMP / – cAMP)
log [cAMP] (M)
d
cAMP 1 μM
cAMP 100 μM
Ratio of populations responding
I306W
I166W
L300W
V190W
L211W

Fig. 31 Contribution of Gip1-G protein complex formation to wide-range chemotaxis. **(a)** Chemotactic behaviors of *gip1Δ* cells expressing Gip1 mutants. Cells (green) migrate towards the tip of a pipette filled with 100 μM cAMP. Representative images with cell trajectories (magenta lines) are shown before (0') and 120 min after (120') the micropipette chemotactic assay. Scale bar, 50 μm. **(b)** Chemotactic index (upper) and motility speed (lower) calculated from the assay in Fig. 31a. The data represent the mean ± SEM (n = 285-1737 data points from at least 103 cells). Distribution of vector, WT, D208A, and ΔC-tail are colored in black, gray, red, and blue, respectively. **(c)** Chemotactic response to various cAMP concentrations. The data represent the mean ± SEM of three independent experiments. Vector, WT, D208A, and ΔC-tail are shown by the black-filled diamond, gray-filled circle, red-filled triangle, and blue-filled square, respectively. **(d)** Chemotactic response to 1 and 100 μM cAMP. The mutant cells with tryptophan substitution in the hydrophobic cavity were analysed as in Fig. 31c. The data represent the mean ± SEM of at least three independent experiments (n = 4 for vector (cAMP 100 μM) and WT (cAMP 100 μM), n = 3 for the other experiments). **(e)** Gα2 translocation dependent on cAMP stimulation in the presence of LatA. Representative images are from before (-cAMP) and after (+cAMP) the addition of 10 μM cAMP. Scale bar, 5 μm. **(f)** Dose dependency of Gα2 translocation in response to different cAMP concentrations. The data represent the mean ± SD ($n \geq 60$ cells). Vector, WT, D208A, and ΔC-tail are shown by the black-open diamond, gray-open circle, red-open triangle, and blue-open square, respectively.

IV. Discussion

G proteins bind to a guanine nucleotide and switch their activities by exchanging GDP and GTP by GEF or GAP enzymes. In addition to such GDP/GTP exchange reaction, accumulating studies report that G proteins change their intracellular localization and exert appropriate activities. This spatial regulation mechanism has been revealed in mainly small G proteins (Rho, Ras, Rab). Recently, Gip1 was identified to be a key factor of subcellular translocation of heterotrimeric G proteins during eukaryotic chemotaxis in a *Dictyostelium* cell. In this doctoral thesis, I unveiled how Gip1 sequesters heterotriemric G proteins in the cytosol with structural, biochemical, and imaging techniques. In this section, I discuss the mechanism of complex formation between Gip1 and G proteins, mainly focusing on the binding mode, the binding specificity, the regulation mechanism and the physiological relevance.

IV-1 Binding mode

I determined two crystal structures of C-terminal G protein binding region of Gip1. Gip1 had a centrally located hydrophobic cavity and accommodated a bacterial phospholipid inside the cavity. The overall structure was similar to those of TNFAIP8, TIPE2 and TIPE3. TIPE2 and TIPE3 involve in the lipid transfer [Fayngerts *et al.,* 2014; Fayngerts *et al.,* 2017], and TNFAIP8 can bind to PE [Kim *et al.*, 2017]. In addition, Gip1 binds to heterotrimeric G proteins, which are subjected to lipid-modification. Taken together, these results suggest that Gip1 interacts with the lipid-modified moiety of G proteins through the hydrophobic cavity. Consistent with the previous report that Gip1 mainly binds to Gβγ [Kamimura *et al.*, 2016], Gip1 was not able to interact with the geranylgeranylation-deficient Gγ(ΔCAAX) mutant. Furthermore, complex formation of Gip1 and G proteins was competitively inhibited by geranylgeranyl pyrophosphate and impaired by introduced steric blockage into the cavity (Figs. 23a, 26). These results strongly support that Gip1 binds to G proteins via the hydrophobic cavity and geranylgeranyl-moiety on the C-terminal Gγ (Fig. 32). A previous report

provides another model that TNFAIP8 interacts with Gαi through the cavity-bound PE, which occupies the cavity and forms hydrogen bonds with three charged residues around the cavity entrance [Kim *et al.*, 2017]. This report did not focus on the lipid-modifications. Thus, it could be worth reconsidering if TNFAIP8 directly binds to Gαi through its lipid-modification.

The solved Gip1 structures accommodated the phospholipid inside the hydrophobic cavity. The lipid might artificially enter the cavity during the protein purification. In this study, it cannot be concluded whether the bound-lipid has a physiological function or not. The amount of endogenous cytosolic Gβ was a little less than Gip1, and hence almost all cytosolic G proteins were thought to be complexed with Gip1. This means that some Gip1 proteins do not complex with G proteins. Since overexpressed Gip1 is stable without N-terminal PH domain in a cell [Kamimura *et al.*, 2016], C terminus of Gip1 stably exists in the solvent by itself. This result may indicate that PH domain is not involved in stabilizing the C terminus in absence of G proteins. It seems unlikely that a highly hydrophobic area is usually exposed to the solvent. TIPE2 interacts with both PIP2 and prenyl-modified Rac1 [Wang *et al*., 2012; Fayngerts *et al.,* 2017]. Since TIPE2 is structurally similar to Gip1 and Gip1 has not been reported to interact with another binding partner so far, Gip1 could bind to a lipid compound to stabilize its structure in absence of G proteins. To investigate the possibility, it is worth exploring if Gip1 contains certain lipids in *Dictyostelium* cells.

Solubilization factors have reported to capture their cargos in two different ways. RhoGDI gets close to the plasma membrane by interacting to the cargo through the regulatory arm, directs to the appropriate orientation, and then accommodates the lipid-moiety transiently dissociated from the plasma membrane [Nomanbhoy *et al.*, 1999]. Through these steps, RhoGDI changes its cavity size [Keep *et al*., 1997; Qureshi *et al*., 2018]. On the other hand, PDEδ captures the spontaneously dissociated cargos with the open cavity [Qureshi *et al*., 2018]. Gip1 contained a phospholipid in the determined structures. This result may indi-

cate that the cavity is open before complex formation. In addition, Gip1 localized in the cytosol but not on the plasma membrane (Fig. 24). These results suggest that Gip1 forms open cavity and captures the geranylgeranyl-moiety on Gγ spontaneously dissociated for the plasma membrane in the PDEδ-like manner.

The complex formation between Gip1 and G proteins were affected by geranylgeranyl pyrophosphate but not by myristic acid, which is a derivative of acyl-moiety of Gα2 (Figs. 21, 23). This result demonstrates that Gip1 does not interact with the myristyl-moiety on Gα2. Since the number of modified lipids is of significance to the frequency of dissociation [Rocks *et al.*, 2005; Rocks *et al.*, 2010; Chandra *et al*., 2012], shielding the geranylgeranyl-moiety alone from the solvent may be adequate to the G protein solubilization.

Gip1 preferentially bind to heterotrimeric G proteins rather than Gβγ alone, and solubilize the ternary complex in the cytosol. So far, it has been reported that phosducin and UNC119 also solubilize Gβγ and Gα subunits, respectively [Sokolov *et al*., 2004; Zhang *et al.*, 2011, Sinha *et al*., 2013]. Especially, UNC119 forms a hydrophobic cavity and contains acyl-moiety on N-terminal Gα in the cavity for complex formation [Zhang *et al.*, 2011]. However, both phosducin and UNC119 bind to only dissociated G protein subunits. Phosducin shares the binding interface of Gβ with many effectors (e.g. Gα, GRK, PLCβ2 and SIGK) [Lambright *et al*., 1996; Gaudet *et al.*, 1996; Ford *et al.*, 1998; Leow *et al.*, 1998; Tesmer *et al*., 2005; Davis *et al.*, 2005]. Likewise, UNC119 overlaps the binding interface of Gα with Gβγ [Cheguru *et al*., 2015]. In both cases, binding effectors inhibit interaction of dissociated subunit. Since Gip1 maintains the heterotrimeric form of G proteins, it is possible that Gip1 binds to G proteins in a distinct manner from other effector proteins.

IV-2 Binding specificity for heterotrimeric G proteins

Besides the hydrophobic cavity, Gip1 required the C-terminal tail region for the complex formation with G proteins (Fig. 30). The tail region was connected with α3-helix through the

hydrogen bonding network including Asp208. This hydrogen bonding network was rearranged to induce rotational movement of α1- and α6-helices and to change the cavity size. PDEδ and UNC119 change their cavity size to dissociate their bound-cargo by interacting with dissociation factors (e.g. Arl2-GTP) [Hanzal-Bayer *et al*., 2002; Ismail *et al*., 2011; Ismail *et al*., 2012]. Similarly, the C-terminal tail may regulate the cavity size and hence binding affinity with G proteins. Indeed, deletion of the tail region or alanine mutation of Asp208, which connected α3-helix and the tail region, severely impaired the binding ability with G proteins (Fig. 30). Interestingly, C-terminal deleted Gip1 was able to interact with G proteins in in vitro-assay. More surprisingly, both wild-type and C-tail deleted Gip1 bound to geranylgeranyl-modified CAAX box alone from RasG in in vitro-assay, although RasG did not bind to Gip1 in in vivo-assay (Figs. 25c, 30c). To sum up, the C-terminal tail may provide the binding specificity for G proteins on the physiological conditions, but not adequate to restrict binding partners in artificial conditions. It is suggested that unknown proteins or environmental factors might suppress the non-specific binding through the C-terminal tail region.

The tail region included Glu307, which dramatically impaired the complex formation by alanine substitution. Glu307 changed the orientation of its side chain between two forms of Gip1 structures, but the residue did not form any hydrogen bonds with other intramolecular atoms within the structures. These data may demonstrate that Glu307 is important for intermolecular interaction. UNC119 and PDEδ distinguish the amino acid sequence near the lipid-modified regions, resulting in the binding specificity to their cargos besides the hydrophobic cavity [Fansa *et al*., 2016; Dharmaiah *et al.*, 2016; Jaiswal *et al.*, 2016]. Since Glu307 resides in the vicinity of the cavity entrance, Glu307 may be involved in distinguishing the C-terminal sequence of Gγ. Interestingly, TNFAIP8 family proteins have glutamic acid at the corresponding position as Glu307 of Gip1 (Table 9). However, the directions of the C-terminal tail regions of TNFAIP8 family proteins extend to the different orientation from that of Gip1 (Fig. 20d). According to the information, it is enigmatic if the glutamic ac-

id on the C terminal tail in TNFAIP8 family exerts the same function as Glu307.

Electrostatic surface potential affected the complex formation between Gip1 and heterotrimeric G proteins. Gip1 had a positively charged patch on the water-exposed surface between α2- and α5-helices, where alanine mutations remarkably decreased the binding ability with G proteins (Fig. 20a,c). Since this positively charged patch was conserved in Gip1 and TNFAIP8 family proteins, the charged area may contribute to a common function in Gip1 and TNFAIP8 family. On the other hand, there was also a positively charged area between α3- and α4-helices. This charge was attributed to Lys239, which was significantly affected by alanine scanning. Contrary to the positive charged patch described above, Lys239 was found only in Gip1 but not conserved in TNFAIP8 family. Since this residue did not form any hydrogen bonds within intramolecular atoms, Lys239 could function for intramolecular binding in a Gip1-specific manner, resulting in the determination of binding specificity.

IV-3 Regulation mechanism of G protein translocation

Two forms of Gip1 structures indicated that rotational movement at α1- and α6-helices rearranged the hydrogen bonding network around the cavity entrance and changed the cavity size approximately 30%. PDEδ reduces its cavity size by interacting with Arl2-GTP on the target membrane and releases its cargo to the appropriate location [Ismail *et al.*, 2011]. On the other hand, UNC119 release its cargos by widening the cavity [Jaiswal *et al*., 2016]. These results may suggest that Gip1 releases G proteins by changing the cavity size induced by cAMP stimulation. Gip1 has a PH domain at its N terminus that is essential for regulating cAMP-dependent G protein translocation [Kamimura *et al.*, 2016]. Therefore, cAMP-dependent signal could induce the conformational change of N-terminal PH domain, resulting in the rotational movement of α1- and α6-helices to modulate the cavity size and release G proteins from the cavity.

IV-4 G protein translocation in mammalian cells

Mammalian TNFAIP8 family proteins only have a DUF758 domain but lack a PH domain. As explained above, PH domain is essential for regulating G protein translocation in Gip1. TNFAIP8 and TIPE2 are reported to interact with Gαi and Rac1, respectively [Laliberté *et al.,* 2010; Wang *et al.*, 2012]. In mammalian cells, TNFAIP8 family proteins might serve as solubilization factors for G proteins in the same way as C terminus of Gip1 in *Dictyostelium*. In addition, TNFAIP8 family proteins might have partner proteins for regulating G protein translocation as is the case with PH domain for Gip1. Since GPCR signaling is widely used in broad biological phemnomena, it is exciting if G protein shuttling, a spatial regulation mechanism of heterotrimeric G proteins, are conserved in mammal cells.

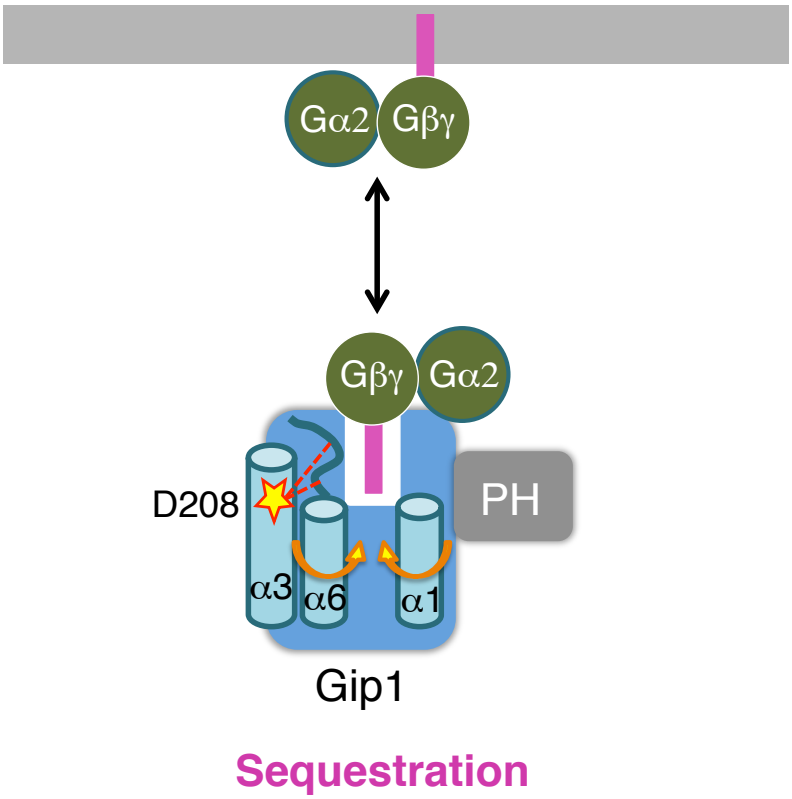

Fig. 32 Schematic model of G protein sequestration in the cytosol.

In the resting state, G proteins are sequestered in the cytosol by complex formation with Gip1. C-terminal region of Gip1 is a cylinder-like structure composed of six α-helices, and accommodates the prenyl-moiety on Gγ subunit via the central hydrophobic cavity. In addition to the cavity, C-terminal tail region is critical for the complex formation with G proteins. The tail region and α3 helix are connected with a hydrogen bonding network around Asp208. Both α1 and α6 are movable and have potential to change the cavity shape.

V. References

Abràmoff, M. D., Magalhães, P. J. & Ram, S. J. Image processing with ImageJ. *Biophotonics International* **11**, 36-42 (2004).

Adams, P. D. *et al.* PHENIX: a comprehensive Python-based system for macromolecular structure solution. *Acta Crystallogr. D Biol. Crystallogr.* **66**, 213-221 (2010).

Afonine, P. V. *et al.* Towards automated crystallographic structure refinement withphenix.refine. *Acta Crystallogr. D Biol. Crystallogr.* **68**, 352-367 (2012).

Akgoz, M., Kalyanaraman, V. & Gautam, N. Receptor-mediated reversible translocation of the G protein βγ complex from the plasma membrane to the golgi complex. *J. Biol. Chem.* **279**, 51541–51544 (2004).

Akgoz, M., Kalyanaraman, V. & Gautam, N. G protein βγ complex translocation from plasma membrane to Golgi complex is influenced by receptor γ subunit interaction. *Cell. Signal.* **18**, 1758–1768 (2006).

Alexander, S. P. H. *et al.* The concise guide to pharmacology 2017/18: G protein-coupled receptors. *Br. J. Pharmacol.* **174**, S17–S129 (2017).

Ames, G. F. Lipids of Salmonella typhimurium and Escherichia coli: Structure and metabolism. *J. Bacteriol.* **95**, 833–843 (1968).

An, Y. *et al.* Geranylgeranyl switching regulates GDI-Rab GTPase recycling. *Structure* **11**, 347–357 (2003).

Antony, P., Baby, B. & Vijayan, R. Molecular insights into the binding of phosphoinositides to the TH domain region of TIPE proteins. *J. Mol. Model.* **22**, 272 (2016).

Azpiazu, I., Akgoz, M., Kalyanaraman, V. & Gautam, N. G protein βγ11 complex translocation is induced by Gi, Gq and Gs coupling receptors and is regulated by the α subunit type. *Cell. Signal.* **18**, 1190–1200 (2006).

Bligh, E. G. & Dyer, W. J. A rapid method of total lipid extraction and purification. *Can. J. Biochem. Physiol.* **37**, 911–917 (1959).

Bonner, J. T. *et al*. Acrasin, acrasinase, and the sensitivity to acrasin in Dictyostelium discoideum. *Dev. Biol.* **20,** 72-87 (1969).

Brann, M. R. & Cohen, L. V. Diumal expression of transducin mRNA and translocation of transducin in rods of rat retina. *Science* **235**, 585–587 (1987).

Brooks, C. *et al.* Farnesylation of the transducin G protein gamma subunit is a prerequisite for its ciliary targeting in rod photoreceptors. *Front. Mol. Neurosci.* **11**, 16 (2018).

Cao, X., Yan, J., Shu, S., Brzostowski, J. A. & Jin, T. Arrestins function in cAR1 GPCR-mediated signaling and cAR1 internalization in the development of Dictyostelium discoideum. *Mol. Biol. Cell* **25**, 3210–3221 (2014).

Cao, X. *et al.* Human tumor necrosis factor (TNF)-alpha-induced protein 8-like 2 suppresses hepatocellular carcinoma metastasis through inhibiting Rac1. *Mol. Cancer* **12**, 1–10 (2013).

Caterina, M. J., Devreotes, P. N., Borleis, J. & Hereld, D. Agonist-induced loss of ligand binding is correlated with phosphorylation of cAR1, a G protein-coupled chemoattractant receptor from Dictyostelium. *The Journal of Biological Chemistry* **270**, 8667–8672 (1995).

Chandra, A. *et al.* The GDI-like solubilizing factor PDEδ sustains the spatial organization and signalling of Ras family proteins. *Nat. Cell Biol.* **14**, 148–158 (2012).

Cheguru, P. *et al.* The solution structure of the transducin-α-uncoordinated 119 protein complex suggests occlusion of the Gβ1γ1-binding sites. *FEBS J.* **282**, 550–561 (2015).

Chisari, M., Saini, D. K., Kalyanaraman, V. & Gautam, N. Shuttling of G protein subunits between the plasma membrane and intracellular membranes. *J. Biol. Chem.* **282**, 24092–24098 (2007).

Davis, T. L., Bonacci, T. M., Sprang, S. R. & Smrcka, A. V. Structural and molecular characterization of a preferred protein interaction surface on G protein βγ subunits. *Biochemistry* **44**, 10593–10604 (2005).

Deverotes, P. N. & Zigmond, S. H. Chemotaxis in eukaryotic cells: a focus on leukocytes and Dictyostelium. *Annu. Rev. Cell Biol.* **4**, 649-686 (1988).

Devreotes, P. N. *et al.* Excitable signal transduction networks in directed cell migration. *Annu. Rev. Cell Dev. Biol.* **33**, 103–123 (2017).

Dharmaiah, S. *et al.* Structural basis of recognition of farnesylated and methylated KRAS4b by PDEδ. *Proc. Natl. Acad. Sci. U. S. A.* **113**, E6766–E6775 (2016).

Dundas, J. *et al.* CASTp: computed atlas of surface topography of proteins with structural and topographical mapping of functionally annotated residues. *Nucleic Acids Res.* **34**,

W116-W118 (2006).

El-Gebali, S. *et al.* The Pfam protein families detabase in 2019. *Nucleic Acides Res.* (2019) doi: 10.1093/nar/gky995.

Elzie, C. A., Colby, J., Sammons, M. A. & Janetopoulos, C. Dynamic localization of G proteins in Dictyostelium discoideum. *J. Cell Sci.* **122**, 2597–2603 (2009).

Emsley, P., Lohkamp, B., Scott, W. G. & Cowtan, K. Features and development of Coot. *Acta Crystallogr. D Biol. Crystallogr.* **66**, 486-501 (2010).

Fansa, E. K., Kösling, S. K., Zent, E., Wittinghofer, A. & Ismail, S. PDE6δ-mediated sorting of INPP5E into the cilium is determined by cargo-carrier affinity. *Nat. Commun.* **7**, 11366 (2016).

Fayngerts, S. A. *et al.* Direction of leukocyte polarization and migration by the phosphoinositide-transfer protein TIPE2. *Nat. Immunol.* **18,** 1353–1360 (2017).

Fayngerts, S. A. *et al.* TIPE3 is the transfer protein of lipid second messengers that promote cancer. *Cancer Cell* **26**, 465–478 (2014).

Fey, P., Dodson, R., Basu, S. & Chisholm, R. L. One stop shop for everything Dictyostelium: dictyBase and the Dicty Stock Center. *Methods Mol. Biol.* **983**, 59-92 (2013).

Fisher, P. R., Merkl, R. & Gerisch, G. Quantitative analysis of cell motility and chemotaxis in Dictyostelium discoideum by using an image processing system and a novel chemotaxis chamber providing stationary chemical gradients. *J. Cell Biol.* **108**, 973–984 (1989).

Fivaz, M. & Meyer, T. Reversible intracellular translocation of KRas but not HRas in hippocampal neurons regulated by Ca2+/calmodulin. *J. Cell Biol.* **170**, 429–442 (2005).

Florio, S. K., Prusti, R. K. & Beavo, J. A. Solubilization of membrane-bound rod phosphodiesterase by the rod phosphodiesterase recombinant δ subunit. *J. Biol. Chem.* **271**, 24036–24047 (1996).

Ford, C. E. *et al.* Molecular basis for interactions of G protein βγ subunits with effectors. *Science* **280**, 1271–1274 (1998).

Gaudet, R., Bohm, A. & Sigler, P. B. Crystal structure at 2.4 Å resolution of the complex of transducin βγ and its regulator, phosducin. *Cell* **87**, 577–588 (1996).

Giri, L. *et al.* A G-protein subunit translocation embedded network motif underlies GPCR regulation of calcium oscillations. *Biophys. J.* **107**, 242–254 (2014).

Gosser, Y. Q. *et al.* C-terminal binding domain of Rho GDP-dissociation inhibitor directs N-terminal inhibitory peptide to GTPases. *Nature* **387**, 814–819 (1997).

Grizot, S. *et al.* Crystal structure of the Rac1-RhoGDI complex involved in NADPH oxidase activation. *Biochemistry* **40**, 10007–10013 (2001).

Gus-Brautbar, Y. *et al.* The anti-inflammatory TIPE2 is an inhibitor of the oncogenic Ras. *Mol. Cell* **45**, 610–618 (2012).

Hanzal-Bayer, M., Renault, L., Roversi, P., Wittinghofer, A. & Hillig, R. C. The complex of Arl2-GTP and PDEδ: From structure to function. *EMBO J.* **21**, 2095–2106 (2002).

Hereld, D., Vaughan, R., Kim, J. Y., Borleis, J. & Devreotes, P. Localization of ligand-induced phosphorylation sites to serine clusters in the C-terminal domain of the Dictyostelium cAMP receptor, cAR1. *J. Biol. Chem.* **269**, 7036–7044 (1994).

Hoffman, G. R., Nassar, N. & Cerione, R. A. Structure of the Rho family GTP-binding protein Cdc42 in complex with the multifunctional regulator RhoGDI. *Cell* **100**, 345–356 (2000).

Iijima, M. & Devreotes, P. Tumor suppressor PTEN mediates sensing of chemoattractant gradients. *Cell* **109**, 599–610 (2002).

Ismail, S. A. *et al.* Structural basis for Arl3-specific release of myristoylated ciliary cargo from UNC119. *EMBO J.* **31**, 4085–4094 (2012).

Ismail, S. A. *et al.* Arl2-GTP and Arl3-GTP regulate a GDI-like transport system for farnesylated cargo. *Nat. Chem. Biol.* **7**, 942–949 (2011).

Jaiswal, M. *et al.* Novel biochemical and structural insights into the interaction of myristoylated cargo with Unc119 protein and their release by Arl2/3. *J. Biol. Chem.* **291**, 20766–20778 (2016).

Janetopoulos, C., Jin, T. & Devreotes, P. Receptor-mediated activation of heterotrimeric G-proteins in living cells. *Science* **291**, 2408–2411 (2001).

Jiang, H. *et al.* Protein lipidation: Occurrence, mechanisms, biological functions, and enabling technologies. *Chem. Rev.* **118**, 919–988 (2018).

Jin, T., Ning, Z., Yu, L., Parent, C. A. & Devreotes, P. N. Localization of the G Protein

complex in living cells during chemotaxis. *Science* **287**, 1034–1036 (2000).

Johnson, R. L., Saxe, III, C. L., Gollop, R., Kimmel, A. R. & Devreotes, P. N. Identification and targeted gene disruption of cAR3, a cAMP receptor subtype expressed during multicellular stages of Dictyostelium development. *Genes Dev.* **7**, 273–282 (1993).

Jurrus, E. *et al.* Improvements to the APBS biomolecular solvation software suite. *Protein Sci.* **27**, 112-128 (2018).

Kabsch, W. XDS. *Acta Crystallogr. D Biol. Crystallogr.* **66**, 125-132 (2010).

Kamimura, Y., Tang, M. & Devreotes, P. Assays for chemotaxis and chemoattract-ant-stimulated TorC2 activation and PKB substrate phosphorylation in *Dictyostelium*. *Methods Mol. Biol.* **571**, 255-270 (2009).

Kamimura, Y., Miyanaga, Y. & Ueda, M. Heterotrimeric G-protein shuttling via Gip1 extends the dynamic range of eukaryotic chemotaxis. *Proc. Natl. Acad. Sci. U. S. A.* **113**, 4356–4361 (2016).

Kang, Y. *et al.* Crystal structure of rhodopsin bound to arrestin by femtosecond X-ray laser. *Nature* **523**, 561–567 (2015).

Karunarathne, W. K. A., O'Neill, P. R., Martinez-Espinosa, P. L., Kalyanaraman, V. & Gautam, N. All G protein βγ complexes are capable of translocation on receptor activation. *Biochem. Biophys. Res. Commun.* **421**, 605–611 (2012).

Kataria, R. *et al.* Dictyostelium Ric8 is a nonreceptor guanine exchange factor for heterotrimeric G proteins and is important for development and chemotaxis. *Proc. Natl. Acad. Sci. U. S. A.* **110**, 6424–6429 (2013).

Keep, N. H. *et al.* A modulator of rho family G proteins, rhoGDI, binds these G proteins via an immunoglobulin-like domain and a flexible N-terminal arm. *Structure* **5**, 623–633 (1997).

Kim, J.-S. *et al.* The Tnfaip8-PE complex is a novel upstream effector in the anti-autophagic action of insulin. *Sci. Rep.* **7**, 1–13 (2017).

Kim, J.-Y. *et al.* Phosphorylation of chemoattractant receptors is not essential for chemotaxis or termination of G-protein-mediated responses. *J. Biol. Chem.* **272,** 27313–27318 (1997).

Klein, P. S. *et al.* A chemoattractant receptor controls development in Dictyostelium

discoideum. *Scienc* **241**, 1467–1472 (1988).

Konijn, T. M., van de Meene, J. G. C., Chang, Y. Y., Barkley, D. S. & Bonner, J. T. Identification of adenosine-3',5'-monophosphate as the bacterial attractant for myxamoebae of Dictyostelium discoideum. *J. Bacteriol.* **99**, 510–512 (1969a).

Konijn, T. M., Chang, Y.-Y. & Bonner, J. T. Synthesis of cyclic AMP in DIctyostelium discoideum and Polysphondylium pallidum. *Nature* **224,** 1211–1212 (1969b).

Krissinel, E. & Henrick, K. Secondary-structure matching (SSM), a new tool for fast protein structure alignment in three dimensions. *Acta Crystallogr D Biol Crystallogr* **60**, 2256-2268 (2004).

Kumar, D. *et al.* Expression of SCC-S2, an antiapoptotic molecule, correlates with enhanced proliferation and tumorigenicity of MDA-MB 435 cells. *Oncogene* **23**, 612–616 (2004).

Kumar, D., Whiteside, T. L. & Kasid, U. Identification of a novel tumor necrosis factor-α-inducible gene, SCC-S2, containing the consensus sequence of a death effector domain of Fas-associated death domain-like interleukin-1β-converting enzyme-inhibitory protein. *J. Biol. Chem.* **275**, 2973–2978 (2000).

Laliberté, B. *et al.* TNFAIP8: A new effector for Galpha(i) coupling to reduce cell death and induce cell transformation. *J. Cell. Physiol.* **225**, 865–874 (2010).

Lambright, D. G., Noel, J. P., Hamm, H. E. & Sigler, P. B. Structural determinants for activation of the α-subunit of a heterotrimeric G protein. *Nature* **369**, 621–628 (1994).

Lambright, D. G. *et al.* The 2.0 Å crystal structure of a heterotrimeric G protein. *Nature* **379,** 311–319 (1996).

Larkin, M. A. et al. Clustal W and Clustal X version 2.0. Bioinformatics **23**, 2947-2948 (2007).

Lee, R. H., Lieberman, B. S. & Lolley, R. N. A novel complex from Bovine visual cells of a 33000-dalton phosphoprotein with β- and γ-transducin: Purification and subunit structure. *Biochemistry* **26**, 3983–3990 (1987).

Levchenko, A. & Iglesias, P. A. Models of eukaryotic gradient sensing: Application to chemotaxis of amoebae and neutrophils. *Biophys. J.* **82**, 50–63 (2002).

Levi, S., Polyakov, M. & Egelhoff, T. T. Green fluorescent protein and epitope tag fusion

vectors for Dictyostelium discoideum. *Plasmid* **44**, 231–238 (2000).

Linding, R., Russell, R. B., Neduva, V. & Gibson, T. J. GlobPlot: exploring protein sequences for globularity and disorder. *Nucleic Acids Res.* **31**, 3701-3708 (2003)

Loew, A., Ho, Y.-K., Blundell, T. & Bax, B. Phosducin induces a structural change in transducin βγ. *Structure* **6**, 1007–1019 (1998).

Macnab, R. M. & Koshland Jr, D. E. The gradient-sensing mechanism in bacterial chemotaxis. *Proc. Natl. Acad. Sci. U. S. A.* **69**, 2509–2512 (1972).

McCoy, A. J. *et al.* Phasercrystallographic software. *J. Appl. Crystallogr.* **40**, 658-674 (2007).

Miyanaga, Y., Kamimura, Y., Kuwayama, H., Devreotes, P. N. & Ueda, M. Chemoattractant receptors activate, recruit and capture G proteins for wide range chemotaxis. *Biochem. Biophys. Res. Commun.* **507**, 304–310 (2018).

Murphy, P. M. *et al.* Structural Homologue of the N-Formyl Peptide Receptor. *J. Biol. Chem.* **267**, 7637–7643 (1992).

Nancy, V., Callebaut, I., Marjou, A. E. l. & de Gunzburg, J. The δ subunit of retinal rod cGMP phosphodiesterase regulates the membrane association of Ras and Rap GTpases. *J. Biol. Chem.* **277**, 15076–15084 (2002).

Noel, J. P., Hamm, H. E. & Sigler, P. B. The 2.2 Å crystal structure of transducin-α complex with GTPγS. *Nature* **366**, 654–663 (1993).

Nomanbhoy, T. K. & Cerione, R. A. Characterization of the interaction between RhoGDI and Cdc42Hs using fluorescence spectroscopy. *J. Biol. Chem.* **271**, 10004–10009 (1996).

Nomanbhoy, T. K., Erickson, J. W. & Cerione, R. A. Kinetics of Cdc42 membrane extraction by Rho-GDI monitored by real-time fluorescence resonance energy transfer. *Biochemistry* **38**, 1744–1750 (1999).

O'Neill, P. R., Karunarathne, W. K. A., Kalyanaraman, V., Silvius, J. R. & Gautam, N. G-protein signaling leverages subunit-dependent membrane affinity to differentially control βγ translocation to intracellular membranes. *Proc. Natl. Acad. Sci. U. S. A.* **109**, E3568–E3577 (2012).

Otwinowski, Z. & Minor, W. Processing of X-ray diffraction data collected in oscillation mode. *Meth. Enzymol.* **276,** 307-326 (1997).

Parent, C. A., Blacklock, B. J., Froehlich, W. M., Murphy, D. B. & Devreotes, P. N. G protein signaling events are activated at the leading edge of chemotactic cells. *Cell* **95**, 81–91 (1998).

Philp, N. J., Chang, W. & Long, K. Light-stimulated protein movement in rod photoreceptor cells of the rat retina. *FEBS Lett.* **225**, 127–132 (1987).

Porturas, T. P. *et al.* Crucial roles of TNFAIP8 protein in regulating apoptosis and Listeria infection. *J. Immunol.* **194**, 5743–5750 (2015).

Pylypenko, O. *et al.* Structure of doubly prenylated Ypt1:GDI complex and the mechanism of GDI-mediated Rab recycling. *EMBO J.* **25**, 13–23 (2006).

Qureshi, B. M. *et al.* Mechanistic insights into the role of prenyl-binding protein PrBP/δ in membrane dissociation of phosphodiesterase 6. *Nat. Commun.* **9**, (2018).

Rak, A. *et al.* Structure of Rab GDP-dissociation inhibitor in complex with prenylated YPT1 GTPase. *Science* **302**, 646–650 (2003).

Rasmussen, S. G. F. *et al.* Crystal structure of the β2 adrenergic receptor-Gs protein complex. *Nature* **477**, 549–555 (2011).

Resh, M. D. Trafficking and signaling by fatty-acylated and prenylated proteins. *Nat. Chem. Biol.* **2**, 584–590 (2006).

Rocks, O. *et al.* The palmitoylation machinery is a spatially organizing system for peripheral membrane proteins. *Cell* **141**, 458–471 (2010).

Rocks, O. *et al.* An acylation cycle regulates localization and activity of palmitoylated Ras isoforms. *Science* **307**, 1746–1752 (2005).

Saini, D. K., Kalyanaraman, V., Chisari, M. & Gautam, N. A family of G protein βγ subunits translocate reversibly from the plasma membrane to endomembranes on receptor activation. *J. Biol. Chem.* **282**, 24099–24108 (2007).

Saini, D. K. *et al.* Regulation of Golgi structure and secretion by receptor-induced G protein βγ complex translocation. *Proc. Natl. Acad. Sci. U. S. A.* **107**, 11417–11422 (2010).

Sasaki, A. T., Chun, C., Takeda, K. & Firtel, R. A. Localized Ras signaling at the leading edge regulates PI3K, cell polarity, and directional cell movement. *J. Cell Biol.* **167**, 505–518 (2004).

Saxe, C. L. III *et al.* CAR2, a prestalk cAMP receptor required for normal tip formation and

late development of Dictyostehum discoideum. *Genes Dev.* **7**, 262–272 (1993).

Saxe, C. L. III, Jhonson, R. L., Devreotes, P. N. & Kimmel, A. R. Expression of a cAMP receptor gene of Dictyostelium and evidence for a multigene family. *Genes Dev.* **5**, 1–8 (1991).

Schalk, I. *et al.* Structure and mutational analysis of Rab GDP-dissociation inhibitor. *Nature* **381**, 42–48 (1996).

Scheffzek, K., Stephan, I., Jensen, O. N., Illenberger, D. & Gierschik, P. The Rac–RhoGDI complex and the structural basis for the regulation of Rho proteins by RhoGDI. *Nat. Struct. Biol.* **7**, 122–126 (2000).

Schiffmann, E., Corcoran, B. A. & Wahl, S. M. N-formylmethionyl peptides as chemoattractants for leucocytes. *Proc. Natl. Acad. Sci. U. S. A.* **72**, 1059–1062 (1975).

Schmick, M. *et al.* KRas localizes to the plasma membrane by spatial cycles of solubilization, trapping and vesicular transport. *Cell* **157**, 459–471 (2014).

Senarath, K. *et al.* Gγ identity dictates efficacy of Gβγ signaling and macrophage migration. *J. Biol. Chem.* **293**, 2974–2989 (2018).

Sinha, S., Majumder, A., Belcastro, M., Sokolov, M. & Artemyev, N. O. Expression and subcellular distribution of UNC119a, a protein partner of transducin α subunit in rod photoreceptors. *Cell. Signal.* **25**, 341–348 (2013).

Sokolov, M. *et al.* Massive light-driven translocation of transducin between the two major compartments of rod cells: A novel mechanism of light adaptation. *Neuron* **33**, 95–106 (2002).

Sokolov, M. *et al.* Phosducin facilitates light-driven transducin translocation in rod photoreceptors. *J. Biol. Chem.* **279**, 19149–19156 (2004).

Sondek, J., Bohm, A., Lambright, D. G., Hamm, H. E. & Sigler, P. B. Crystal structure of a GA protein Gβγ dimer at 2.1 Å resolution. *Nature* **379**, 369–379 (1996).

Sperlich, B., Kapoor, S., Waldmann, H., Winter, R. & Weise, K. Regulation of K-Ras4B membrane binding by calmodulin. *Biophys. J.* **111**, 113–122 (2016).

Sun, H. *et al.* TIPE2, a negative regulator of innate and adaptive immunity that maintains immune homeostasis. *Cell* **133**, 415–426 (2008).

Sun, H. *et al.* TIPE2 controls innate immunity to RNA by targeting the phosphatidylinositol

3-kinase−Rac pathway. *J. Immunol.* **189**, 2768–2773 (2012).

Swaney, K. F., Huang, C.-H. & Devreotes, P. N. Eukaryotic chemotaxis: A network of signaling pathways controls motility, directional sensing, and polarity. *Annu. Rev. Biophys.* **39**, 265–289 (2010).

Tang, M. *et al.* Evolutionarily conserved coupling of adaptive and excitable networks mediates eukaryotic chemotaxis. *Nat. Commun.* **5**, 5175 (2014).

Taylor, S. J., Resnick, R. J. & Shalloway, D. Nonradioactive determination of Ras-GTP levels using activated Ras interaction assay. *Methods Enzymol.* **333**, 333–342 (2001).

Terwilliger, T. C. *et al.* Iterative model building, structure refinement and density modification with the PHENIX AutoBuild wizard. *Acta Crystallogr. D Biol. Crystallogr.* **64**, 61-69 (2008).

Tesmer, V. M., Kawano, T., Shankaranarayanan, A., Kozasa, T. & Tesmer, J. J. G. Snapshot of activated G proteins at the membrane: the Gαq-GRK2-Gβγ complex. *Science* **310**, 1686–1690 (2005).

Tnimov, Z. *et al.* Quantitative analysis of prenylated RhoA interaction with its chaperone, RhoGDI. *J. Biol. Chem.* **287**, 26549–26562 (2012).

Tomchik, K. J. & Devreotes, P. N. Adenosine 3',5'-monophosphate waves in Dictyostelium discoideum: A demonstration by isotope dilution-fluorography. *Science.* **212**, 443–446 (1981).

Tsang, N., Macnab, R. & Koshland Jr, D. E. Common mechanism for repellents and attractants in bacterial chemotaxis. *Science* **181**, 60–63 (1973).

Vagin, A. A. *et al.* REFMAC5 dictionary: organization of prior chemical knowledge and guidelines for its use. *Acta Crystallogr. D Biol. Crystallogr.* **60**, 2184-2195 (2004).

Wang, Z. *et al.* TIPE2 protein serves as a negative regulator of phagocytosis and oxidative burst during infection. *Proc. Natl. Acad. Sci. U. S. A.* **109**, 15413–15418 (2012).

Wätzlich, D. *et al.* The interplay between RPGR, PDEδ and Arl2/3 regulate the ciliary targeting of farnesylated cargo. *EMBO Rep.* **14**, 465–472 (2013).

Winn, M. D. *et al.* Overview of the CCP4 suite and current developments. *Acta Crystallogr. D Biol. Crystallogr.* **67**, 235-242 (2011).

Xu, X. *et al.* GPCR-controlled membrane recruitment of negative regulator C2GAP1 locally

inhibits Ras signaling for adaptation and long-range chemotaxis. *Proc. Natl. Acad. Sci. U. S. A.* **114**, E10092–E10101 (2017).

Yan, J. *et al.* A Gβγ effector, ElmoE, transduces GPCR signaling to the actin network during chemotaxis. *Dev. Cell* **22**, 92–103 (2012).

You, Z., Ouyang, H., Lopatin, D., Polver, P. J. & Wang, C.-Y. Nuclear factor-κB-inducible death effector domain-containing protein suppresses tumor necrosis factor-mediated apoptosis by inhibiting caspase-8 activity. *J. Biol. Chem.* **276**, 26398–26404 (2001).

Yumura, S., Mori, H. & Fukui, Y. Localization of actin and myosin for the study of ameboid movement in Dictyostelium using improved immunofluorescence. *J. Cell Biol.* **99**, 894–899 (1984).

Zha, Z. *et al.* A non-canonical function of Gβ as a subunit of E3 ligase in targeting GRK2 ubiquitylation. *Mol. Cell* **58**, 794–803 (2015).

Zhang, H. *et al.* UNC119 is required for G protein trafficking in sensory neurons. *Nat. Neurosci.* **14**, 874–880 (2011).

Zhang, S., Charest, P. G. & Firtel, R. A. Spatiotemporal regulation of Ras activity provides directional sensing. *Curr. Biol.* **18**, 1587–1593 (2008).

Zhang, X. *et al.* Crystal structure of TIPE2 provides insights into immune homeostasis. *Nat. Struct. Mol. Biol.* **16**, 89–90 (2009).

Zhang, Z. *et al.* TIPE1 induces apoptosis by negatively regulating Rac1 activation in hepatocellular carcinoma cells. *Oncogene* **34**, 2566–2574 (2015).

Zigmond, S. H. Mechanism of sensing chemical gradients by polymorphonuclear leukocytes. *Nature* **249**, 450–452 (1974).

VI. Acknowledgements

This study was carried out in Laboratory of Single Molecule Biology, Graduate School of Frontier Biosciences, Osaka University, and Laboratory for Cell Signaling Dynamics, RIKEN Center for Biosystems Dynamics Research (BDR).

I would like to express my sincere gratitude to Prof. Masahiro Ueda and Dr. Yoichiro Kamimura for helpful discussions and encouragements. I am deeply grateful to Dr. Hiroyasu Koteishi and Assistant Prof. Yukihiro Miyanaga for teaching me a lot including experimental methods as well as their continuous supports, helpful advices and discussion. I am also grateful to Dr. Kohei Takeshita for teaching me experimental advices and suggestions on crystallization and structural refinement. I would like to thank all members in Laboratory of Single Molecule Biology and Laboratory for Cell Signaling Dynamics for daily discussion.

I wish to express my sincere thanks to Prof. Masaru Ishii, Prof. Atsushi Nakagawa, and Associate Prof. Shuji Tachibanaki for evaluating my doctoral thesis.

I would like to show my greatest appreciation to Prof. Kiyoshi Takeda, Prof. Yasushi Okamura, Prof. Masayuki Miyasaka, and staffs of Interdisciplinary Program for Biomedical Sciences (IPBS) for giving me precious opportunity to study interdisciplinary fields, stimulating discussion from various viewpoints, and continuous supports.

Finally, I thank my family for their financial support and encouragement.

March 2019

Takero Miyagawa

VII. Achievements

Publication

1. Miyagawa, T., Koteishi, H., Kamimura, Y., Miyanaga, Y., Takeshita, K., Nakagawa, A. & Ueda, M. Structural basis of Gip1 for cytosolic sequestration of G protein in wide-range chemotaxis. *Nat. Commun.* **9**, 4635 (2018)

Presentations in international conferences

1. ○Miyagawa, T., Masui, R., & Kuramitsu, S.

   「Nucleotide binding extremely stabilizes a protein kinase from *Thremus thermophilus* HB8」, 『The 2nd Annual Meeting for Whole-Organism Science Society』, SPring-8 Public Relations Center, 2012 年 9 月 28-29 日, ポスター番号 24（9 月 28 日）(査読なし, ポスター発表)

2. ○Miyagawa, T., Iio, Y., Masui, R., & Kuramitsu, S.

   「Biochemical and genetic analysis of functionally unknown protein from *Thermus thermophilus* HB8」, 『The 3rd Annual Meeting for Whole-Organism Science Society』, Osaka University, 2013 年 9 月 21-22 日, ポスター番号 39 （9 月 21 日）(査読なし, ポスター発表)

Presentations in domestic conferences

1. ○宮川武朗, 飯尾洋太, 増井良治, 倉光成紀

   「高度好熱菌丸ごと一匹解析：異なるファミリーに属するプロテインキナーゼは異なる耐熱化機構を持つ」, 『第 85 回日本生化学会大会』, 福岡国際会議場・マリンメッセ福岡, 2012 年 12 月 14-16 日, 演題番号 2T01-11（12 月 15 日）, ポスター番号 2P-653（12 月 15 日）(査読あり, 口頭発表, ポスター発表)

2. ○藤野友輔, 宮川武朗, 井上真男, 藤井裕己, 倉光成紀, 増井良治

「Effectts of ligands on structural stability of protein kinase TpkD from *Thermus thermophiles* HB8」, 『第 89 回日本生化学会大会』, 仙台国際センター/東北大学川内北キャンパス, 2016 年 9 月 25-27 日, ポスター番号 P128 (9 月 25 日) (査読あり, ポスター発表)

3. ○藤野友輔, 宮川武朗, 井上真男, 藤井裕己, 倉光成紀, 増井良治

「Effectts of ligands on structural stability of protein kinase TpkD from *Thermus thermophiles* HB8」, 『第 16 回日本蛋白質科学会年会』, 福岡国際会議場, 2016 年 6 月 7-9 日, ポスター番号 2P-022 (6 月 8 日) (査読あり, ポスター発表)

4. ○藤野友輔, 宮川武朗, 井上真男, 藤井裕己, 倉光成紀, 増井良治

「高度好熱菌 protein kinase TpkD の構造安定性に対するリガンドの効果」, 『第 63 回日本生化学会近畿支部例会』, 神戸薬科大学, 2016 年 5 月 21 日, ポスター番号 B20 (査読あり, ポスター発表)

5. ○宮川武朗, 上村陽一郎, 小手石泰康, 竹下浩平, 中川敦史, 上田昌宏

「三量体 G 蛋白質シャトリングを支える Gip1-Gγ複合体形成の構造解析」, 『第 17 回日本蛋白質科学会年会』, 仙台国際センター, 2017 年 6 月 20-22 日, ポスター番号 2P-002 (6 月 21 日) (査読あり, ポスター発表)

6. ○宮川武朗, 上村陽一郎, 小手石泰康, 竹下浩平, 中川敦史, 上田昌宏

「Gip1 は Gγの脂質修飾部位を疎水性空隙で覆うことで三量体 G 蛋白質を細胞基質に隔離する / Gip1 sequesters heterotrimeric G proteins in the cytosol by masking their lipid-modification site with the hydrophobic cavity」, 『第 55 回日本生物物理学会年会』, 熊本大学 黒髪北地区, 2017 年 9 月 19-21 日, ポスター番号 2Pos033 (9 月 20 日) (査読あり, ポスター発表)

7. ○宮川武朗

「三量体 G タンパク質の細胞質局在を支える分子構造基盤の解明」, 『理研シンポジウム「細胞システムの動態と論理 X」』, 国立研究開発法人理化学研究所　生

物科学研究棟, 2018 年 4 月 12-13 日 (4 月 13 日) (査読なし, 口頭発表)